Magnetically-active polymer scaffolds printed by electrical field-assisted 3D printing

Bc. Danila Gorgol

Master's thesis
2020

Tomas Bata University in Zlín
Faculty of Technology

Univerzita Tomáše Bati ve Zlíně
Fakulta technologická
Ústav inženýrství polymerů

Akademický rok: 2019/2020

ZADÁNÍ DIPLOMOVÉ PRÁCE

(projektu, uměleckého díla, uměleckého výkonu)

Jméno a příjmení:	**Bc. Danila Gorgol**
Osobní číslo:	**T18243**
Studijní program:	**N2808 Chemie a technologie materiálů**
Studijní obor:	**Inženýrství polymerů**
Forma studia:	**Prezenční**
Téma práce:	**Magneticky aktivní polymerní scafoldy vytisknuté pomocí elektrickým polem asistovaného 3D tisku**

Zásady pro vypracování

Technologie 3D tisku je v současnosti velmi rychle se rozvíjejícím odvětvím v oblasti zpracování polymerních materiálů. Standardní technologie 3D tisku jako je např. stereolitografie je omezena na určitý typ materiálu a určitou teplotu. Naproti tomu elektrickým polem asistovaný (EPA) 3D tisk disponuje kombinací zvýšené teploty a aplikovaného elektrického pole s cílem zlepšit schopnost daného materiálu pro získání jeho finálního tvaru. Tato technologie je také velmi často využívaná na přípravu scafoldů pro kultivaci buněk.

Student se bude v rešeršní části zabývat 3D tiskem obecně. Podrobně se bude věnovat elektrickým polem asistovanému (EPA) 3D tisku. Popíše různé typy materiálů, které jsou vhodné EPA 3D tisk. Nedílnou součástí rešeršní práce bude popsat principy EPA 3D tisku a požadavky na materiál, který se pro tyto účely používá. Dále pak uvede několik příkladů, kompozitních materiálů obsahující různá plniva a podrobně magnetická plniva, které se pro 3D tisk využívají obecně.

V experimentální části připraví student polymerní kompozity na bázi termoplastických polyolefinů obsahující magnetické plnivo. Tyto systémy bude charakterizovat pomocí různých analytických metod, spektroskopických technik, termických metod a mechanických vlastností. Nakonec provede EPA 3D tisk připravených systémů do formy scafoldů a bude hodnotit jejich vlastnosti pod vlivem různé intenzity magnetického pole.

Forma zpracování diplomové práce: **Tištěná/elektronická**
Jazyk zpracování: **Angličtina**

Seznam doporučené literatury:

1. Petcu, E. B., Midha, R., McColl, E., Popa-Wagner, A., Chirila, T. V., Dalton, P. D., 3D printing strategies for peripheral nerve regeneration, Biofabrication, 2018, vol. 10, pp. 032001.
2. Wunner, F. M., Wille, M. L., Noonan, T. G., Bas, O., Dalton, P. D., De-Juan-Pardo, E. M., Hutmacher, D. W., Melt Electrospinning writing of Highly Ordered Large Volume Scaffold Architectures, Advanced Materials, 2018, vol. 30, pp. 1706570.

Vedoucí diplomové práce: **Ing. Miroslav Mrlík, Ph.D.**
Centrum polymerních systémů

Datum zadání diplomové práce: **2. ledna 2020**
Termín odevzdání diplomové práce: **15. května 2020**

L.S.

prof. Ing. Roman Čermák, Ph.D.
děkan

doc. Ing. Tomáš Sedláček, Ph.D.
ředitel ústavu

Ve Zlíně dne 17. února 2020

PROHLÁŠENÍ AUTORA
DIPLOMOVÉ PRÁCE

Beru na vědomí, že:

- diplomová práce bude uložena v elektronické podobě v univerzitním informačním systému a dostupná k nahlédnutí;
- na moji diplomovou práci se plně vztahuje zákon č. 121/2000 Sb. o právu autorském, o právech souvisejících s právem autorským a o změně některých zákonů (autorský zákon) ve znění pozdějších právních předpisů, zejm. § 35 odst. 3;
- podle § 60 odst. 1 autorského zákona má Univerzita Tomáše Bati ve Zlíně právo na uzavření licenční smlouvy o užití školního díla v rozsahu § 12 odst. 4 autorského zákona;
- podle § 60 odst. 2 a 3 autorského zákona mohu užít své dílo – diplomovou práci nebo poskytnout licenci k jejímu využití jen s předchozím písemným souhlasem Univerzity Tomáše Bati ve Zlíně, která je oprávněna v takovém případě ode mne požadovat přiměřený příspěvek na úhradu nákladů, které byly Univerzitou Tomáše Bati ve Zlíně na vytvoření díla vynaloženy (až do jejich skutečné výše);
- pokud bylo k vypracování diplomové práce využito softwaru poskytnutého Univerzitou Tomáše Bati ve Zlíně nebo jinými subjekty pouze ke studijním a výzkumným účelům (tj. k nekomerčnímu využití), nelze výsledky diplomové práce využít ke komerčním účelům;
- pokud je výstupem diplomové práce jakýkoliv softwarový produkt, považují se za součást práce rovněž i zdrojové kódy, popř. soubory, ze kterých se projekt skládá. Neodevzdání této součásti může být důvodem k neobhájení práce.

Prohlašuji,

- že jsem diplomové práci pracoval samostatně a použitou literaturu jsem citoval. V případě publikace výsledků budu uveden jako spoluautor.
- že odevzdaná verze diplomové práce a verze elektronická nahraná do IS/STAG jsou obsahově totožné.

Ve Zlíně dne:

Jméno a příjmení studenta:

……..

podpis studenta

ABSTRAKT

Hlavním cílem této diplomové práce byla příprava a charakterizace scafoldů na bázi elastomeru s přídavkem magnetických částic, jenž potenciálně umožní kultivaci buněk v magnetickém poli. Tato práce zahrnuje teoretickou část zaměřenou na objasnění klíčových faktorů ve funkci, struktuře a výrobě scafoldů a taktéž popis metodologie provedených měření. Praktická část obsahuje postup přípravy polymerních masterbatchů obsahující elastomerní matrici a magnetické plnivo a poté samotnou výrobu scafoldů pomocí elektrickým polem asistovaným 3D tiskem včetně jejich charakterizace rastrovacím elektronovým mikroskopem, hodnocení viskoelastických a kalorimetrických vlastností, a nakonec testů na jejich cytotoxicitu, jako potvrzení použitelnosti v medicinálních aplikacích.

Klíčová slova: elastomer, magnetické částice, scafold, medicína, magnetické pole

ABSTRACT

The main goal of this master's thesis was preparation and characterization of the scaffolds based on copolymer with a magnetic additive potentially enabling a cell cultivation in magnetic field. This work includes theoretical part aimed on the clarifying of crucial factors in scaffold function, structure and production as well as the description of the methodology of the performed measurements. The practical part contains preparation of the polymer masterbatches including elastomeric matrix and magnetic filler and then fabrication procedure of the scaffolds using electric filed-assisted 3D printing and their characterization using scanning electron microscopy, investigation of the viscoelastic and calorimetric properties and finally cytotoxicity evaluation, as a confirmation of their utilization in medical applications.

Keywords: elastomer, magnetic particles, scaffold, medicine, magnetic field

ACKNOWLEDGEMENTS

I am glad to have this opportunity to express gratitude to all of the Polymer engineering department members for their support. I am grateful to Ing. Miroslav Mrlík Ph.D. for valuable advices and patience. I thank my family for the unceasing encouragement and attention. I am grateful to my life partner Bc. Leona Mahelová who supported me through this thesis. I also thank Ing. Zdenka Capáková Ph.D. for cytotoxicity evaluation and Ing. Pavel Bažant, Ph.D. for training on SEM device and time.

I hereby declare that the print version of my Bachelor's/Master's thesis and the electronic version of my thesis deposited in the IS/STAG system are identical.

CONTENTS

INTRODUCTION

During whole history of humankind people were looking for materials and technologies that could improve their life quality. Over the past two decades, regenerative medicine and tissue engineering have invested in the regeneration and reconstruction of pathologically altered tissues such as cartilage, bone tissue, skin, heart valves, nerves and many others components of human organism (Pina et al., 2019). The term "tissue engineering" was at first officially specified in 1988 by the National Science Foundation Workshop, which means ‘the application of principles and methods of engineering and life sciences toward the basic insight of structure-function relationships in normal and pathological mammalian tissues and the development of biological substitutes to not only renew but aslo improve or maintain tissue function (O'Brien, 2011). Three-dimensional based scaffolds and hydrogels alone or in cooperation with bioactive molecules or cells and gens are able of driving the development of functional tissue engineering and providing stable mechanical support during implantation and using in vivo (Pina et al., 2019). Also scaffold could be presented such as a temporary or permanent host for cells a controlled drug release system and also a biodegradable tissue engineering biomaterials. Scaffolds are gradually able to fully replace bone as a result for example of bone injuries caused by an accident, a shortage of a bone tissue after tumor surgery and bone malformations or by providing a temporary spacer when a bone implant failure because of some infection (Ronca et al., 2017). As base for scaffold can serve natural and synthetic polymers, biologically resorbable organic and inorganic materials (Pina et al., 2019).

The main goal of this work was an attempt to create suitable material for a further muscle tissue scaffold which could be active in magnetic field and fabricated due to melt-electrowriting technique. As material was chosen composition of thermoplastic elastomer (Vistamaxx) and magnetic particles (Carbonyl Iron Powder). The properties of the composite were measured using viscoelastic characterization, dynamic mechanical analysis, differential scanning calorimetry. The structure and content were observed due to optical and scanning electron microscope. Biocompatibility was tested by cytotoxicity tests. This thesis provides a brief overview on the thermoplastic elastomer scaffolds, magnetic particles and deeper exploring of tissue engineering and scaffold with fabrication methods.

I. THEORY

1 CRUCIAL PARAMETERS FOR SCAFFOLD

The main goal in the field of regenerative medicine is to provide a substitute for lost or damaged tissues because of disease, trauma, or congenital abnormalities. In the case of such system as scaffolds, the biomaterial component is generally defined as a naturally or synthetically derived substance designed to interact with complex biological systems and support functional tissue (Chung et al., 2017).

Scaffolds (Fig. 1) can play a role of great importance in regenerative medicine because they can act not only as an ordinary substrate for promoting cell growth, but also as forming specific structures, regulating behavior of cells, a sustained local delivery system for growth factors or signaling molecules and improving cell function and tissue regeneration (Saadatmand et al., 2019). Tissue engineering in medicine is widely applied to recover or recreate the original properties of damaged tissues and organs. The tissue - engineering scaffold is the one of the most crucial element of properly regenerating tissues. Generally scaffold is a 3D structure that promotes cell growth, suitable adhesion, and the formation of functional tissues. To regenerate different types of tissues for example such bone, muscles, skin, nerves, or tendons, bioprinting techniques have been utilized to create 3D platforms with or without cells. A content of the human body consists of a wide range of unique biological fibril structures, and the geometry of fibril array is mostly specific to the tissue's distinct functional complexity (Kim et al., 2018).

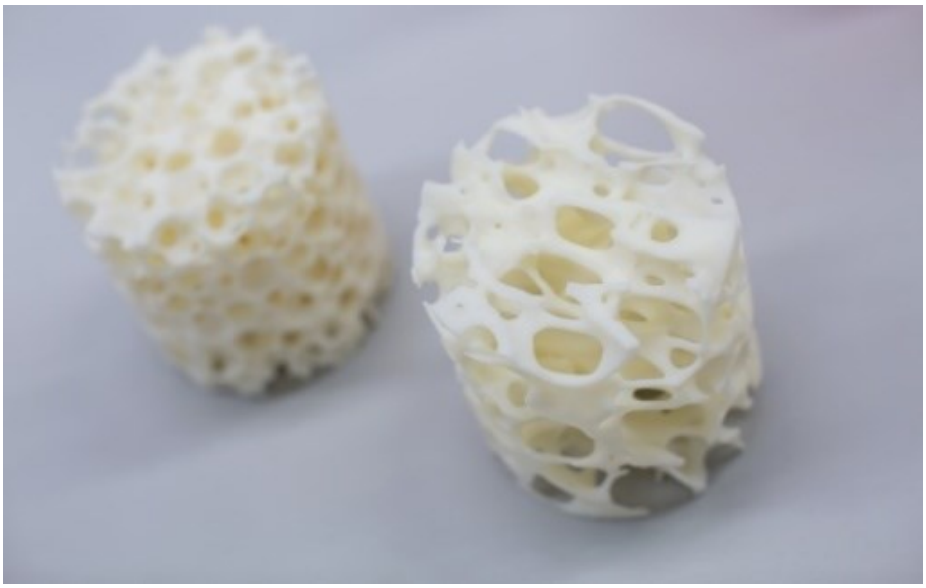

Figure 1 Bioglass scaffolds ("Chemistry Society, SS, HKUSU", 2020).

Generally, the tissue engineering should serve three general purposes: (1) to create the space that will be sufficient for forming of the regenerating tissue, (2) to temporarily provide a functionality in the defected tissue, and (3) to facilitate tissue growth and possibly allow inoculation of the cells, proteins and genes to improve tissue regeneration. The first requirement is fulfilled if the shape of the regenerated tissue agrees with the original shape of the tissue (Lanfer et al., 2009). Numerous scaffolds made of different biomaterials were fabricated using a variety of manufacturing techniques used in the field in attempts to regenerate distinct tissues and organs in the human body. Regardless of the tissue type, several key considerations are significant when determining or designing the suitability of scaffolds to be applied in tissue engineering:

(a) Biocompatibility

(b) Biodegradability

(c) Mechanical properties

(d) Scaffold structure

(e) Drug delivery

1.1 Biocompatibility

The fundamental requirement to every scaffold for tissue engineering is that it surely has to be biocompatible; cells have to get proper adherence, normal functionality, and migration onto the surface and eventually through some pores of the scaffold structure and begin to proliferate before laying down new matrix. After implantation, tissue engineered construct or the scaffold has to bring out a negligible immune reaction in order to prevent it causing such a severe inflammatory response that it might worsen healing or make rejection by the body (Ronca et al., 2017). Some additives can increase biocompatibility. For example, cell attachment studies show the fact that graphene oxide (GO) present in the composite scaffolds provided a favorable environment for cell proliferation and attachment (Sivashankari & Prabaharan, 2020).

1.2 Biodegradability

The goal of tissue engineering is to enable the cells of own body to replace the implanted scaffold or tissue engineering construct over time. Scaffolds are not permanent implants. The scaffold has to therefore be biodegradable to allow the cells of organism to produce their

own extracellular matrix. The side products of this degradation should also be non-toxic and be able to leave the body without any negative interference with other organs, accumulation is not acceptable too. To allow degradation along with tissue formation, an inflammatory response is required to be associated with a controlled infusion of cells such as macrophages. Recently it was explored, that tissue engineering strategies are more routine in clinical practice, immunology plays an increasingly important role in the research field (Ronca et al., 2017). Some architecture change in structure or simply degradation of some scaffold parts could be useful for drug release. The usage of bioceramic scaffolds for a controlled drug release, makes the treatment much more effective especially for a disease such as cancer. Due to method, drug tends to efficiently release at the site of disease from loaded biocompatible scaffold to either extirpate the disease or stimulate bone healing (Farzin et al., 2017).

1.3 Mechanical properties

In ideal case, the scaffold should have such mechanical properties as original tissue or organ site into which it is to be implanted and, on practical side, has to be strong enough to allow surgical handling during operation. While this is important in all tissues, it presents some complications, especially for cardiovascular and orthopaedic applications. The production of scaffolds with suitable mechanical behavior is one of the greatest challenges in attempting to create cartilage or bone. In this type of tissues, the implanted scaffold should have satisfactory mechanical chariness since the moment of implantation to completion of the remodeling process (O'Brien, 2011).

The crucial information for mechanically optimal scaffold are about what scaffold stiffness is best for application, what average amount of pores and their size is the best for tissue regeneration, or any other of the many various scaffold parameters, firstly requires scaffold microstructure (microstructure could be defined as a structure size ranging from 100 up to 1000 μm) for possibility to operate structurally. Design optimization is necessary too because of possible complication with a conflict of many different design requirements. In addition, the scaffold microstructures can be relatively complicated and demand detailed production control. Detailed management of microstructure production is readily achievable only by solid free mold (SFM) techniques. The use of SFF for scaffolding has been rapidly increasing during the last 5 years (Ronca et al., 2017). Another complication is that the speed of healing depends on age of a patient; for example, young patients show faster healing,

while fractures usually heal to the acceptable point in approximately six weeks, full mechanical integrity requires about one year after the fracture, but in the older age, the speed of healing decreases. This should also be considered when creating scaffolds for orthopedic applications. Nevertheless, as time spreads, much attention is paid to an attempt to generate a scaffold with mechanical properties quite similar to bone tissue and cartilage. A lot of materials were made with excellent mechanical properties, but at the expense of maintaining high porosity, and many materials that demonstrated potential in vitro failed in vivo, the reason is insufficient vascularization capacity. Obviously, the right balance between mechanical properties and suitable porous structure to enable cellular infiltration and vascularization is crucial for successful function of every scaffold (O'Brien, 2011).

1.4 Scaffold structure

The major goal of polymeric scaffold utilization in tissue engineering is to act like a 3D template matrix that can fulfill several requests. The temporary artificial matrix has to provide mechanical stability in terms of maintaining stress and support the loading generated during in vitro or in vivo regeneration (Tanasa et al., 2020). A basic requirement for tissue architecture is the management of cell-matrix interactions. Completing this goal by mimicking the original environment of cells is a main plot for many scientific disciplines, for tissue engineering too (Lanfer et al., 2009). These 3D constructs provide the physicochemical and mechanical upkeep for in vitro ECM (natural extracellular matrix formation), being slowly degraded, metabolized, or resorbed upon in vivo implantation. In addition, heterogenic structure improves the tissue vascularization and formation of new tissue (Pina et al., 2019). As example, an alginate/bioceramic scaffold consisting of hollow pipe struts (outer diameter of 1 mm and inner diameter of 500 μm) were fabricated by a 3D printing process was proposed for bone tissue regeneration because the hollow struts can induce the rapid migration of host blood vessels through the hollow channels, thereby successfully increasing bone tissue regeneration (Lee & Kim, 2020). Extracellular matrix is outer space between cells in tissue. That is not empty zone at all, ECM is filled by various structural components such as collagen, elastin, firbrin and others. The type of cell and complex of all these proteins creates a structure and a functionality of tissue including proliferation, differentiation, adhesion and orientation. For example collagen is organized as parallel fiber bundles in tendons and ligaments, as concentric waves in bone and as oriented fibrils in the surface zone of articular cartilage (Lanfer et al., 2009).

All scaffolds should have some volume of interconnected pores to provide an essential enviroment for cells (O'Brien, 2011). Such factors as the sum of pores, pore sizes, and interconnectivity have an enormous influence at all whole scaffold functionality. High level of porosity is crucial for ECM colonization and cell infiltration, which is directly influenced by size of pores too. Further, a porous interconnected architecture is necessary to allow in general molecular transport and diffusion of scaffold waste products. Scaffold degradation products have to be able to leave the body without any negative interference with another organs and surrounding tissues. The issue of degradation of core resulting from insufficient vascularization and the removal of waste from the center of scaffold, is a main tissue engineering problem (Pina et al., 2019), (Lanfer et al., 2009).

Next key component is the average pore size in the scaffold (Figs. 2 and 3). Cells primarily interact with scaffolds by chemical groups (ligands) on the surface of the material. Scaffolds that are synthesized from natural extracellular materials such as collagen naturally possess ligands in the form of Arg-Gly-Asp (RGD) that create connection with a cell, while scaffolds produced from synthetic materials could need deliberate incorporation of these ligands by way of example: protein adsorption. The density of the ligand depends on the specific surface area, i.e., the available pore surface, where cells are able to adhere. It influenced by the average pore size in the tissue engineering material. Thus, the pores must be large enough to allow the cells to migrate to a structure where they ultimately bind to ligands within the scaffold, but small enough to create a sufficiently high specific surface, resulting in a minimum of ligand density to allow effective binding of critical mass cells (O'Brien, 2011). In case of the mechanical point of view, the level of porosity is a more significant factor than pore size. Scaffolds with porosities bigger than 40% are more likely to substitute trabecular bones. While for in vitro and in vivo performances, pore size appeared more influential feature and co-existence of macropores with micropores led to better bone formation (Jodati, Yılmaz & Evis, 2020). Porosity could be regulated by some additives. Biodegradable polymer scaffolds that were prepared with a spherical porogen, as example could be soft gelatin or paraffin microspheres, were reported to exhibit greater pore interconnectivity and lower fluid flow resistance compared with a cubic NaCl porogen (Conrad & Roeder, 2020).

In every case, structure of a scaffold has an enormous effect on the mechanical properties and biological traits of the tissue, such as cell proliferation, cell migration, cell adhesion, and cell growth (Hedayati et al., 2020).

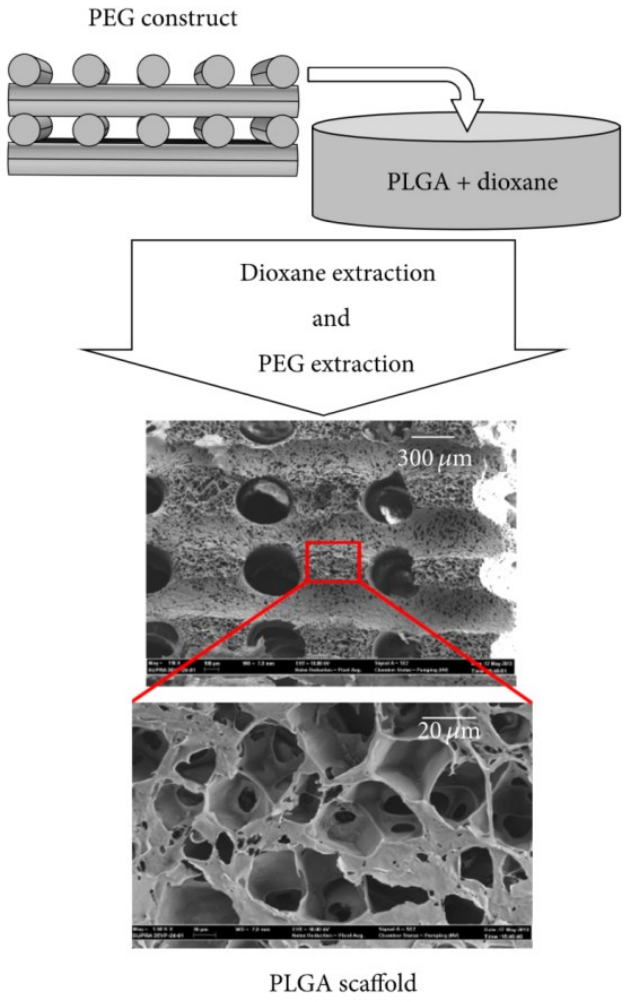

Figure 2 Hierarchy of structure (Yousefi et al., 2016).

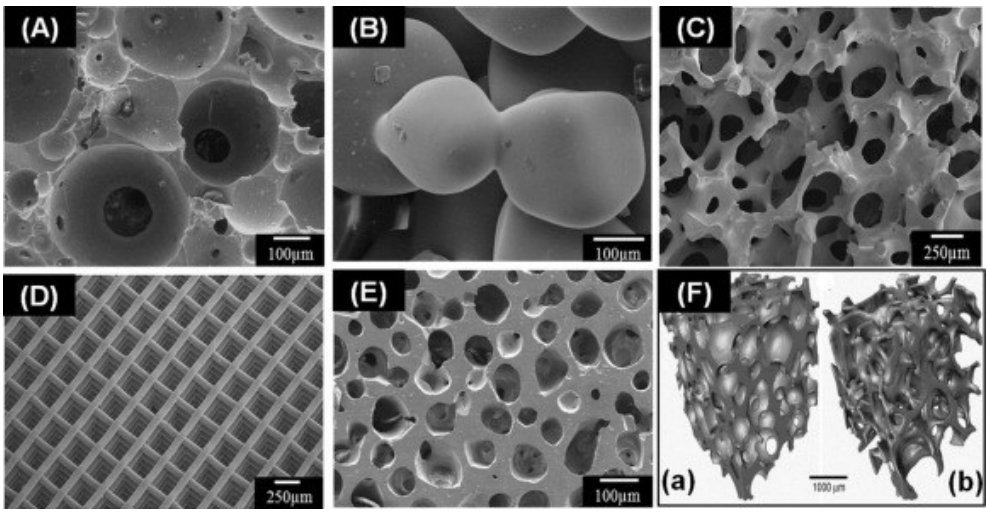

Figure 3 Different types of porosity (Owens et al., 2016).

1.5 Drug delivery

To improve the effectiveness in case of drug delivery of some new tissue formation in the biodegradable porous scaffolds, different types of growth factors such as bone morphogenetic protein 2 are often incorporated into the scaffold for local delivery. While delivered locally, the growth factors enable to help in cellular signaling processes such as migration and differentiation which can promote tissue formation. In a moment when growth factors are regularly incorporated into biodegradable system, there are ultimately limits to protein delivery, including poor delivery and protein stability in reason of protein size, and even immune responses. An alternative way may be small molecule (vitamin B, lidocaine, pilocarpine) delivery, but the incorporation of small drug molecules into porous degradable scaffolds has not been extensively studied yet. Due to the potential effective combination of therapeutic effects of a quite small molecule drug with a scaffold, there has been a rising attention in the field of development of such tissue regenerative biodegradable scaffold drug delivery systems, particularly for bone-tissue engineering applications. As example could be a case of osteosarcoma the co-administration a chemotherapeutic to treat remaining cells, along with a scaffold to repair the bone defect created from surgical tumor removal (Cyphert et al., 2020), (Mahato, 2017). In Fig. 4 is possible to see one of possible way for creating drug delivery scaffolds. Fig. 5 shows, that in case of drug delivery scaffold ibuprofen tends to spread gradually.

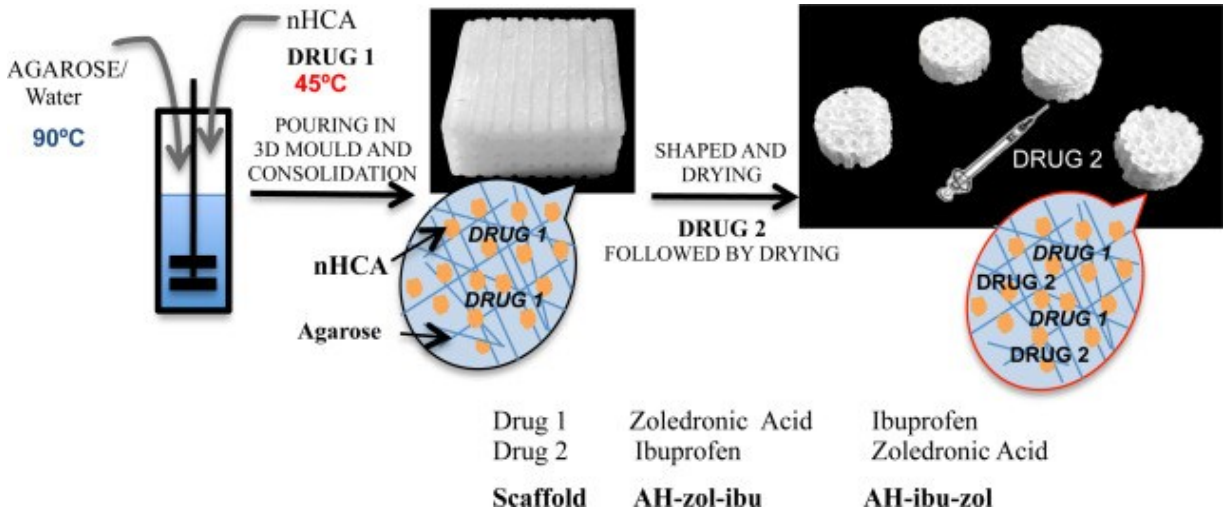

Figure 4 Creating drug delivery scaffold (Paris et al., 2015).

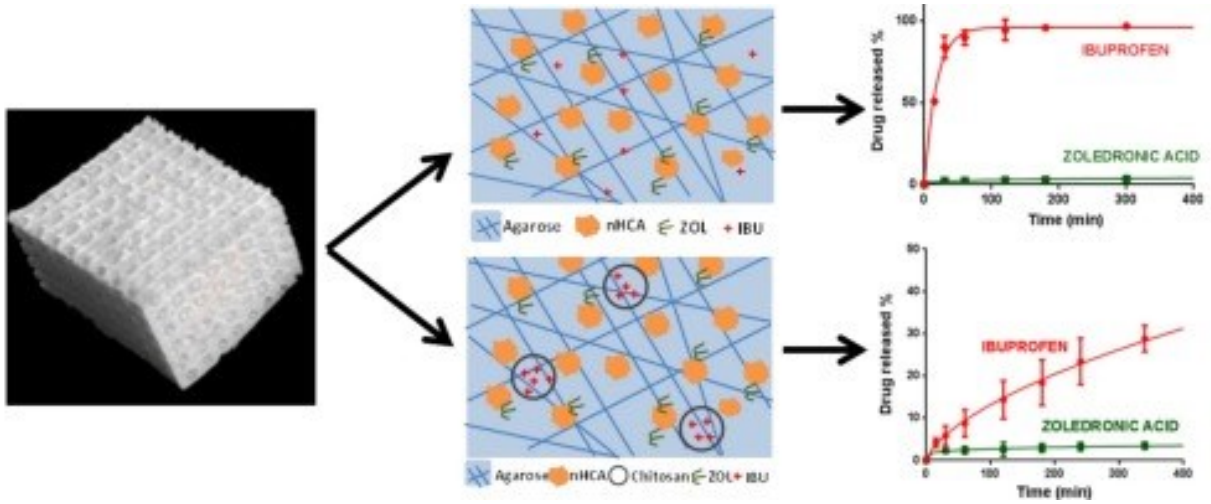

Figure 5 Efficiency of drug delivery (Paris et al., 2015).

2 SCAFFOLD APPLICATION IN DIFFERENT TYPES OF TISSUE

According to average lifespan, the human heart usually pumps nearly 200 million liters of blood delivered by approximately 3 billion heartbeats. Because of this fact that it is not some surprising information that native myocardium under this demand is quite extraordinarily complex, structurally as well as functionally (Pomeroy, et al., 2019). Nowadays myocardial infarction has become the most common heart illness in the whole Western world, in reason of heart failure, and it is becoming a leading global danger (Jin & Li, 2014).

2.1 Cardiac tissue engineering

The situation of regeneration of cardiac muscle (Fig. 6) injury is quite complicated: In case a cardiac muscle injury happens, fibroblasts tend to replace the loss of cardiomyocytes to form scar tissue, leading to arrhythmia and heart remodeling (Dong et al., 2020). Different biomimetic scaffolds and stem cells are applied in cardiac tissue engineering to support reconstruction and regeneration of the heart. As known, the cardiac muscle is an electrically active tissue that is able to conduct electrical signals and allowing the heart to work. According to previous information, the option is to use a number of conductive materials, that can be applied in cardiac tissue engineering to promote cardiomyocyte proliferation and to guide stem cell differentiation. The synergy effect of conductive materials and multipotent stem cells provides a chance to overcome myocardial infarction. One of adepts between the conductive polymers is polyaniline (PANi), it has been used in cardiac engineering and it has been shown that an ordered poly(lactic-co-glycolic acid) (PLGA) / PANi nanofiber scaffold successfully provides synchronous beating of cultured isolated cardiomyocyte clusters (Jin & Li, 2014). Growing evidence supports that cardiomyocytes are able to undergo limited self-renewal through natural processes of de-differentiation and proliferation, with ongoing attempts to potentiate these effects after myocardial injury, however, safety and efficacy of these strategies are not proven in large animals and humans yet (Pomeroy, et al., 2019).

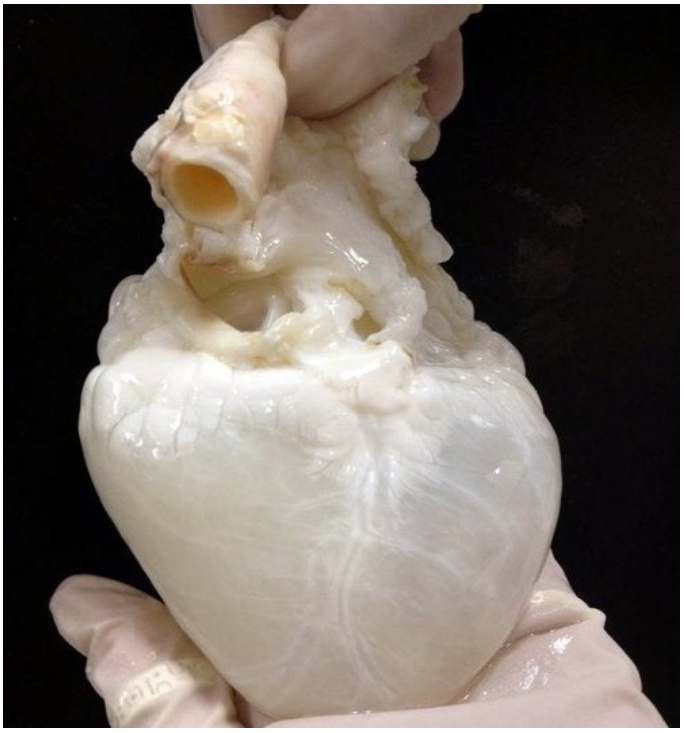

Figure 6 Cardiac tissue ("Drained of blood, the heart is white : woahdude", 2020).

2.2 Bone tissue engineering

Human bone has variety of structures (Fig. 7). Bone tissue contains cortical and cancellous part. Cortical bone has high density, showing a porosity of only 5–10%, at time of cancellous bone with a spongy-like structure, has a porosity of 50–90%. Cortical bone accounts for up to 80% of the weight of human skeleton structure while cancellous bone accounts only around 20%. Cortical bone has much higher compressive strength and Young's modulus than cancellous bone. The regeneration of a bone tissue is complicated process because it involves a number of molecular, cellular, biochemical and mechanical factors. Therefore, porous bone tissue engineering scaffolds with suitable shape, degradability, biocompatibility, porosity, pore size, mechanical properties and desirable cellular responses are needed to provoke bone regeneration. Hence, the printed bone tissue scaffolds certainly should have match mechanical properties in order to provide ample mechanical support and avoid stress shielding (Wang et al., 2020). The volume of bone fractions of the formed bone almost in all cases were comparable to selected natural cancellous bones, except the Young's moduli that were greater than the natural cancellous bones (Shi, Shui, Chen & Li, 2020). The discovery of the natural conductive properties of a bone tissue is proven by a lot of studies on bone regeneration and fracture healing with the use of an electric field. Meantime, in bone

tissue engineering, the topographical cues of bone grafts were presented to promote cell attachment, migration, proliferation and differentiation. The synergistic effect of topographic cues and electrical stimulation may decently promote elongation of osteoblasts. Also, graphene can play a role of the driving power of bone cell formation process, regardless of the underlying substrates (Jin & Li, 2014).

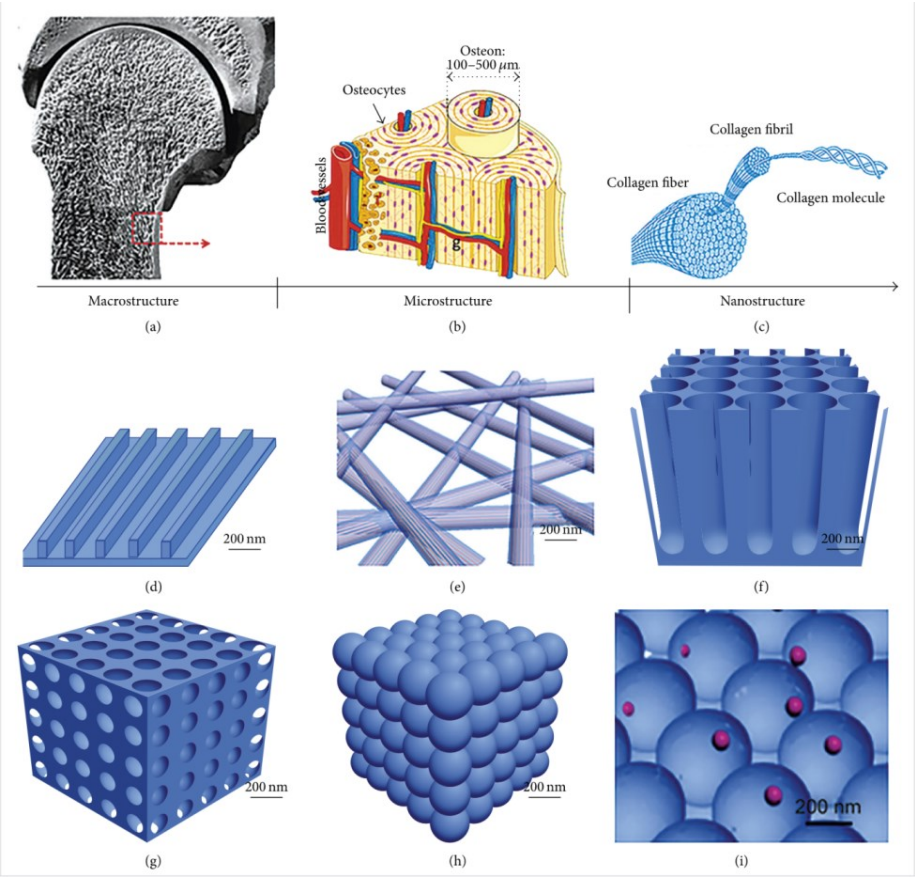

Figure 7 The microstructure and nanostructure of bone system and the nanostructured material used in bone regeneration. (a) At level of macrostucture, bone consists of a dense shell of cortical bone with porous cancellous bone at both ends. (b) Microstructure has repeating osteon units within cortical bone. The osteons consist of 20–30 concentric layers of collagen fibers, called lamellae, containing blood vessels and nerves. (c) At nanostructure level, collagen fibers (100–2000 nm) are composed of collagen fibrils. Structures of nano scale with the features of nanopattern (d), nanofibers (e), nanotubers (f), nanopores (g), nanospheres (h), nanocomposites (i) and nanocomposites with structural components with a feature size in the nanoscale (Yousefi et al., 2016).

2.3 Nerve tissue engineering

Because of a risk of the common exposure to physical injuries, peripheral nerves can easily be damaged. The most usual cases of nervous system traumas (as example could be spinal cord injury and stroke) are still neurological deficits. The autologous nerve graft is the stable standard for nerve reparation (Jin & Li, 2014). Conventional treatment usually includes an autologous nerve graft transplant at the injury site. There are, however, some limitations in gap restriction (maximum 50 mm) for autograft transplantation, donor nerve size mismatch, prolonged recovery time and formation of neuroma (Pillai et al., 2020). The usage of tissue engineered nerve grafts made from nanomaterials is an alternative way to do a nerve therapy and it has yielded unexpected results and useful possibilities. In addition, the connection was found, that electrical stimulation can positively influence the development and function of electro-active tissues, especially in a nerve tissue engineering. (Jin & Li, 2014).

2.4 Muscle tissue engineering

Muscle tissues play has a essential function in human body, comprising more than 50% of body mass and controlling force generation, body movement and internal function of organs. Muscle tissues as soft tissues are quite easy to get injured. In case of injuries when mass loss is higher than 20%, the endogenic regeneration is helpless, and fibrosis and scarring will certainly happen (Dong et al., 2020). Skeletal muscle tissue is surrounded with basement membranes containing large ECM proteins on the scale of 50–300 μm and it is made up of highly aligned fibrous bundles of muscle tissue that enable to induce muscle function. Due to their biophysical structure, one of the most major design parameters for muscle scaffolds is the duplication of the topographical shape of native myofibers (Kim et al., 2020). The scaffolds are considered as critical medical structures because they are able to directly provide a microcellular environmental condition for obtaining proper myogenesis and significantly support a high degree of muscle-tissue regeneration. Consequently, the scaffolds have to be created with micro/nanostructural cues to promote the arrangement, differentiation, and maturation of myoblasts (Yeo & Kim, 2019). A commonly known example is the uniaxially aligned microfibrils in skeletal muscles, which contain myofibers which are coated with laminin and type-IV collagen. Because of the fact that myoblasts cultured in the functional structures tend to mimic the native muscle structure — which can provide physiologically realistic cues (such as cell-to-cell interactions and biochemical and biomechanical signals) — the scaffolds should be designed in way to imitate native muscle

architecture (Kim et al., 2018). To mimic the original structure of the muscle tissue, various techniques could be used. For example such as electrospinning in order to produce nanoscale aligned fibers, micromolding to obtain an imprinted grooved pattern, wet electrospinning, and a combination of wet electrospinning and three-dimensional (3D) printing to attain microfibrous aligned bundles. Every microscale or nanoscale structure with topographically aligned cues induced a high degree of myotube formation and a myotube orientation fully ordered in the needed direction, compared with the structures with no any topographical cue (Kim, Kim & Kim, 2020). The conductive biomaterials demonstrate tendency to support skeletal and cardiac muscle tissue formation by numerous studies. Nevertheless, the principle how the conductive biomaterials regulate these specific processes is still unknown. Actually, researchers only know that the conductive materials provide a specific charge of the cells, which cannot happen in other non-conductive scaffolds. Moreover, cellular behaviors, including cell attachment, cell proliferation and protein expression, are influenced by the ion transfer and movement across the membrane due to the conducted charge-made local electrical fields inside the scaffolds (Dong et al., 2020).

3 MATERIALS FOR SCAFFOLDS

Artificial materials are usually composed of chemically manufactured polymers such as polyesters, polyethers, ceramics, and others. With the driven composition of synthetic materials, implants enable to be reproducibly processed and manufactured with a wide range of chemical and physical properties (Sadtler et al., 2019). The biodegradability and biocompatibility of synthetic polymers are partially limited compared to those of natural polymers (Bakshi et al., 2020).

Naturally based scaffolds are usually created from natural materials and biopolymers such as peptides, proteins, and sugars in many different forms. This type of scaffold can also be derived from many tissues in the body such as bladder, intestine, and cardiac tissue (Chung et al., 2017). Sometimes some additives could be bonded to scaffold. For example, the presence of such protein as keratin reduces the crystallinity and improves the thermal behavior of scaffolds (Naderi et al., 2020). However, usually materials found abundant in nature have quite low reactivity and ability to process for further applications. Naturally based polymers get great attention due to their structural similarity with biological macromolecules, it makes them easily recognized by the environment and therefore easily metabolized to residues that are nontoxic and naturally eliminated (Bakshi et al., 2020).

3.1 Natural materials

3.1.1 Collagen

Collagen (Fig.8) is the one of the most important and essential proteins in scaffold development is the selection of a initial material; usually one that is available and to some extent achieves added value when it is processed (Bazrafshan & Stylios, 2019). This protein has structure of fibrous protein that plays a significant role in tissue healing, providing the biological microenvironment for cell growth and supporting cell attachment, proliferation, and migration. At the same time, it is biocompatible, biodegradable and low immunogenic (Andonegi et al., 2020). Collagen belongs to a superfamily of at least 28 different collagen types that consist of more than 40 distinct polypeptide chains. Fibrillar collagen enable to form multiple hierarchical structures, namely collagen α-chain, tropocollagen, collagen fibril, and collagen fiber (Tian et al., 2020). The protein is usually available in the extracellular matrices of a lot of connective tissues of mammals, comprising about 25–35% of the whole-body protein contents (Bazrafshan & Stylios, 2019). Among all others types of

collagen, type I in the dentine matrix provides focal sites for calcification and its good biocompatibility with natural tissues and low antigenicity makes it a popular scaffold material among scientists and clinics. Collagen causes the organization of pre-ontoblasts and the adhesion of newly created odontoblasts to dental pulp, thus providing a framework for dentinogenesis. The evoking ability of collagen to differentiate scaffold-inoculated stem progenitor cells is significantly beneficial for tissue engineering of pulp. Collagen sponge and gel scaffolds support the proliferation of dental pulp stem cells (DPSC) and their differentiation into odontoblasts, as well as the synthesis of much harder tissues, suggesting that it is a suitable material for scaffolding construction in reconstruction of pulp-dentin (Tanasa et al., 2020). Scaffolds of collagen and hyaluronic acid with collagen could be fabricated by using 3D printing and cross-linked by dehydrothermal treatment (Bavaresco et al., 2020).

3.1.2 Chitosan

Chitosan is the only one known alkaline polysaccharide in nature, whereas others like cellulose, dextran, pectin, agar-agar, starch, etc. are either neutral or acidic. It is not toxic, odorless, biodegradable and biocompatible. It is a biocompatible material that degrades slowly to harmless products that are absorbed completely in body. A lot of researchers see chitosan as a source of potential bioactive material during the past few decades. Sadly, chitosan has several disadvantages for biological applications, such as poor solubility under physiological conditions. In order to overcome these complications, efforts have been made to derivatize chitosan by chemical modifications and hydrolysis. Nowadays, chitosan and chitin are widely used in such applications as industrial and biomedical (Bakshi et al., 2020).

3.1.3 Fibrin

Fibrin (Fig. 8) is widely applied as a natural hydrogel in field of tissue engineering. It is a natural network which is gathered by polymerization of fibrinogen; a glycoprotein presence which is normal in human blood plasma, and extremely important for wound healing and other biological phenomena. Fibrin gel could serve as a transport system for many kinds of mesenchymal cells (Seyedi et al., 2017). Due to its role in the coagulation cascade, fibrin is highly recognized as one of the strongest factors in healing of wounds. The protocol (by Dohan et al.) is a combination of natural fibrin with cytokines, growth factors and platelets not only to regenerate the soft tissue found in the pulp chamber, but in addition to repair the hard tissue that makes dentine. Scaffolds that are based on fibrin are usually used for soft

tissue engineering and dental pulp revascularization due to odontoblastic differentiation (Jazayeri et al., 2020). According to all previous facts, scaffolds from naturally structures are more suitable candidates to generate desirable tissues (Tanasa et al., 2020).

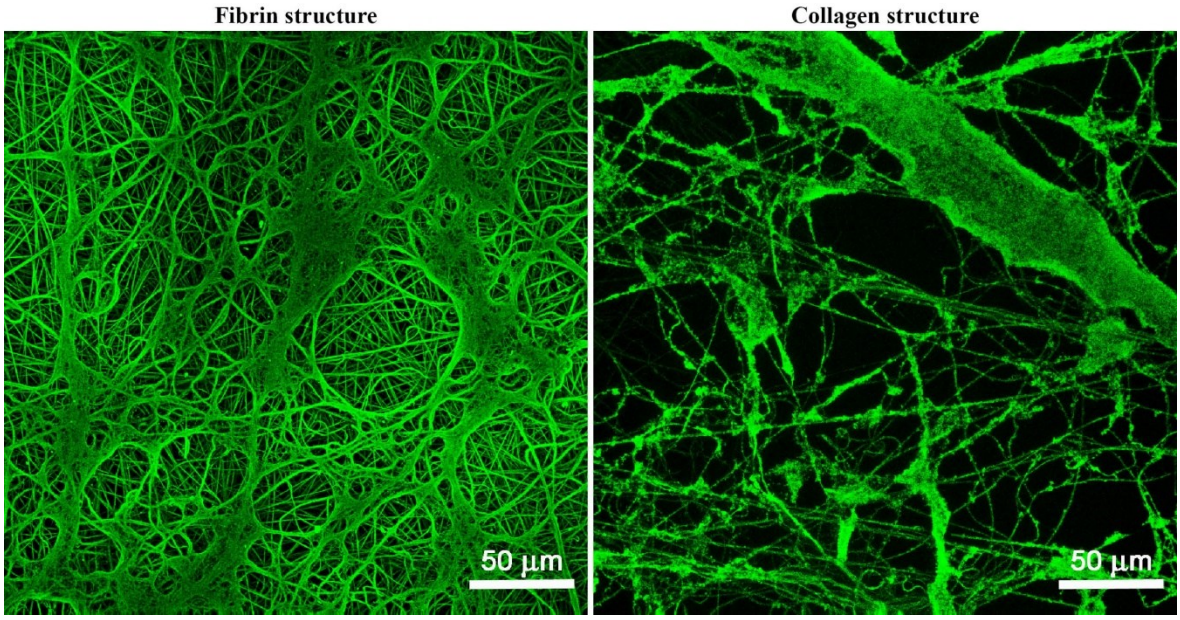

Figure 8 Fibrin and Collagen structure ("Frontiers", 2020).

3.2 Synthetic materials

3.2.1 PLA

PLA (polylactic acid) is a type of biodegradable polyester that promotes the adhesion of undifferentiated cells of dental pulp and ex vivo cells. Chandrahasa et al. made a measure of the proliferation of mature human dental pulp tissue with using three types of tissue engineered scaffolds: (1) open PLA scaffold, (2) bovine collagen scaffold, and (3) calcium phosphate bioceramic scaffolds. Their results revealed the fact that the rate of proliferation of dental pulp was influenced by the chemical composition of the scaffold, and the scaffold PLA was more optimal for scaling mature dental pulp than scaffold collagen or dicalcium phosphate. In addition, the interdependent pore structure of nanofibrous PLA scaffolds has shown successful cell proliferation and angiogenesis. In vivo and in vitro tests have shown that PLA is capable to induce DPSC differentiation into mature odontoblasts and produce both soft and hard tissue that resembles the dentine fiber histoarchitecture. Moreover, tooth slices containing polymer enabled the formation of a microvascular lattice. Due to the advantageous mechanical properties of the PLA scaffold, besides their controllable

degradation rate, PLA is a favorable candidate for tissue engineering of pulp (Jazayeri et al., 2020).

3.2.2 PCL

PCL (polycaprolactone) (Fig. 9) is a biocompatible and biodegradable plus decent elastic polymer with a low degradation rate when used alone, or in a composition of polymers when it is used to modify the brittle polymers such PLA. In case of using blend of polyurea, poly-(serinol hexamethylene urea), and PCL with different ratios for the production of artificial vessels, the results of mechanical tests proved that with increasing the amount of PCL in the electrospinning solution, the elasticity of the scaffold starts to be close to the mammalian arteries. By adding a certain amount of PCL to scaffolds with polyurethane base, is possible to dramatically improve its mechanical properties and increase porosity and cyclic performance (Nejad et al., 2020).

3.2.3 PGA

PGA (polyglycolic acid) is another type of PLA-like biochemical polymer that can be next biocompatible scaffold for tissue engineering of pulp. According to in vitro studies, the PGA composite skeleton can achieve a cell density that corresponds to that of native dental pulp. Buurma et al. had results proving that transplanted human pulp fibroblasts and human gingival fibroblasts synthesized not only the extracellular matrix in the PGA construct, but a vascularized network in vivo too. PGA is various in its application in bioengineering field of dental tissues, including whole crown regeneration. Experimental implants with PGA inoculated with odontogenic cells according to radiographic examinations produced highly mineralized dentine tissue and histological staining further revealed pulp tissue and formation of root mantle epithelium, demonstrating successful pulp regeneration using PGA-based constructions (Jazayeri et al., 2020).

3.2.4 PVDF

PVDF (polyvinylidene fluoride) is a polycrystalline polymer with four crystal forms of α, β, γ and δ. Among them, α crystal is the easiest one to obtain, but it does not exhibit piezoelectricity. Only β form crystal has acceptable piezoelectricity. So, because of that increasing the concentration of β phase in polyvinylidene fluoride is one of the most important ways to improve the piezoelectric performance (Chen et al., 2020). In medical field, PVDF is one of the most widely-investigated piezoelectric polymers for tissue

engineering scaffolds to self-power generators. That is owing to its highest piezoelectric properties and optimal biocompatibility. PVDF and its copolymers have shown better nerve regeneration effect in both peripheral nervous system and central nervous system (Cheng et al., 2020).

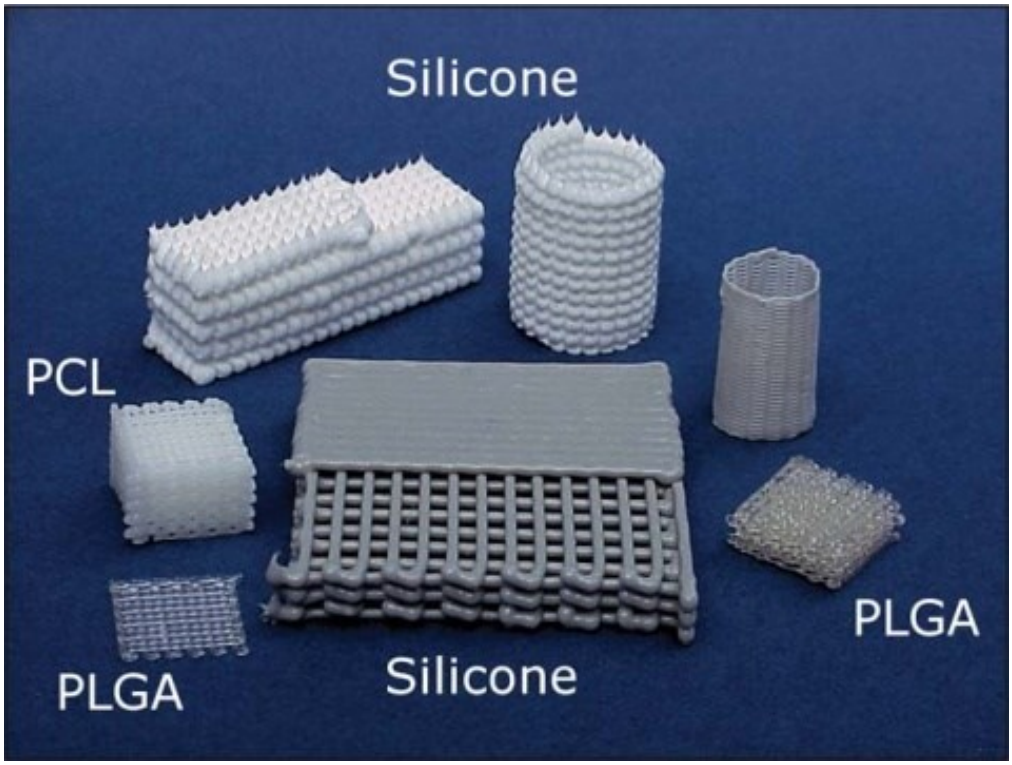

Figure 9 Different types of synthetic polymers (Waterman, 2020).

3.3 Thermoplastic elastomers

The development of thermoplastic elastomers (TPE's) started in the early 1960's and bridged the gap separating elastomers and thermoplastics. (Seymour & Kauffman, 1992). Thermoplastic elastomers are in a class of materials in which a thermoplastic is combined with elastomer particles. TPE composites have advantage of constituents and their behavior changes with their volume fractions. Hence, their properties can be modified according to the desired application. (Parenteau et al., 2014).

Consisting of an elastic matrix that is physically cross-linked by plastic domains, thermoplastic elastomers have properties as any other rubbery materials that are suitable for fabrication with plastic processing techniques. Using high throughput techniques, such as injecting molding and melt extrusion, TPE products could be manufactured in large volumes with quite short production cycles. It is possible to distinguish TPE according to chemical composition and morphology, there are six groups of commercially available TPEs: (1)

styrenic block copolymers, (2) thermoplastic polyurethanes, (3) polyamide-based thermoplastic elastomers, (4) polyetherester-based thermoplastic elastomers, (5) rubbery-polyolefin blends, and (6) dynamically vulcanized polymer blends (Wang et al., 2019). These days, elastic, extensible, and flexible thermoplastic elastomers are essential components in a variety of high technologies that range from aerospace/automotive parts, stretchable electronics, wearable sensors, biomedical devices, to artificial organs (Koo et al., 2020).

4 MAGNETIC SCAFFOLDS

Some physical stimulation, such as tensile and compressive stresses, fluid shear stresses and heat, are known to be able to distinctly enhance bone regeneration and fracture-healing. Moreover, magnetic stimulation from static magnetic fields and electromagnetic fields enable also significantly improve bone repair and regeneration. Magnetic Nanoparticles with magnetic behavior have great potential for bone tissue engineering applications. Used alone, or in combination with a magnetic field, magnetic nanoparticles can be useful in modification and improving the three key factors in bone regeneration: (1) stem cells, (2) scaffolds, and (3) growth factors. Magnetic fields influences the ion channels and cell biochemical pathways (Xia et al., 2018). The activity of magnetic field can turn on sensitive receptors on cell surface and then induce related signaling pathways to enhance cell activity. Magnetic fields, pulsed electromagnetic fields (EMFs), rotating magnetic fields and alternating electromagnetic fields can help with the integration of implants with host tissues, increase the mineral density of newly-formed bone by upper calcium content and improve defect healing (Xia et al., 2018), (Shuai et al., 2020).

Nowadays, the use of superparamagnetic scaffolds to provide mechanical stimulation by external EMF has attracted quite intensive interest. The presence of superparamagnetic nanoparticles (NP) in system changes some mechanical properties of organic scaffolds by manipulating the compressive strength and the modulus of elasticity. Superparamagnetic nanoparticles become magnetized when they are exposed to magnetic fields, in case these fields alternate, such as EMF, making them to rotate and vibrate. When supermagnetic NPs are inside scaffold, these rotational and vibrational forces induce mechanical changes in the scaffold and anything attached thereto, such as cells. Enchanted mechanical properties in three-dimensional scaffolds, in particular elastic modulus values, were shown to promote osteogenic differentiation of mesenchymal stem cells (MSC). Nanocomposite scaffolds based on polymers filled with magnetic particles have an application in drug delivery systems. Lately, the use of superparamagnetic scaffolds Fe_3O_4 and standard EMF has been designed to promote bone formation. Mentioned method uses the combination of two separate stimuli on cells: mechanical, through the vibrational movement of the scaffold when the cells are attached, in moment EMF can change the transmembrane potential by regulating different ion channels and transporters. There is serious evidence supporting the functional role of the transmembrane potential in regulating the proliferation and differentiation of MSC (Aldebs et al., 2020).

4.1 CHARACTERISTICS OF MAGNETIC PARTICLES

When designing particles to control magnetic particles, seven properties need to be considered. When assessing or designing different magnetic particles for a specific purpose, the full spectrum of characteristics has to be considered together because no single characteristic is much important than any other, and to a large extent these characteristics or properties are directly or indirectly related. In terms of material development, disregarding the links between material properties can have a very strong effect on defect pattern creation, even to the extent that the pattern is created at all. During comparing or evaluating magnetic particles, it is relatively easy to be influenced by the fluorescent brilliance of materials. Such comparisons require great care to be sure that the test pieces reflect the work to be performed accurately and to take into account the nature of the magnetic field used. It is also important to consider the effect of material transfer from the laboratory environment to the fabrication process. Some materials can provide marvelous results in the laboratory, but have proven to be complicated to use in manufacturing for some reasons (Lovejoy, 1993). According to Lovejoy, the seven characteristics considered are:

(a) particle size

(b) particle shape

(c) particle density

(d) particle mobility

(e) particle durability

(f) ease of visibility

(g) magnetic properties of the particles

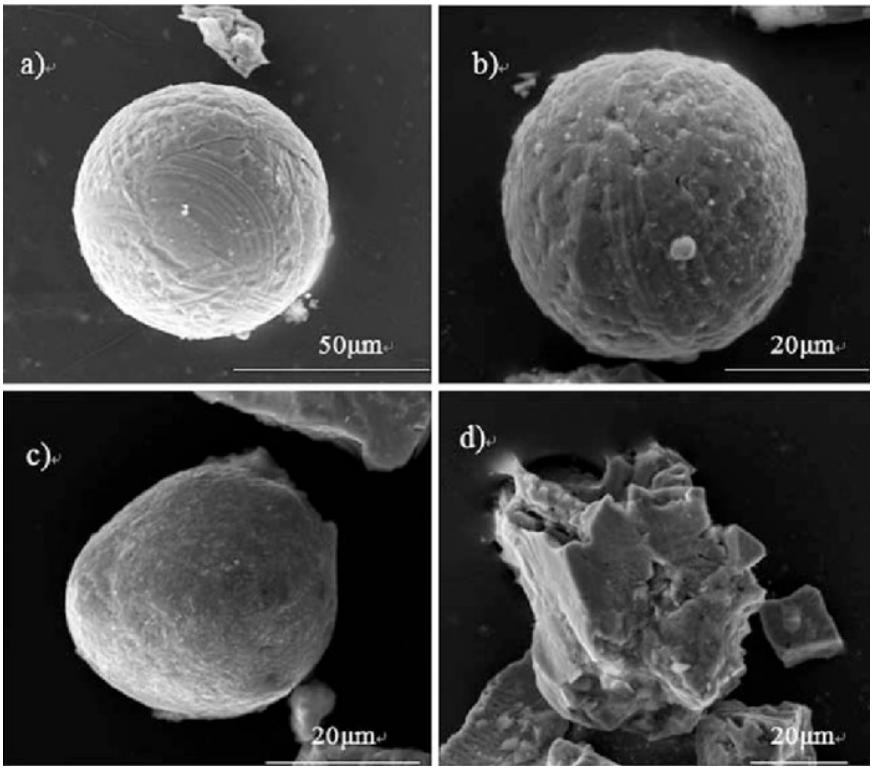

Figure 10 Representative SEM micrographs of magnetic particles. a) Only iron oxide identified, b) Strongly magnetic Fespherule with 'orange-peel' structure and adhered smaller particles on the surface, c) Pear-shaped spherule containing Cd, d) Zr-rich meltedlike irregular particle (Yang, Liu, Chan & Liu, 2007).

Particles (Fig. 10) with magnetic behavior for bioseparation are made of one or more magnetic cores. In general, the magnetic core consists either of maghemite (gamma Fe_2O_3) or magnetite (Fe_3O_4) with superparamagnetic or ferromagnetic properties (http://www.kapelan-media.com, 2020). The reason is that they are biocompatible, show low toxicity, and easy in separation (Liu et al., 2019). As coating matrix of polymers can be silica or hydroxylapatite with terminal functionalized groups (http://www.kapelan-media.com, 2020). In general, magnetic particles in nanoscale (<100 nm at least in one direction) and microscale (1–50 μm) are the most popular MPs used in forensic science (Liu et al., 2019). Carbonyl iron powder (CIP) is one of the most commonly using magnetic particle. CIP is a highly pure iron, that is a metallic magnetic material, it is widely used in sensor applications. Spherical CIP particles which have carbonyl surface functionality and an average particle size is about 5 μm. In comparison to other conductive nano-fillers, CIP can be arranged in a chain structure easily under magnetization (Jang et al., 2020), (Burgaz & Goksuzoglu, 2020).

Superparamagnetism is a case when a single-domain particle has the dipole moment that fluctuates rapidly in the core in reason of the thermal excitation so that there is no magnetic moment for time in macroscopic scale. Thus, these particles are non-magnetic while an external magnetic field is applied but do develop a mean magnetic moment in an external magnetic field. In contrast, ferromagnetism means that the particle has a permanent magnetic moment. So, the biggest effective magnetic anisotropy suppresses the motion of the core-moments activated by thermic signal. The strong point of the superparamagnetic particles is a possibility of easy resuspension, slow sedimentation, large surface area and in addition uniform distribution of the particles in the suspension media. After magnetization, the particles gain behavior just like small permanent magnets, so that they form aggregates or lattice due to magnetic interaction. Main advantages of particles with ferromagnetic behavior are decently strong magnetic properties and therefore the quite fast separation with an external magnetic field even in case of viscous media (http://www.kapelan-media.com, 2020).

Nowadays, the properties of magnetic nanoparticles could have important role in the traditional medical sector because of the possibility of treating the degenerative diseases such type as cancer. Here is possibility to increase contrast for magnetic resonance imaging and control drug release. Nanoparticles have to be at least in one dimension between 10 and 100 nm large. Biocompatible magnetic materials could be used as a potential treatment option for malign tumors. In recent times, a number of studies have been reported the development of fully safe materials, such as magnetic calcium phosphate ceramics and bioactive glass ceramics (Tanasa, 2020).

5 FABRICATION OF THE SCAFFOLDS

3D printing was developed in late 19th century, while such technologies as photosculpture and geomorphology technologies were developed. (Wang et al., 2020). 3D printing or additive manufacturing is a process of connecting materials to make products from 3D model data, according to principle of layer-by-layer, as opposed to subtractive manufacturing methodologies. 3D printing is a versatile technique (Fig. 11), that allows to fabricate a variety types of materials such as polymers, metals, ceramics and composite systems, with possibility to customize shapes and dense or macro/micro porous architecture (Ronca, 2017). Methods of 3D printing have been divided into bioprinting of cellularized constructs, such as laser-assisted bioprinting, inkjet-based, extrusion-based, and a cellular method, such as solid free-form production, powder-fusion printing, and stereolithography. 3D-printed structures can provide structural and mechanical support and a sufficient nutrient supply space for cell migration and growth. Although 3D printing is capable to hardly print a scaffold with nano-scale structures, hence mentioned technologies emphasize its capability to achieve scaffolds in various scales at different areas by combining all other manufacture techniques (Zhao et al., 2017). In addition, additive manufacturing provides a proper approach to fabricate biodegradable tissue-engineered scaffolds with controllable macro/microarchitectures which strongly influences the mechanical and biological properties of the resultant scaffolds (Meng et al., 2020). The application of 3D printed objects is wide in many industries such as manufacturing of turbine blade, jewelry designing, building, tissue engineering, etc. (Ronca, 2017).

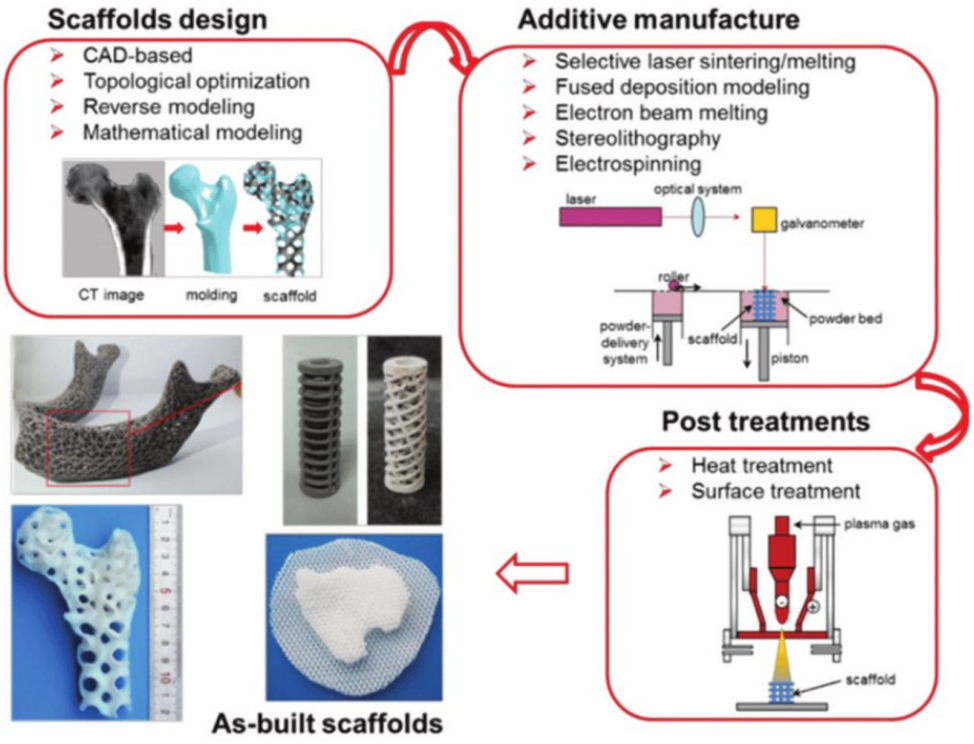

Figure 11 A schematic diagram for the design, additive manufacturing (AM), post-treatments of bone scaffolds, and several typical AM-derived scaffolds (Yang et al., 2018).

5.1 Printing methods

5.1.1 Stereolithography

The method that is called stereolithography is considered to be one of the most universal technique providing the highest precision of a final 3D structure. The main principle of stereolithography is based on spatially controlled solidification of the liquid photo-polymerizable resin. Materials as polymers or composites are often used for tissue engineering applications due to their low cost, production and mechanical properties. However, their surface properties often do not meet the wettability and biocompatibility requirements for cell adhesion and proliferation (Ronca, 2017).

5.1.2 Injection molding

Nowadays the method called injection molding is a commonly adopted technique for fabricating polymer-based products and scaffolds due to its high productivity, design flexibility, and quite low cost. Lately, molding techniques have been combined with some other methods. As an example can be gas foaming technique, to obtain a 3D porous structure

and pores with interconnected structure for scaffolds. A lot of researchers have proposed the injection molding technique to produce biodegradable polymeric scaffolds due to injection molding technique does not need organic solvents. Organic solvents are usually dangerous for cell differentiation and tissue growth. In general, some additives, such as chemical or physical blowing agents, have been added to the polymers to gain scaffolds with interconnected pores (Zhao et al., 2017).

5.1.3 Microcellular injection molding

Microcellular injection molding is another popular technique to for production of scaffolds in reason of its high productivity, flexibility of design, and quite low price. Kramschuster and Turng combined particulate leaching and microcellular injection molding method to create scaffolds with interconnected pores. In previous work, polylactic acid, salt particles, and water-soluble polymer polyvinyl alcohol as particles were mixed by a twin-screw extruder, and then injection-molded by microcellular injection molding. Interconnectivity was attained by the co-continuous blending morphology of the biodegradable PLA matrix with the water-soluble polymer polyvinyl alcohol and the pore size in the scaffolds was under control due to salt particles. However, in the melt blending process, particles of NaCl have a tendency to break easily (Zhao et al., 2017).

5.1.4 Solvent-quenching and salt-leaching technique

In case of solvent-quenching method, the polymer is first dissolved in a solvent with a high freezing point and the polymer or solvent solution immediately gains frozen form at various temperature values (e.g., −20 °C, −80 °C, or in liquid nitrogen) before lyophilization process. The created pores inside the sponges is the result of a rapid freezing of the solvent in the polymer, forming small voids of frozen solvent which are subsequently sublimated from the polymer during lyophilization. In this method, the size of the pores depends on adjusting the freezing temperature point. For the salt-leaching method, sieved sodium chloride (NaCl) crystals are added to a dissolved polymer solution and then are leached out in water once the polymer solution solidifies. The amount and size of the pores in the sponge can be manipulated with adjusted by altering the diameter and amount of salt crystals used in production. In short, solvent-quenching and salt-leaching are universal methods that are able to provide fine-tune control over the porosity of a biodegradable polymeric sponge or scaffold (Cyphert et al., 2020).

5.2 Electrospinning technique

Since the last few decades, electrospinning (Figs. 12, 13) has emerged as an essential tool for the production of 3D nanofibers scaffold with fiber diameters in the nm to μm scale. Probably, nowadays it is one of the most studied method for the scaffold formation (Haider et al., 2020) Electrospun nanofibers are commonly applied in various products such as wound dressing, sensors, drug delivery, filters and membranes and others. This is due to their extraordinary and promising features including high surface-to-volume ratio, tunable porosity and three-dimensional interconnected pore structure (Ranjbari, Bazgir & Shirazi, 2020). The crucial advance of electrospun fiber is high aspect ratio that makes it suitable for many potential applications in various fields. For example tissue engineering, drug delivery, biomedical, textiles, filtration, electronic devices, solar cells, filtration, sensors, energy storage, catalysis, and environmental applications (Sarwar et al., 2019), (Jin & Li, 2014).

Originally, it was considered as a method to design and produce scaffolds for tissue engineering (TE) applications. In many cases, non-woven nettings of sub-micrometer diameter fibers, which look like the fibrils found in native extracellular matrix (ECM), are collected. Nevertheless, the small size of pores associated with the random layering of sub-micrometer diameter fibers is a basic complication for solution electrospun nettings, which are able to act such as a barrier to cell infiltration. In case of randomly located fibers, diameter of fibers has to be at least 4 μm for designing and production a scaffold with a pore size of at least 20 μm in order to promote cell invasion and made this type of scaffolds dynamic structures with at least minimal capacity for maintaining the passive transport of nutrients and waste throughout these microstructures (Brown et al., 2011), (Kajbafzadeh et al., 2014). This limiting matter can be attributed to the natural behavior of the solution during electrospinning process. As the polymer solution is drawn into a jet by electrostatic force, following an initially straight stable zone, bending instabilities amplify in a secondary zone along the flight path of the charged jet. Though this outcome in superfine fibers, it causes a quite big area of collection with chaotic deposition. As a consequence, solution electrospun meshes are most of the time thin and their gathering is random. In cases when some of these techniques gives reasonably ordered structures, charge accumulation effects on solution electrospun fibers has a tendency to restrict the amount of layers which can be collected and remain bound as one coherent structure. One technique to manage better the control over the location of electrospun fiber deposition is to operate in the region of the jet where the flight

way is direct. As other possibility, generally, polymer melts with higher viscosities and lower conductivities in comparison to polymer solutions, enable be electrostatically drawn over quite large distances when maintaining a straight jet path. More powerful disturbance forces are needed to overcome the surface tension in these jets, resulting in extended regions of stability up to many centimeters in length. Ultimately the melt electrospun fibers tend to have larger geometry than the solution electrospun fibers, although there are some exceptions to this rule (Brown et al., 2011).

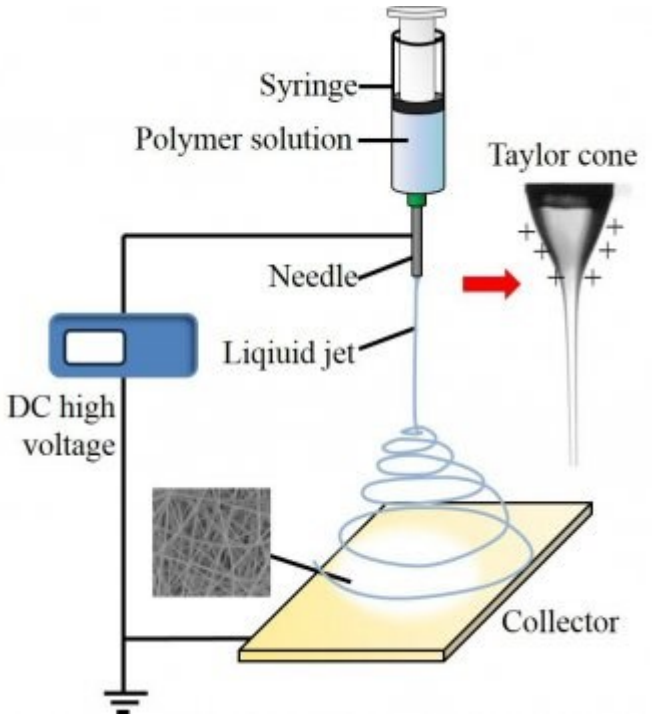

Figure 12 The constuction of electrospinning ("Electrospinning Technique", 2020)

Electrospinning can offer a relatively cost-effective way to fabricate nanofiber scaffolds from various materials. PCL, poly (lactic acid) (PLA), poly (glycolic acid) (PGA), poly (lactic-glycolic acid) (PLGA) and poly (lactic-caprolactone) (PLCL) are the most requisite raw materials due to their simplicity of fabrication, mechanical properties are stable and biocompatibility is good enough (Saadatmand et al., 2019). Polyamide nanofibers showed excellent biocompatibility with several human cells and tissues in reason of similar collagen content of the ECM and active groups (Kajbafzadeh et al., 2014). Natural polymers such type as collagen, gelatin, chitosan and also silk fibroin can also be spun into a form of nanofiber scaffolds (Saadatmand et al., 2019).

In field of applying electrospinned nanofibers in wound dressings and generally in regenerative medicine, therapeutic agents are often incorporated into nanofibers with controlled release. In ideal case wound dressings should have some various goals: combating acute or chronic infection; maintaining a balanced moisture and gas exchange environment; absorption of extrudates and coiled blood; and support cell proliferation and migration and thus wound healing (Saadatmand et al., 2019), (Kajbafzadeh et al., 2014). As the best variant of process, nanofiber formulations for drug delivery to patients should be controlled spatially as well as temporally. Nanofibers are generally controlled in dosage form by local route of administration. Drug release takes place only at the target site, thus avoiding systematic drug exposure. Space control of drug delivery can be easily made by inserting electrospinned nanofibres in place by invasive or non-invasive means. In previous studies, time control of drug release was mostly specified by drug diffusion rate, drug desorption rate, drug dissolution rate, fiber diameter (diffusion barrier length) and polymer degradation. Recent efforts have been devoted to the development of activation and feedback factors of electrospinned nanofibers in order to start the release or control the rate of drug release over time. This type of nanofibres is also called intelligent electrospun nanofibers (Saadatmand et al., 2019). In addition, the one dimensional zinc oxide (ZnO) nanofibers have been fabricated through the sol–gel processing and electrospinning technology could be efficient against Staphylococcus aureus bacteria (Thangavel et al., 2020).

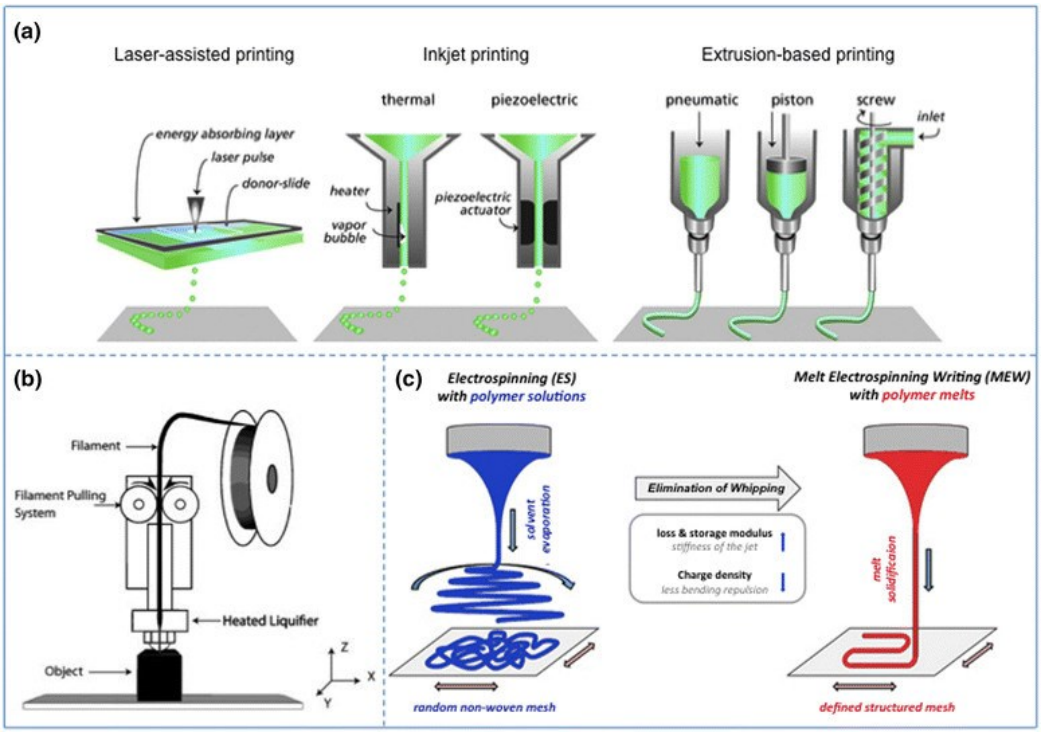

Figure 13 Various types of fabrication (Carter et al., 2016).

5.3 Melt-electrowriting technique

A relative new method in 3D printing field is melt electrowriting (MEW) (Fig. 13), invented in 2011 by Professor Paul Dalton and Professor Dietmar Hutmacher. MEW utilizes an electric field uniquely combined with additive manufacturing AM technology for the controlled deposition of polymer in a molten jet form, which rapidly solidifies into a fiber. These submicron fibers can be permanently folded, resulting in the ability to directly write complex and multi-scaled architectures and structures and overcome the complications of other additive manufacturing technologies (Catt, 2020).

The main principle underlying controlled direct writing with electrified polymer jets was established by Sir Geoffrey Taylor in his seminal 1969 paper on electrically-charged jets. To distinguish “electrowriting” and “electrospinning”, a distinct starting point to electrospinning is clearly needed for describing the technique. It is well-known that a non-electrostatically charged falling fluid breaks into droplets – for example water flow when a tap is opened. Well-known is that the location of these instabilities directly depends on the flow rate of the column of fluid, and the height at which this non-charged fluid is falling from. For a solution of polymer falling in a form like a column, the flow rate that is needed before instabilities is much lower. Nevertheless, prior to instabilities, this fluid can be direct-written onto a moving collector (Dalton, 2017).

A melted polymer just needs suitable cooling to solidify during direct-writing. This happens after the melted jet touching the collector. This process is widely influenced by the processing parameters, and there is a slight embossing on the underneath of range of MEW type scaffolds from the collector. Moreover, electrohydrodynamic quenching occurs during melt electrospinning and then the movement of charged water vapor causes a cooling effect over the jet (Dalton, 2017).

The main difference between electrospinning and electrowriting (Fig. 14) is effectively the magnitude of applied voltage, the physical effect that is established is vastly another. Instead of sub-micron diameter electrospun fibers are created due to whipping process, they are achieved in electrowriting because of lowering of the fluid flow rate and sustaining this with the use of an applied voltage (Dalton, 2017).

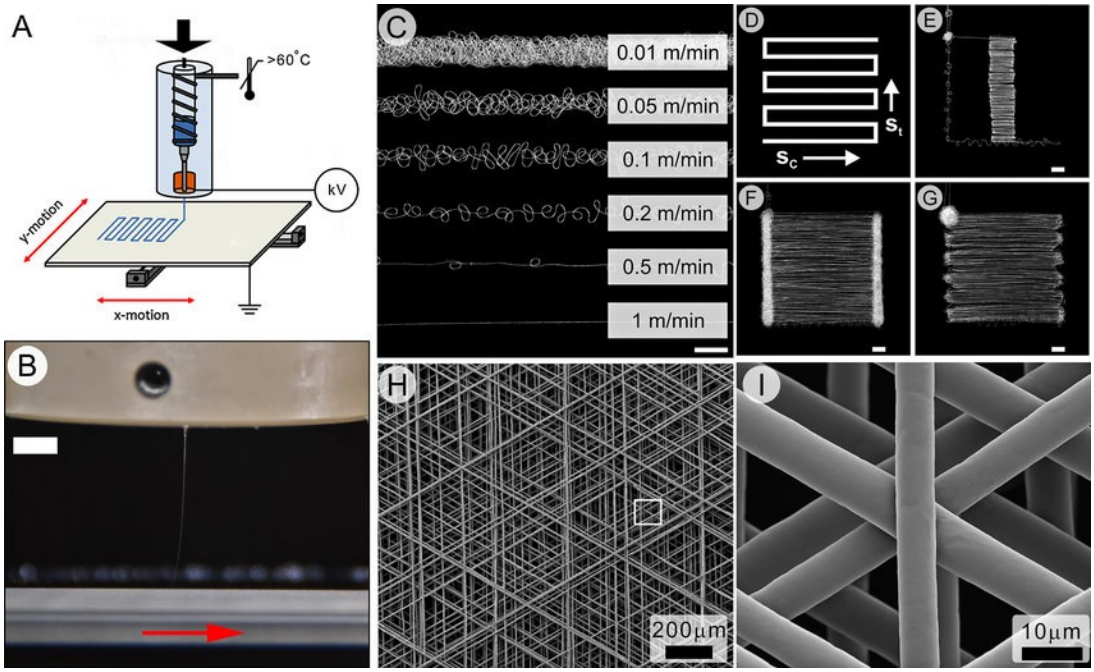

Figure 14 Schematic demonstrating melt electrospinning direct writing and (Brown, Dalton & Hutmacher, 2016).

II. ANALYSIS

6 MAIN AIMS OF THE MASTER'S THESIS

The main aim of this thesis was focused on the fabrication of active scaffolds with potentinal application in medicine. Following steps were planned to be performed.

- Preparation of the magnetic/elastomer composite masterbatches
- Caloremetric, rheological and viscoelastic characterization of prepared masterbatches
- Fabrication of the magnetic scaffolds using melt-electrowriting
- Characterization of scaffolds using optical and scanning electron microscopies
- The proof of suitability of fabricated scaffolds for medical application

7 MATERIALS AND METHODS

The content of the experimental part is made in such a way as to achieve the goals set work.

7.1 Materials

Carbonyl Iron Powder SQ BASF

Table 1 Basic properties of CIP.

Material	Density (g/cm3)	Type	Fe min. (%)	C min. (%)	Particle Size Distribution (microns)
Carbonyl Iron Powder SQ BASF	7.86	Hard	99.5	0.05	3.9-5.0

Vistamaxx 6202 ExxonMobile

Table 2 Basic properties of Vistamaxx 6202.

Material	Density (g/cm3)	Melt index (g/10min)	Ethylene Content (wt%)
Vistamaxx 6202 ExxonMobile	0.862	9.1	15

7.2 Masterbatches preparation

Samples were made by mixing of Vistamaxx (Tab. 1) matrix and Carbonyl Iron Powder (CIP) (Tab. 2) using Microcompounder (Xplore, MC 15 HT, The Netherlands). At first granules of Vistamaxx were inserted to microcompounder with volume capacity 15 cm^3, dynamically melted at 100 °C about 3 minutes and then the CIP of various volume content (0%, 5%, 10%, 30%, 50%) was added. Velocity of the screws was 50 rpm for 5 minutes after the addition v CIP. Prepared masterbatches and their composition is summarized in the Tab. 3.

Table 3 Composition of the prepared masterbatches.

Masterbatches code (vol. %)	Vistamaxx (g)	CIP (g)
0%	12.98	0
5%	12.33	5.98
10%	11.68	11.79
30%	9.08	35.37
50%	6.49	58.95

7.3 Scaffold preparation

Melt electrospinning

MEW scaffolds were fabricated with a custom-built printer as described in previous studies (Fig. 15) (Blum et al., 2019), (Hrynevich et al., 2018). The scaffold production was performed upon following conditions; distance between platform and jet was 3.3 mm, temperature was held at 190 °C, and pressure ensuring the material motion from the nozzle was set to 2.0 bar, voltage was established to constant value 2.8 kV. Box-pore 5-layered scaffolds with CIP amount 0%, 5%, 30% and 50% have surface area 4 mm^2 with 2 mm side and 200 mm distance between individual printed fibers. Collector speed has velocity of 320 mm/min. Scaffolds 10% was not performed, due to the limited access to laboratories from 15th March to 10th May in the COVID-19 period.

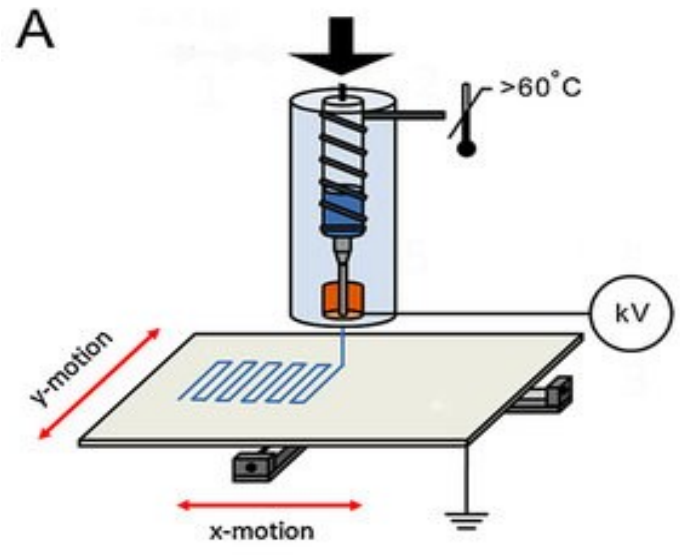

Figure 15 The melt electrospinning scheme.

7.4 Masterbatch characterization

7.4.1 DSC

The experiment was carried out by Differential Scanning Calorimetry (DSC 1, Star System, Mettler Toledo)in temperature range from -75 °C to 225 °C with heating rate was 10 °C/min. The suitable sample weight was between 6.2 and 7.9 mg. The main goal was to obtain dependence heat flow on temperature.

7.4.2 Rheological properties

In order to investigate the viscoelastic properties of samples rotational instrument: Rotational Rheometer (Anton Paar, MCR 502, Austria) with parallel plate geometry PP10, the upper plate with 10 mm in diameter. Constant temperature was achieved using Peltier cell (Anton Paar, MCR 502, Austria) was used. The testing was performed on the melted samples. At first, the linear viscoelastic range was established as is shown in the following part then it was measured dependence of storage and loss moduli on the frequency, to properly see the mechanical performance of the prepared samples as well as further effect of the CIP addition to the Vistamaxx. The investigated frequency range was (0-10 Hz). Measurements were carried out at three different temperatures – 150° C, 170° C and 190° C.

For every sample was determinated dependence of storage modulus and loss modulus on strain and also storage modulus and loss modulus at frequency. In addition, the dependence of tanδ and complex viscosity on frequency was measured too.

7.4.3 Viscoelastical properties

The experiment was carried out by Rotational Rheometer (Anton Paar, MCR 502, Austria) with parallel plate geometry PP10, the upper plate with 10 mm in diameter. Constant temperature was achieved using Peltier cell (Anton Paar, MCR 502, Austria) in temperature range from 0-80 °C in order to obtain the dependence storage and loss moduli on temperature and the dependence complex viscosity on temperature.

7.4.4 DMA

The experiment was carried out by Dynamic Mechanical Analysis (DMA 1, Mettler Toledo) in temperature range from -100 °C to 150 °C with frequency 1 Hz. The main goal was to obtain dependence storage modulus on temperature and tan δ on temperature too.

7.5 Scaffold characterization

7.5.1 Microscopy (optical and SEM+EDX)

Optical microscopy is able to provide possibility to optically explore the structure and texture of prepared material and structure of 3D printed samples. For the exploring, Optical microscope (Leica DVM2500 Digital Camera) was used. In case of SEM this method allows observing a dispersity of CIP in Vistamaxx and find out accurate content of iron in every sample. For this goal Scanning Electron Microscope with EDX (VEGA 2 LMU, TESCAN) was used. Images were acquired in the backscattered electrons (BSE) and the secondary electron (SE) modes. All samples were dried and coated by Au/Pd powder prior to the insertion to SEM microscope. The surface of samples was investigated in order to see the structural properties of the prepared masterbatches and how the structure is affected by presence of the Carbonyl Iron Powder.

7.5.2 Magnetic activity of fabricated scaffolds

Due to changing magnetic field samples enable to be tested for suitable CIP particles amount. In case of needed positive response to magnetic field, sample could be chosen as base for future scaffold. For the scaffolds motion capture, camera (Xiaomi Redmi Note 5) was used. As Figure 64 shows, at the start (2-10 V) magnetic field has quite linear running but after 10 V it has a slower growth. To measure magnetic field Teslameter (FH 51, MAGNET-PHYSIK) was used.

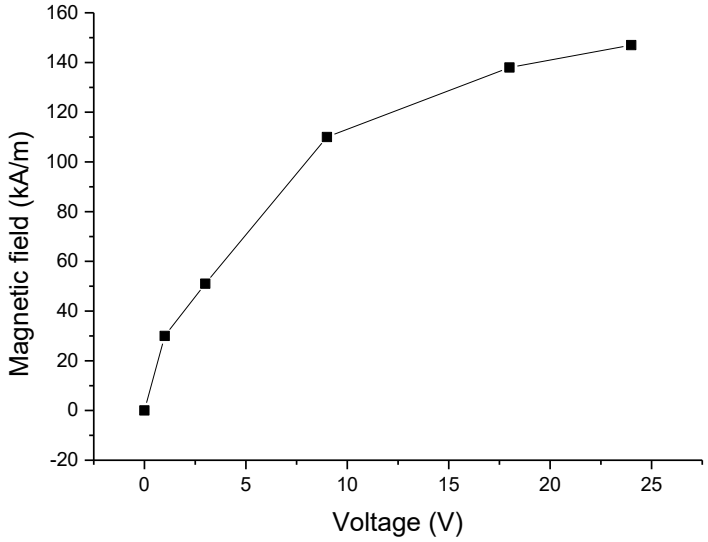

Figure 16 The dependence electric field on voltage.

7.5.3 Cytotoxicity

Cultivation and trypsinization

Cultivation - the technique for increasing cell count.

Trypsinization is the technique for separating the cells from a material.

After confluence, cells were inspected due to microscope and transported to a laminar box. A medium was aspirated from the culture vessel (T75) so as not to damage the cells. The cells were rinsed with 0.2 ml/cm^2 of phosphate buffer (PBS), equivalent to 15 ml, from the media, and then the buffer was aspirated. Additionally, 0.1 ml/cm^2 of trypsin corresponding to 7.5 ml was added to incubate the incubator for 15-20 minutes to break the cell-tocell binding. The release of the cells was continuously checked due to a microscope. After discontinuation of the batch, 7.5 ml of medium was added to the flask and the solution was pipetted into a tube and placed in a centrifuge which had been pre-heated to 37 °C. During centrifugation, which took place for 3 minutes at 1100 rpm, the cells were sedimented, allowing the medium to be aspirated with trypsin. The number of cells thus obtained was approximately 2×10^7, which was then diluted with the medium to a desired concentration of 1×10^5 cells/ml. The cell suspension thus obtained was diluted into a 96-well plate with 1 µl suspension in each well and 12 well plates in each well, where 1 ml of the cell suspension was in each well. Cell plate was incubated for 24 hours.

Extract fabrication and application

To the tested scaffolds, the culture medium was added so that the concentration corresponded to 0.1 g of particles/ml of medium. The slurry thus formed was placed in a shaker for 24 hours at 450 rpm and 37 °C. After 24 hours of cell incubation, the 96-well plate medium was aspirated. 100 µl of the medium was replaced in the reference portion with fresh media and 0%, 5%, 30% and 50% platelets were added to the cells and incubated.

MTT test

After 24 hours of culturing the cells in a 96-well plate with varying concentrations of the extract, the medium was aspirated from all wells. Pure medium and 3-[4,5-dimethylthiazol2-yl]-2,5-diphenyltetrazolium bromide - MTT (Molecular Probes, USA) were added to each well. The cells had to be stored for an additional 4 hours in the incubator. During this time, MTT was metabolized to formazan, which is star-shaped. Furthermore, the medium with MTT was aspirated and 100 µl of dimethyl sulfoxide-DMSO (Molecular Probes, USA) was

added to dissolve formazane, which was allowed to work for 15 minutes. The resulting coloration was then measured by a spectrophotometer at a wavelength of 570 nm, the resulting absorbance corresponding to the number of living cells. With higher live cell counts, the concentration of metabolized formazan will increase and absorption will increase.

The test was provided by EN ISO 10993-5: cytotoxicity equal to 1 corresponds to 100 % cell survival, values of > 0.8 are assigned to no cytotoxicity, 0.6–0.8 mild cytotoxicity, 0.4–0.6 moderate toxicity, < 0.4 severe cytotoxicity.

8 RESULTS AND DISCUSSION

8.1 DSC

Table 4 Melting enthalpy, temperature at peak and glass transition temperature of every sample.

		Enthalpy of exotermic process (W °C/g)	Temperature at peak (°C)	1st Glass transition temperature (°C)	2nd Glass transition temperature (°C)
Sample 0%	1st heating	2.29	213.0	-29.4	41.7
	2nd heating	2.21	186.2	-30.0	-
Sample 5%	1st heating	4.5	196.3	-30.3	42.1
	2nd heating	0.93	9.8	-30.4	-
Sample 10%	1st heating	4.08	192.0	-29.1	40.5
	2nd heating	0.46	9.6	-30.8	-
Sample 30%	1st heating	3.87	204.0	-29.1	41.2
	2nd heating	0.32	10.1	-30.4	-
Sample 50%	1st heating	1.96	200.9	-29.9	44.0
	2nd heating	0.14	9.9	-30.6	-

As could be seen in Tab. 4, the highest enthalpy of exotermic process (4.5 W °C/g) in 1st heating had the sample 5%. The lowest enthalpy value (1.96 W °C/g) had the sample 50%. It seems that small CIP concentration (5%) is able to remarkably increase this enthalpy, but with higher concentration the effect vanishes and with concentration 50% enthalpy is even lower than in case of pure Vistamaxx. The sample 0% had the highest temperature peak position (213.0 °C) (Fig. 17) in 1st heating and the sample 10% had the lowest one (192.0 °C). The differences in glass transition temperatures in both cases at -30 °C as well as at 41 °C for all samples are almost negligible for both scans. Also the presence of the metling peak is visible at 105.0 °C, however no significant change of peak position was observed by addtion of various amounts of CIPs. On the other hand, the metling entalpy slightly decreased with amount of CIPs.

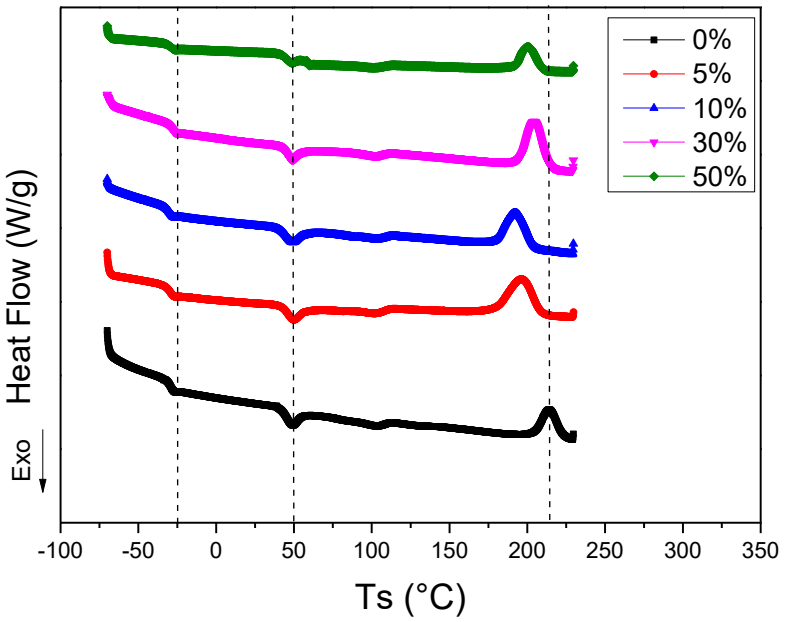

Figure 17 The dependence heat flow on temperature for the all samples with 1st heating.

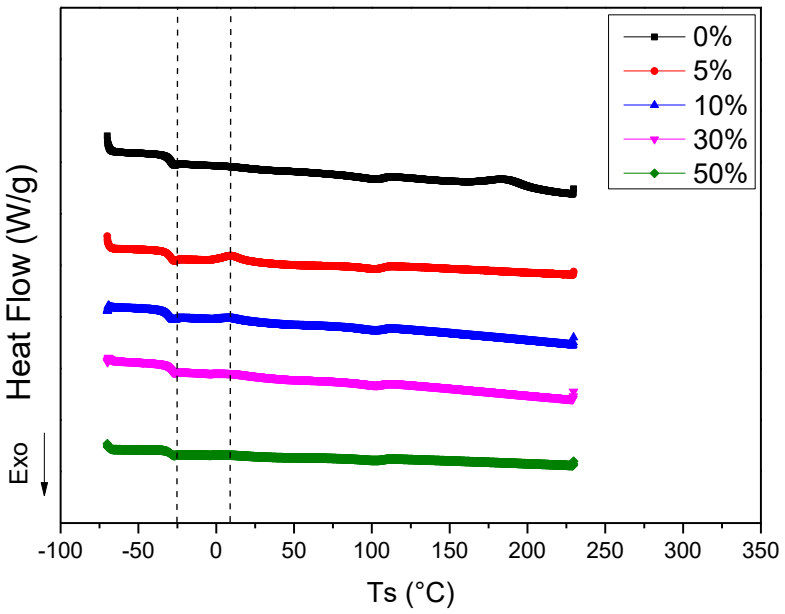

Figure 18 The dependence heat flow on temperature for the all samples with 2nd heating.

As is shown in Fig. 18 (2nd heating cycle) exotermic peak from Fig. 17 dismissed for all composite masterbatches containing CIPs as well as second glass transition temperature at 41 °C. However, the presence of the magnetic particles causes the evolution of cold crystallization peak around 10 °C. Moreover, the enthalpy of this crystallization was significantly decreased from 0.93 W °C/g for 5% sample to 0.14 W °C/g for 50% sample, respectively. The following melting point possition as well as enthalpy was negligibly affected similarly as was observed for 1st heating. Finally, it can be concluded that both magnetic particles as well as heating cycles do not have significant effect on glass transition a melting temperatures.

8.2 Rheological properties

Temperature 150 °C

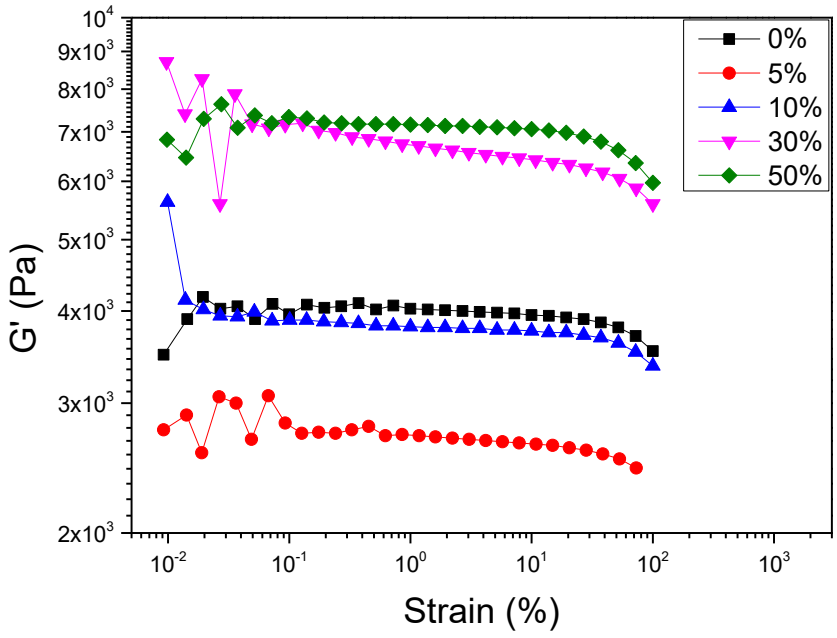

Figure 19 The dependence storage modulus on strain for the all samples for 150 °C at frequency 1 Hz.

As it is shown in Fig. 19 linear viscoelastic region used for further frequency sweep measurements was set to 10%.

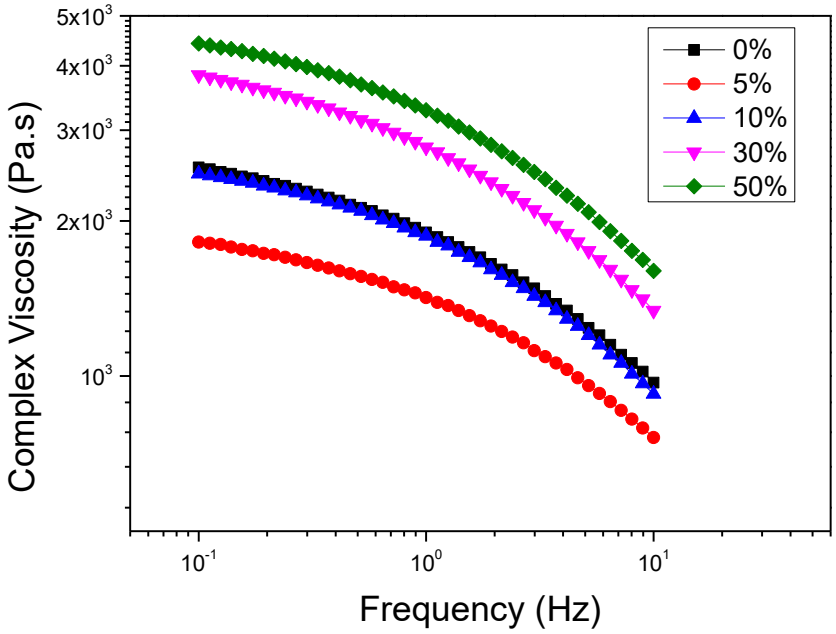

Figure 20 The dependence complex viscosity on frequency for the all samples for 150 °C and strain deformation 10%.

As can be seen in Fig. 20 complex viscosity decreases with increasing applied frequency for all samples, showing their pseudoplastic and shear-thinning behavior. However, small addition of magnetic particles (5% and 10%) decreased values of complex viscosity especially for sample 5%. This is mainly due to the shifted exotermic peak from 213.0 °C to 196.0 °C and 192.0 °C, respectively. However, addition of 30% and 50% of particles lead to significant increase of the complex viscosity, even though the melting peak was 204.0 °C and 200.0 °C, respectively. Here, the amount of the particles plays a crucial role on the complex viscosity increase, rather than exotermic peak position.

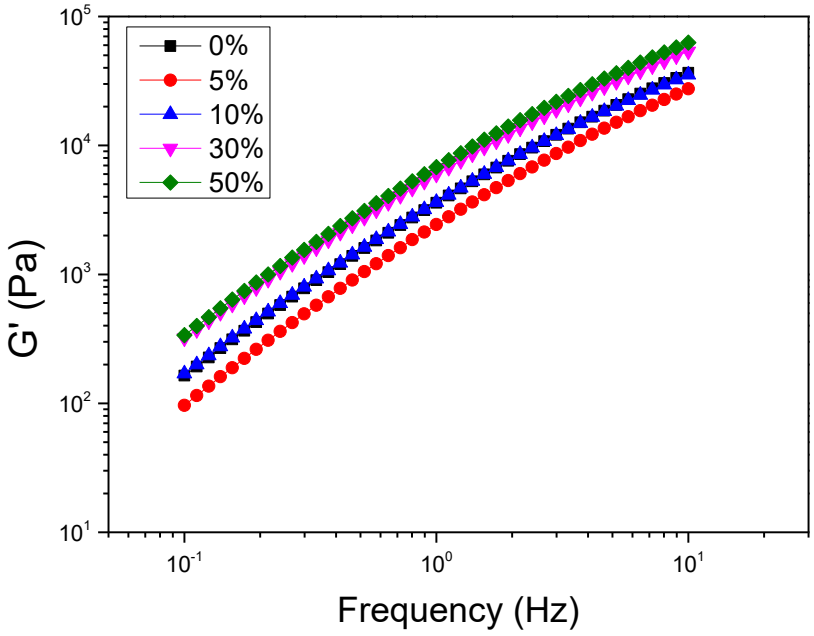

Figure 21 The dependence storage moduli on frequency for the all samples for 150 °C and strain deformation 10%.

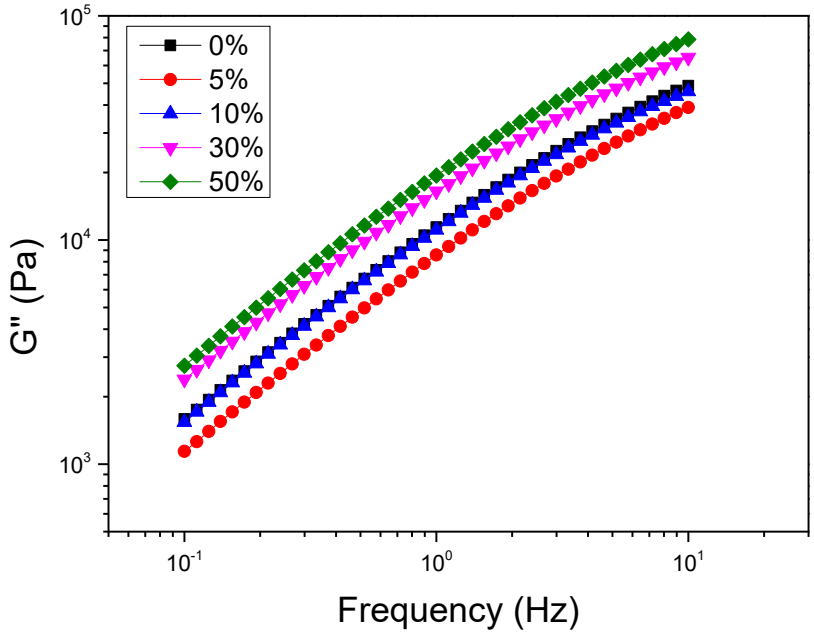

Figure 22 The dependence loss moduli on frequency for the all samples for 150 °C and strain deformation 10%.

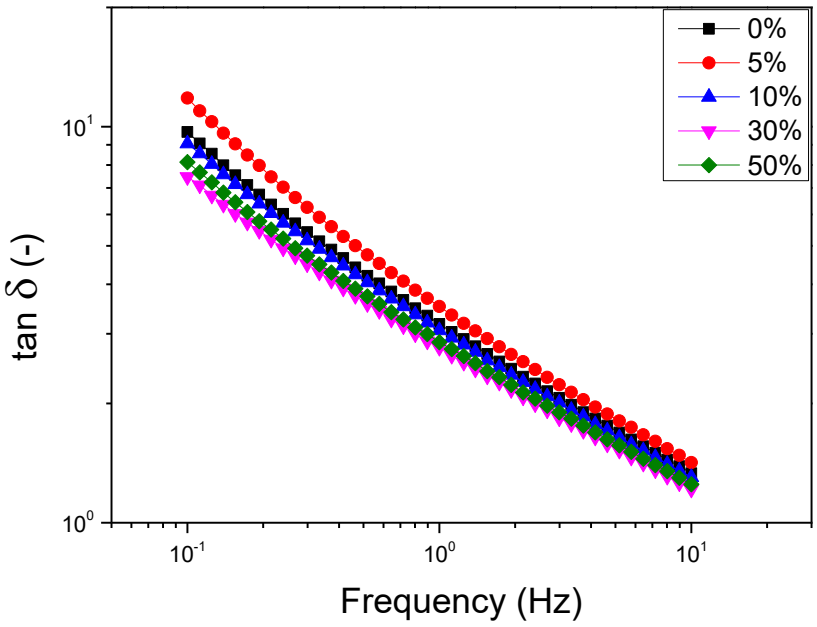

Figure 23 The dependence tan δ on frequency for the all samples for 150 °C and strain deformation 10%.

According to Figs. 20 and 23, it can be seen, that the small amount (5% and 10%) of CIP improves masterbatch flow properties, samples with higher CIP ratio show a little bit worse flow properties instead due to the presence of the high amount of the particles (30 % and 50 %). From the Fig. 23 is clearly visible that the softest sample is 5% showing the highest values of tan δ.

Temperature 170°C

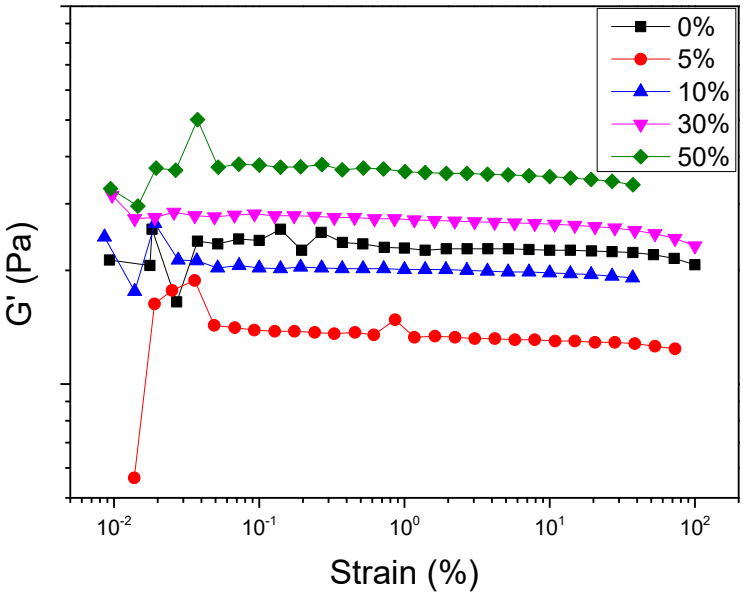

Figure 24 The dependence storage modulus on strain for the all samples for 170 °C at frequency 1 Hz.

As it is shown in Fig. 24 linear viscoelastic region used for further frequency sweep measurements was set to 10%.

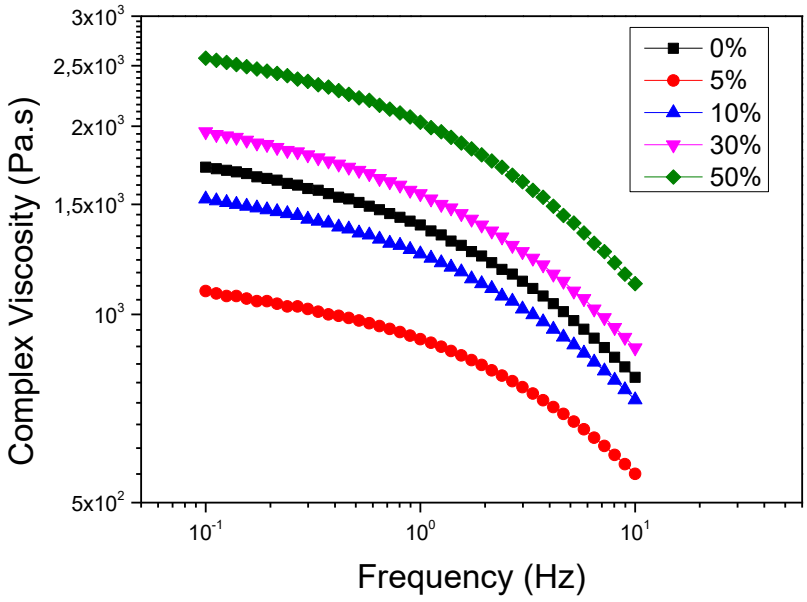

Figure 25 The dependence complex viscosity on frequency for the all samples for 170 °C and strain deformation 10%.

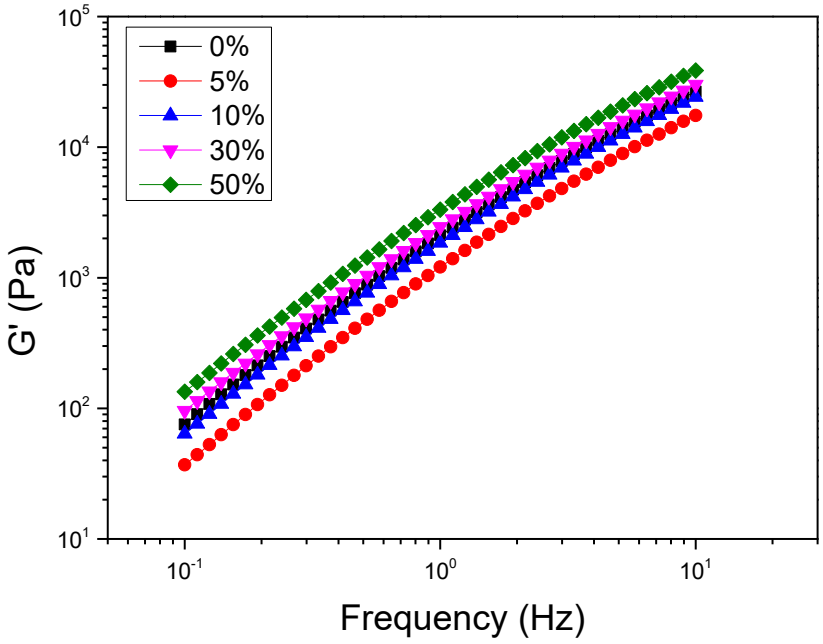

Figure 26 The dependence storage moduli on frequency for the all samples for 170 °C and strain deformation 10%.

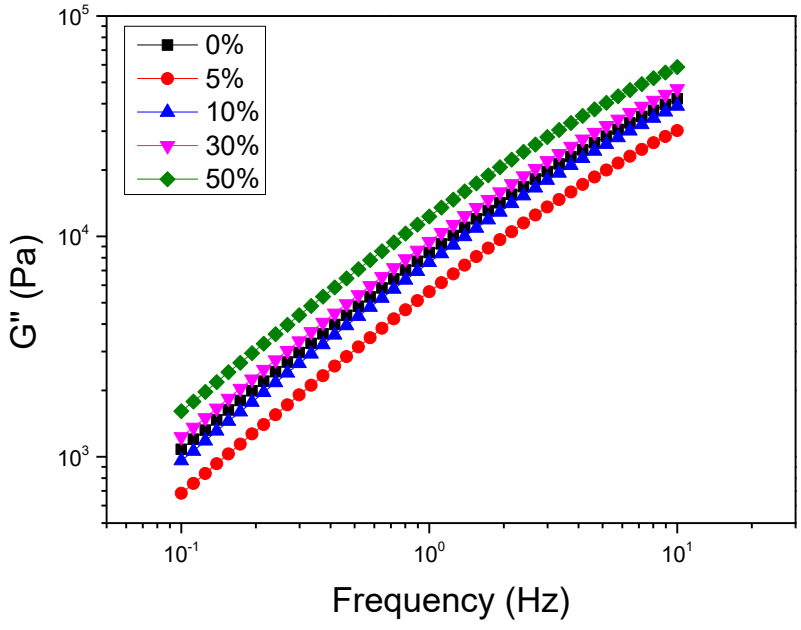

Figure 27 The dependence loss moduli on frequency for the all samples for 170 °C and strain deformation 10%.

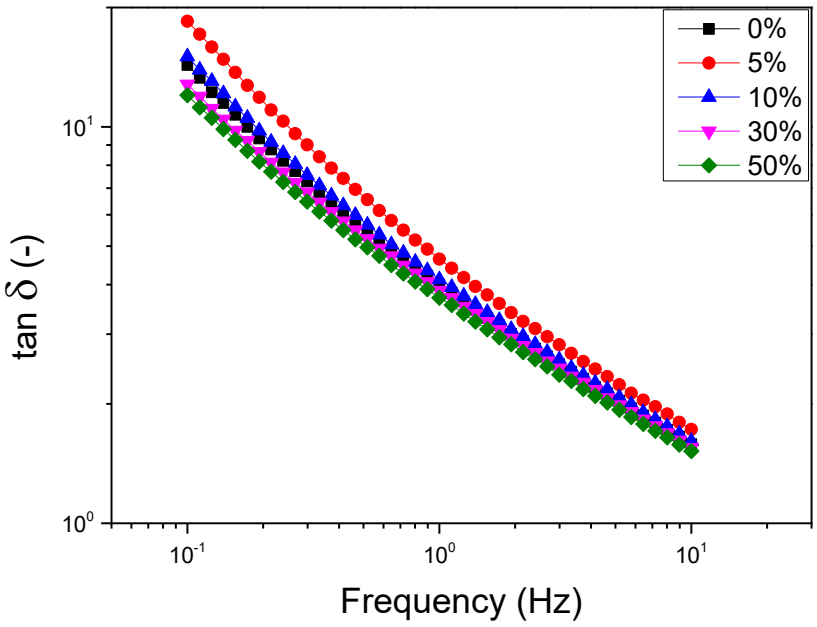

Figure 28 The dependence tan δ on frequency for the all samples for 170 °C and strain deformation 10%.

In case of rheological investigations at 170 °C the curves have nearly the same trends in comparison to measurements at 150 °C. Just differences in complex viscosities are more pronounced.

Temperature 190°C

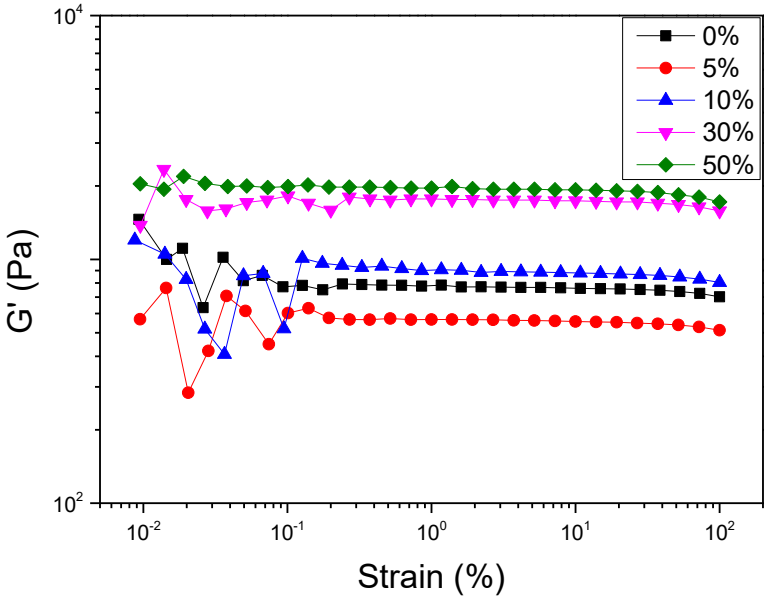

Figure 29 The dependence storage modulus on strain for the all samples for 190 °C at frequency 1 Hz.

As it is shown in Fig. 29 linear viscoelastic region used for further frequency sweep measurements was set to 10%.

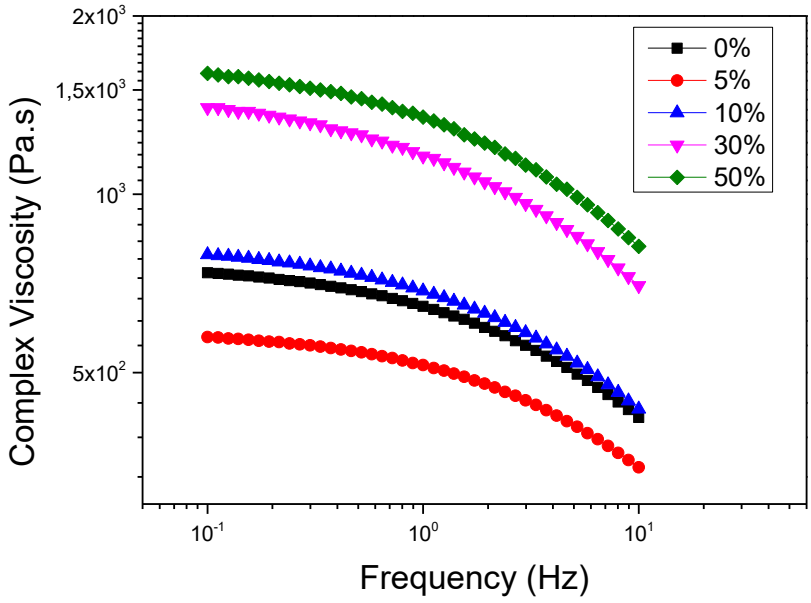

Figure 30 The dependence complex viscosity on frequency for the all samples for 190 °C and strain deformation 10%.

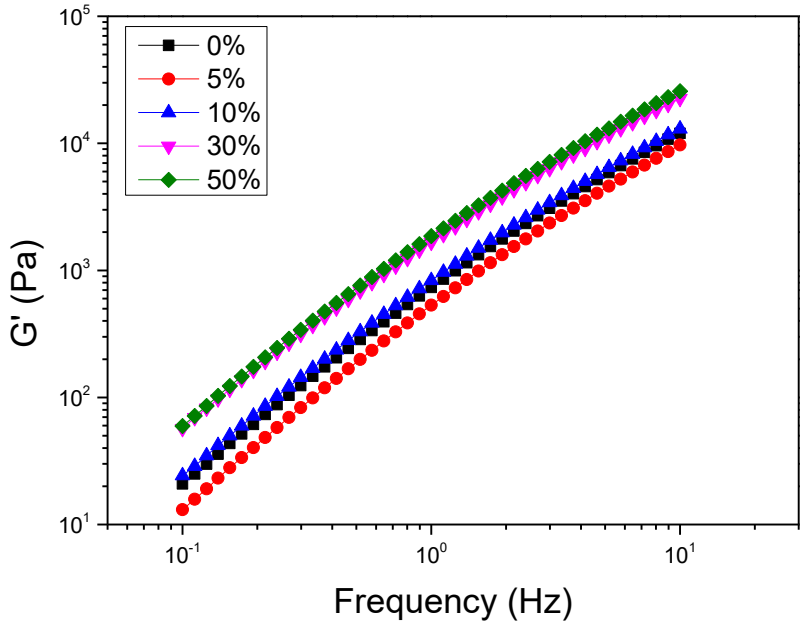

Figure 31 The dependence storage moduli on frequency for the all samples for 190 °C and strain deformation 10%.

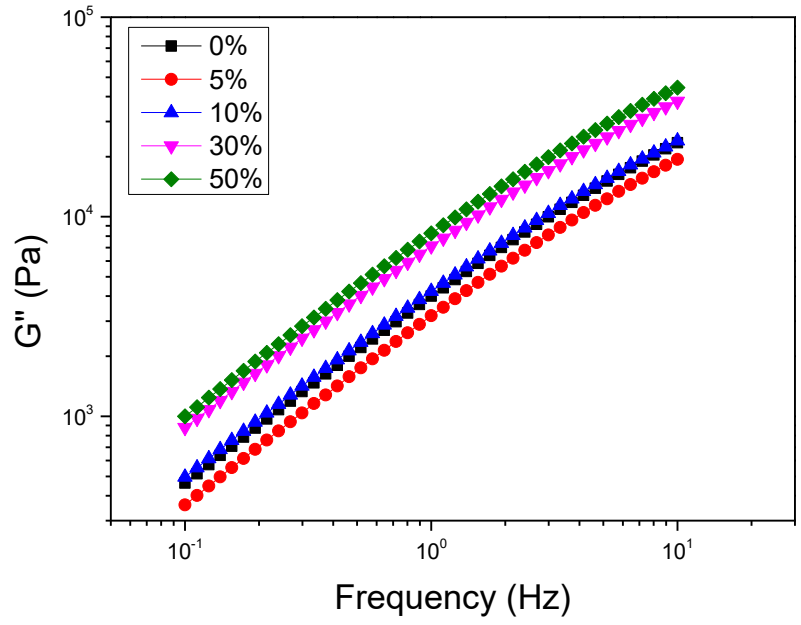

Figure 32 The dependence loss moduli on frequency for the all samples for 190 °C and strain deformation 10%.

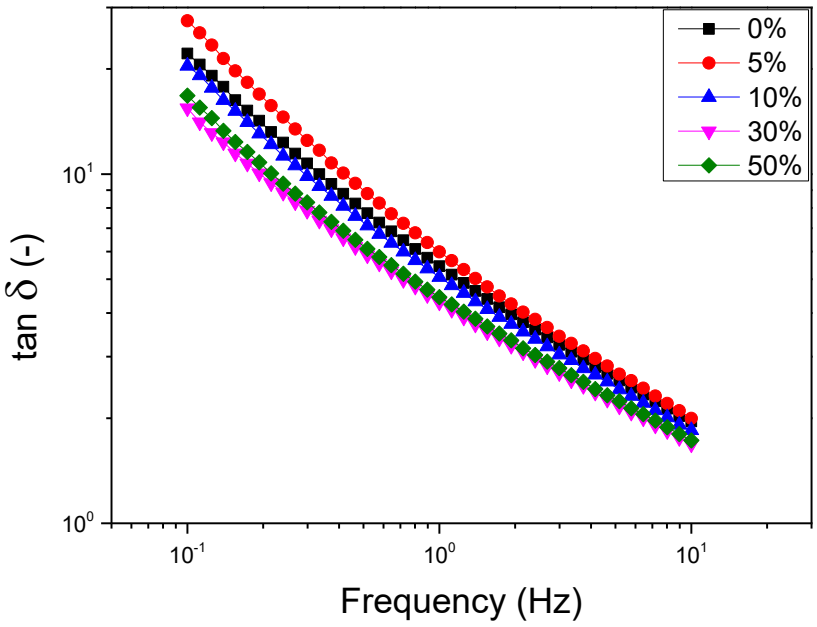

Figure 33 The dependence tan δ on frequency for the all samples for 190 °C and strain deformation 10%.

According to Figs. 20, 25 and 30, with increasing temperature, complex viscosity significantly decreases, and the shape of the curve sustain nearly same, still confirming the shear-thinning behavior. In case of sample 50% the difference is about 2000 Pa.s between 150 °C and 190 °C. Similar trends were also observed for the rest of the samples (5%, 10% and 30%). This fact clearly indicates, that masterbatch 50% can be effectively produced by melt-electrowriting technique as well.

8.3 Viscoelastic properties

In order to investigate the mechanical performance of the prepared masterbatches, the evaluation of the viscoelastic properties using dynamic mechanical analyzer (tensile mode) and rotational rheometer (shear mode) was used. From this point of view two main attributes were measured. Firstly, dependence of the viscoelastic moduli on the strain, to obtain the linear viscoelastic region. Secondly, dependence on the temperature providing the information, of the overall mechanical performance using storage moduli and tan δ.

8.3.1 Viscoelastic properties using tensile mode

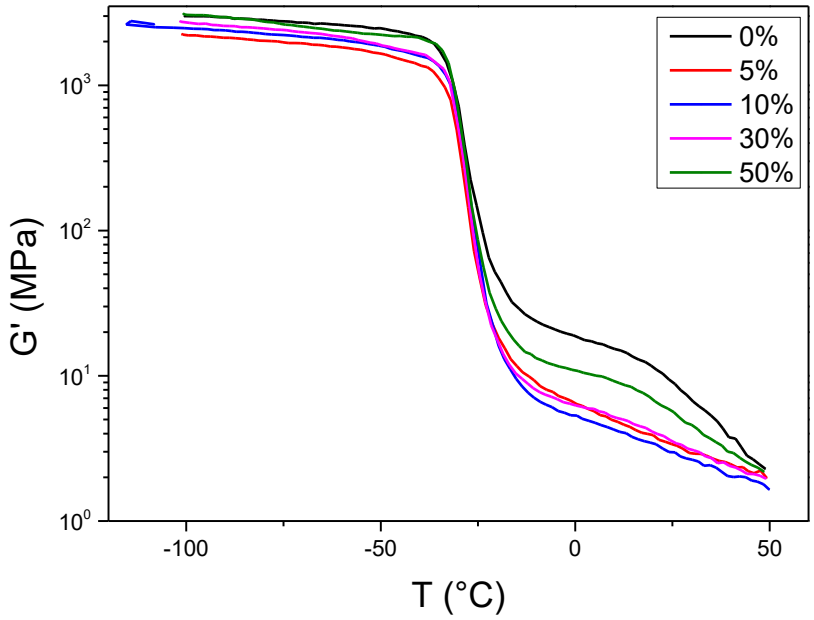

Figure 34 The dependence storage modulus on temperature for the all samples (frequency 1 Hz).

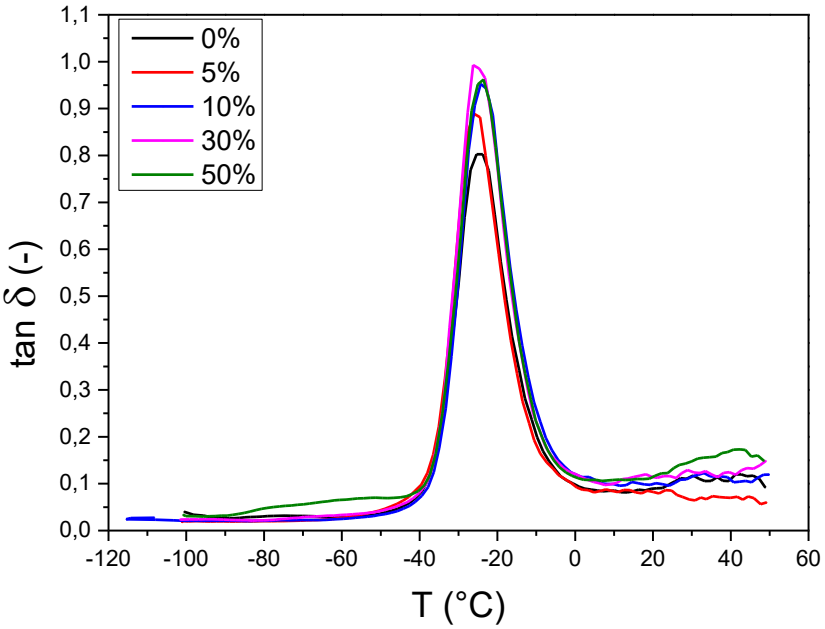

Figure 35 The dependence tan δ on temperature for the all samples (frequency 1 Hz).

As is shown in Fig. 34 the samples have very similar values of the storage moduli starting on 3000 MPa for neat sample and 50% and having around 2200 MPa for sample 5%. However the situation is significantly different after the first glass transition temperature, where still 0% and 50% are the highest however, here the sample 10% showing the lowest values. Moreover, it seems that there is a second drop around 50 °C of the storage modulus indicating the second glass transition temperature. This will be the aim of investigation using shear mode, due to the fact that sample in tensile clamps are not fully clamped and results are very scattered.

In Fig. 35 the peak of tan δ clearly shows the glass transition temperature around -26 °C for all investigated samples. Slight deviation from the DSC results is usual, since the calorimetric principles of investigation are different, significantly increases and then rapidly decreases. As was already discussed with increasing temperature the contact between the samples and clamps were not appropriate and therefore the investigation at higher temperatures was performed using rotational rheometer in shear mode.

8.3.2 Viscoelastic properties using shear mode

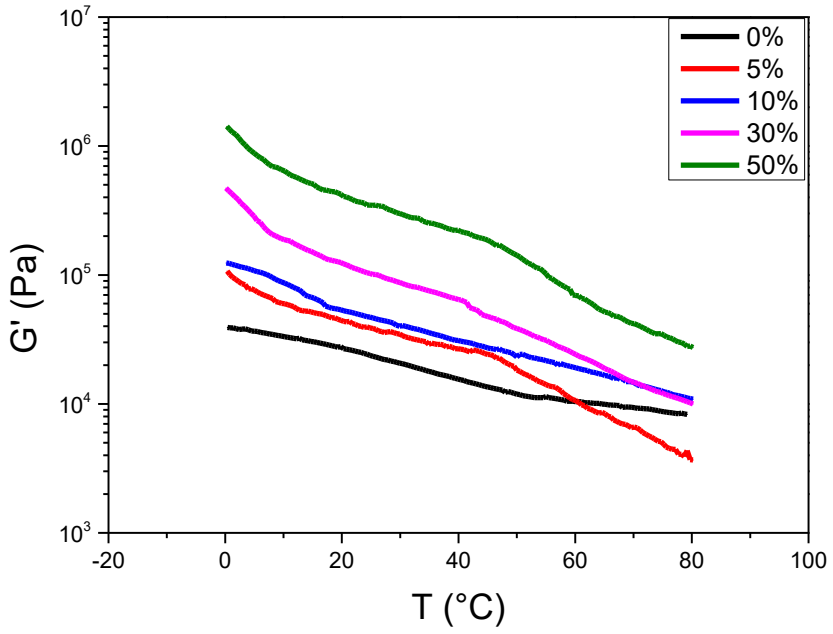

Figure 36 The dependence storage moduli on temperature for the all samples.

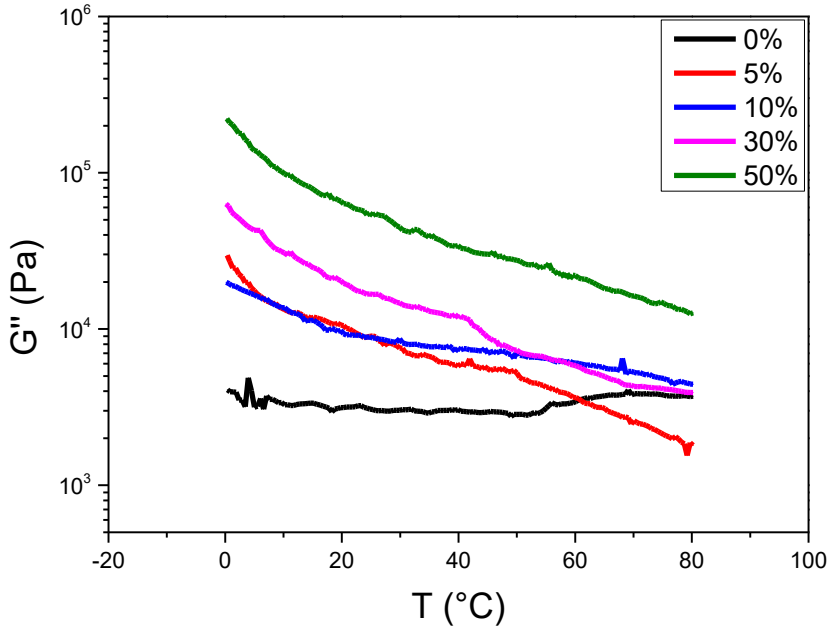

Figure 37 The dependence loss moduli on temperature for the all samples.

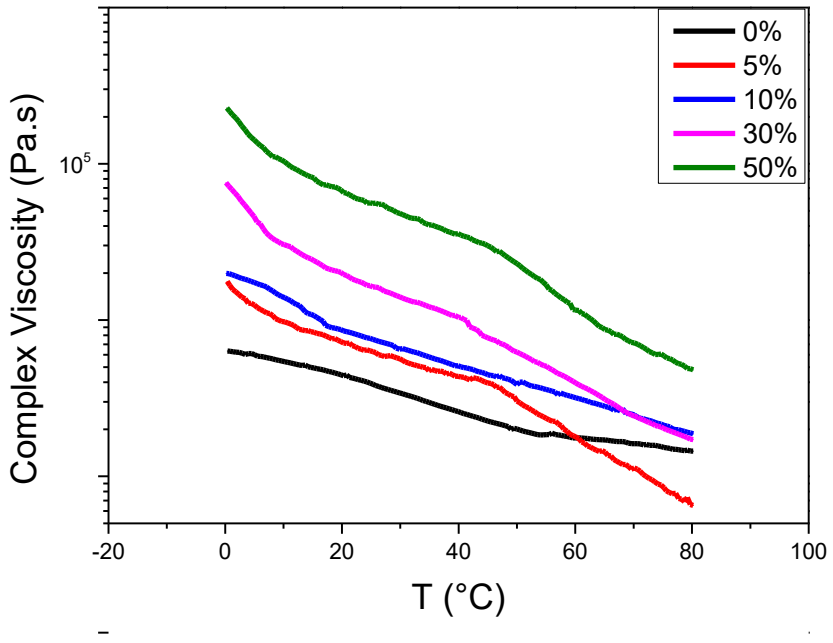

Figure 38 The dependence complex viscosity on temperature for the all samples.

In order to investigate the second glass transition temperature the measurement on rotational rheometer in shear mode from 0 °C to 80 °C was performed (Figs. 38 and 39). It can be seen that there is significant difference in tensile and shear mode. Here the sample 0% has the

lowest values, while sample 50% still on the top from storage modulus point of view. This can be the reason of the contact between the sample and clamps in case of tensile mode above 0 °C. However, the rest of the samples shows similar trends in comparison to tensile mode. Moreover, the above 50 °C the samples with magnetic particles have significant drop of storage modulus and complex viscosity most probably connected to the glass transition temperature, however this evidence is not clear from the investigated data and deeper measurements and evaluations should be performed. In addition, from the data can be seem that with further temperature increase, the sample 5% and sample 10% drop down the 0% sample which is in good agreement to rheological investigation from 150 °C to 190 °C.

8.4 Optical microscope

In this work the samples had a form of 3D printed 5 layers structure with crossing angle 90°. The main goal of optical microscopy was attempt to ensure that the net is printed correctly and every sample has different amount of CIP.

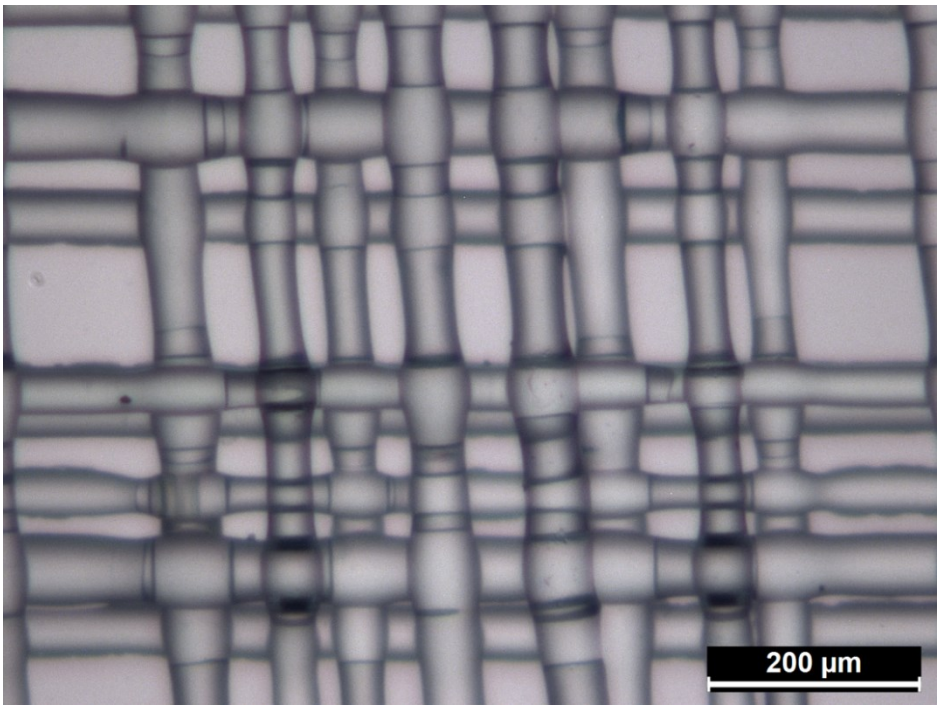

Figure 39 Image of the 5-layered scaffold 0%.

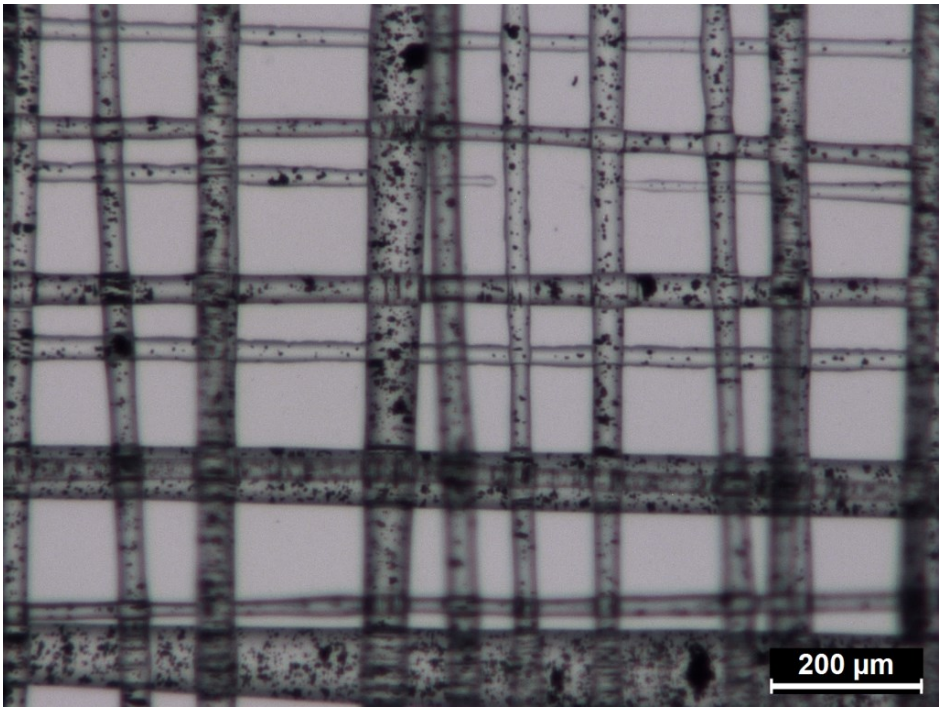

Figure 40 Image of the 5-layered scaffold 5%.

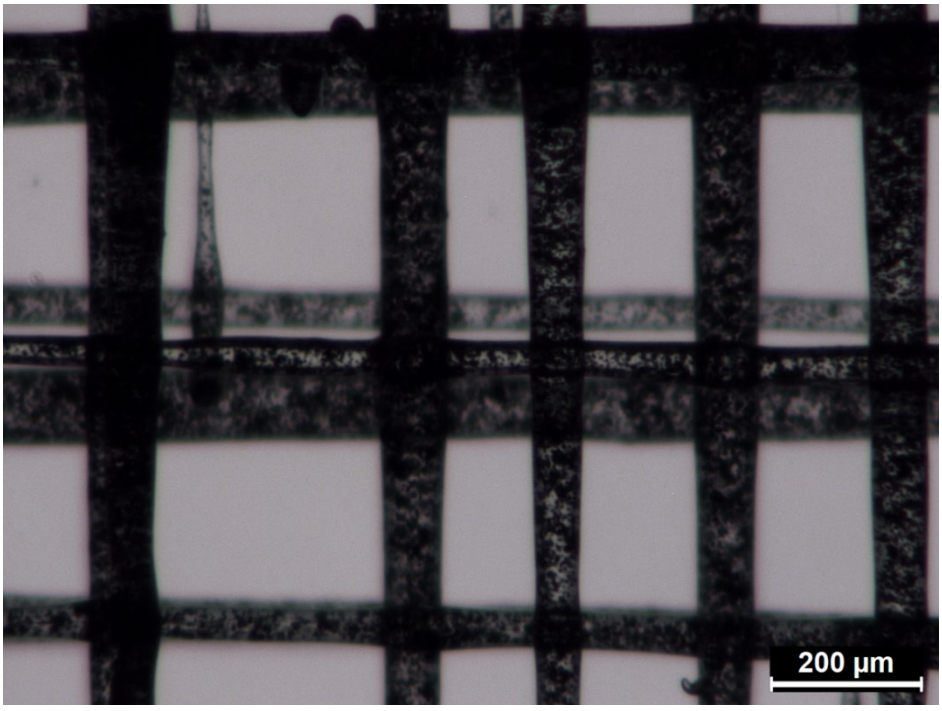

Figure 41 Image of the 5-layered scaffold 30%.

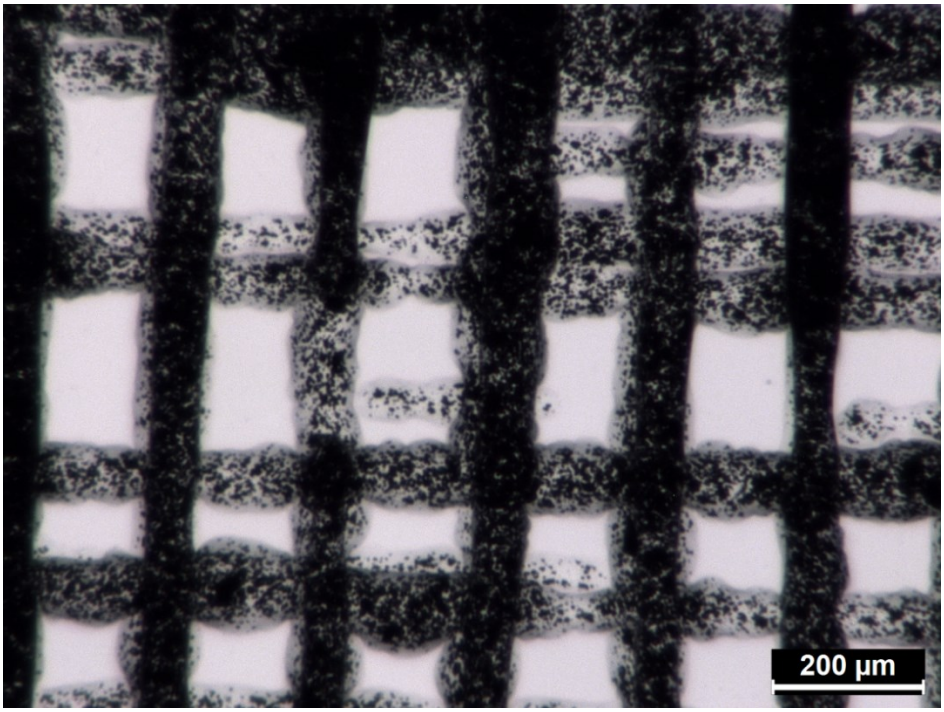

Figure 42 Image of the 5-layered scaffold 50%.

According to performed images melt-electrowriting technology is able to create scaffold structure from prepared masterbatches as composite of thermoplastic elastomer and CIP in various ratio. As can been seen in the Fig. 39, scaffold 0% has the decent structure with negligible anomalies. The sample does not contain CIP particles at all, so it is almost transparent. Figs. 40 and 41 show scaffolds 5% and 30 % with acceptable structure and increasing amount of CIP. Somewhere small deviations like unconnected fibers (Fig. 40) can be observed. Fig. 42 presents scaffold 50% that has the biggest amount of CIP in structure and thus have the fibers with highest diameter.

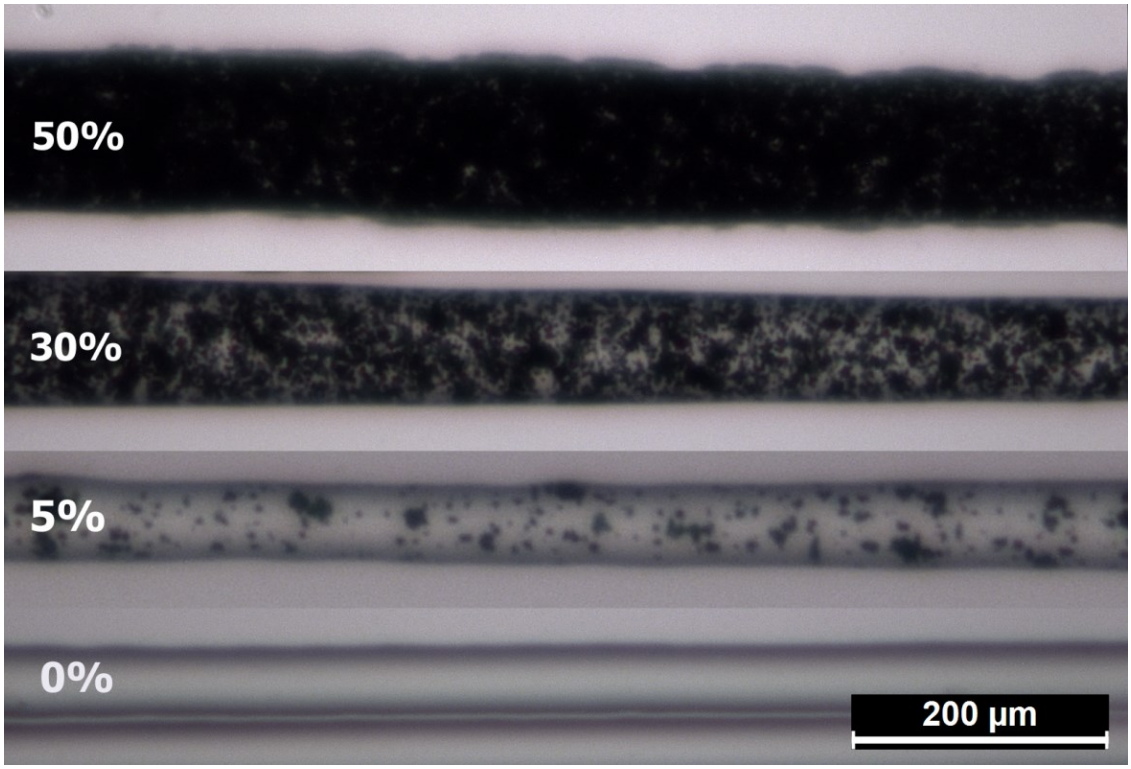

Figure 43 The comparison of CIP amount in fibers.

Fig. 43 shows the difference between various CIP content in samples. It is obvious that with increasing CIP amount decreases scaffold transparency and the fiber width starts to be bigger. The fiber width of the sample 0% is around (45 ± 3) µm, the fiber of the sample 5% - (55 ± 5) µm, the fiber of the sample 30% - (80 ± 15) µm, the fiber of the sample 50% - (135 ± 22) µm.

8.5 SEM

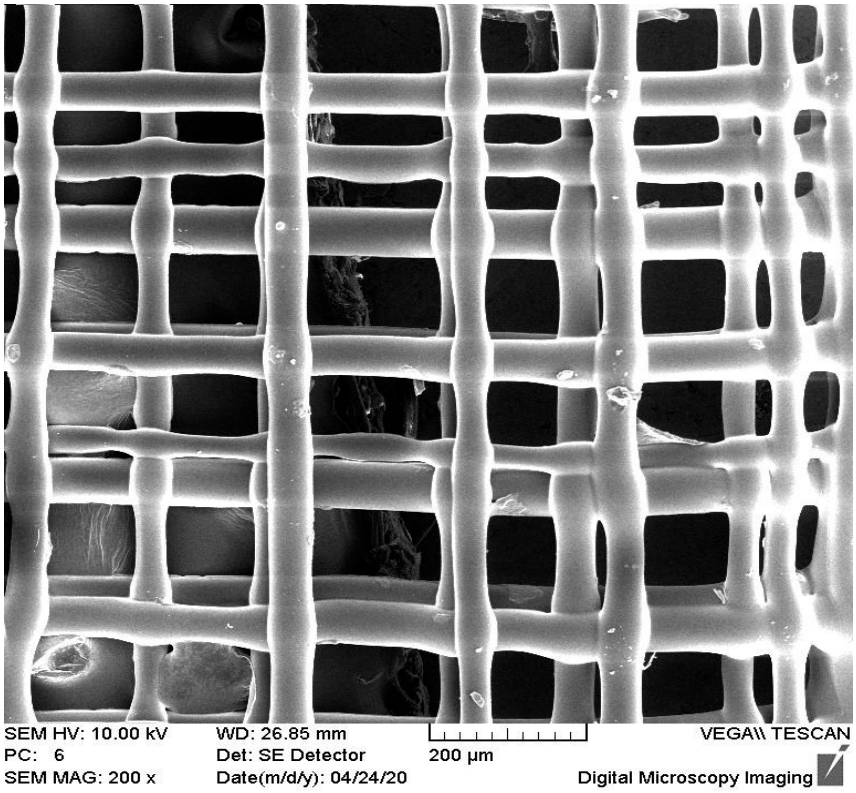

Figure 44 SEM SE image of 3D printed scaffold 0%.

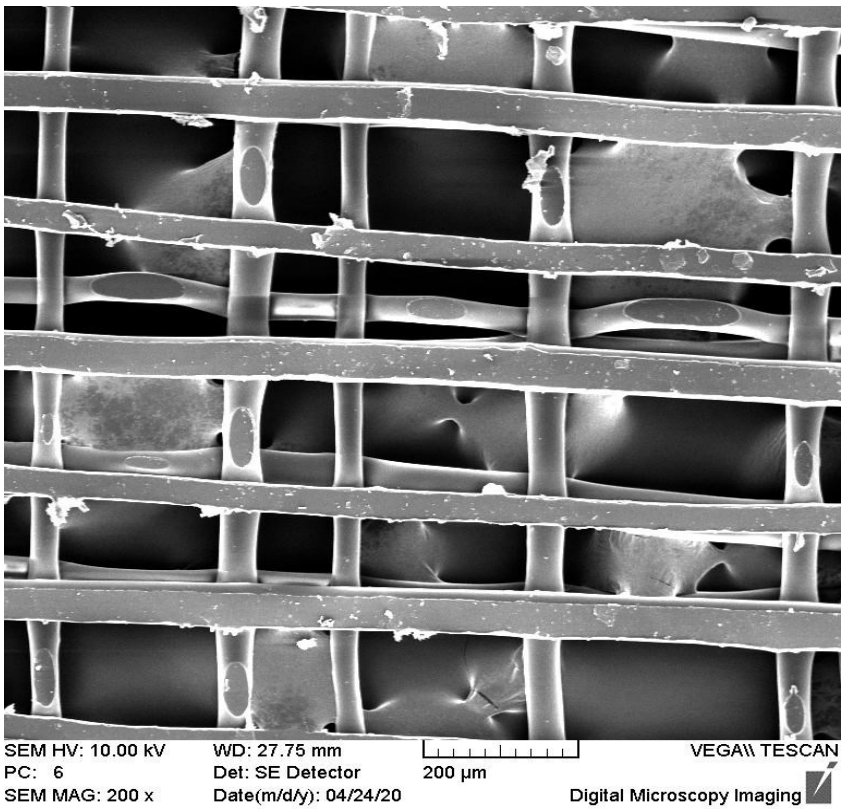

Figure 45 SEM SE image of 3D printed scaffold 5%.

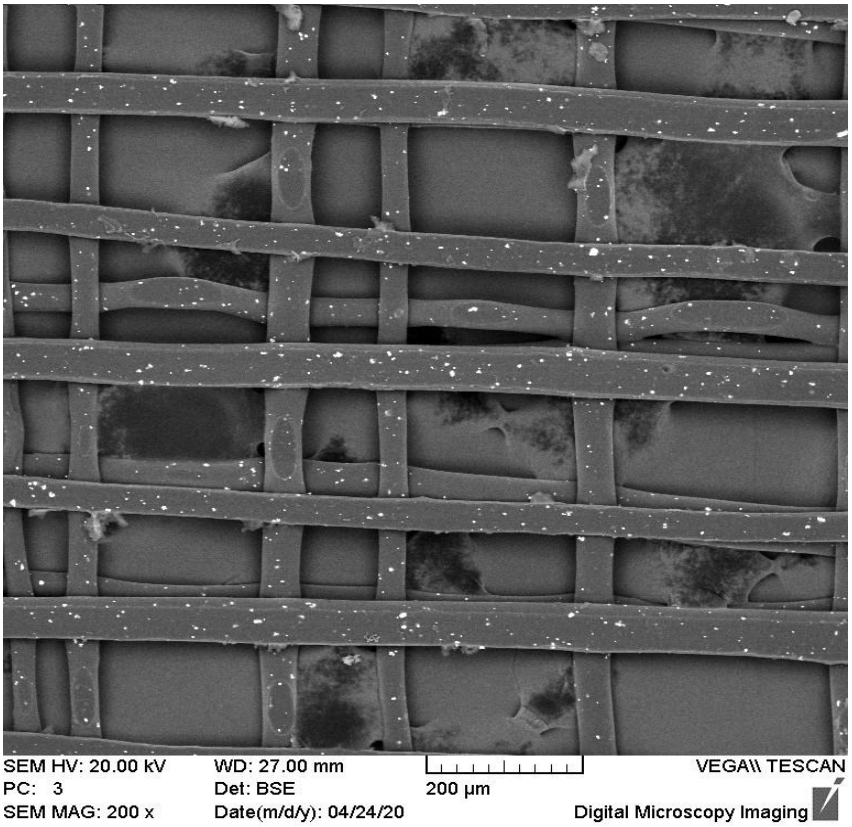

Figure 46 SEM BSE image of 3D printed scaffold 5%.

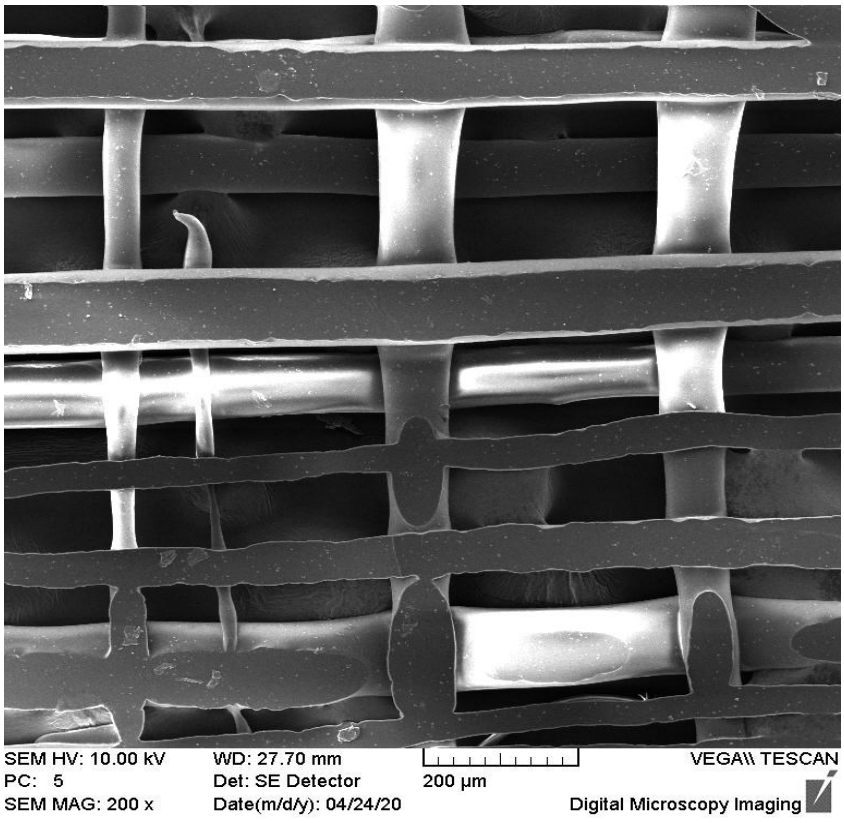

Figure 47 SEM SE image of 3D printed scaffold 30 %.

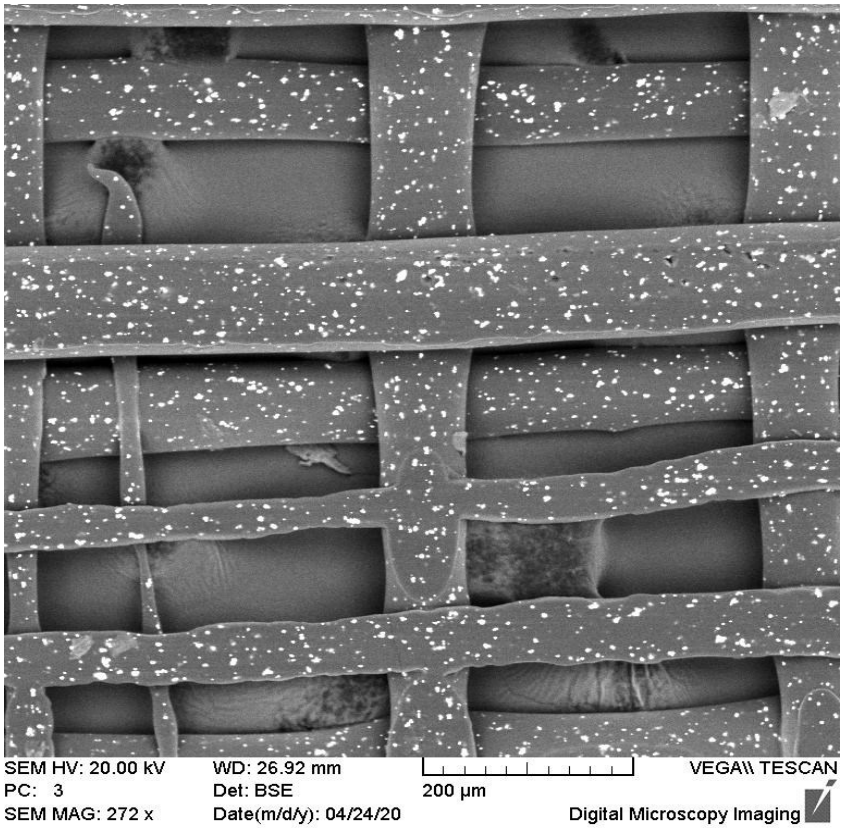

Figure 48 SEM BSE image of 3D printed scaffold 30%.

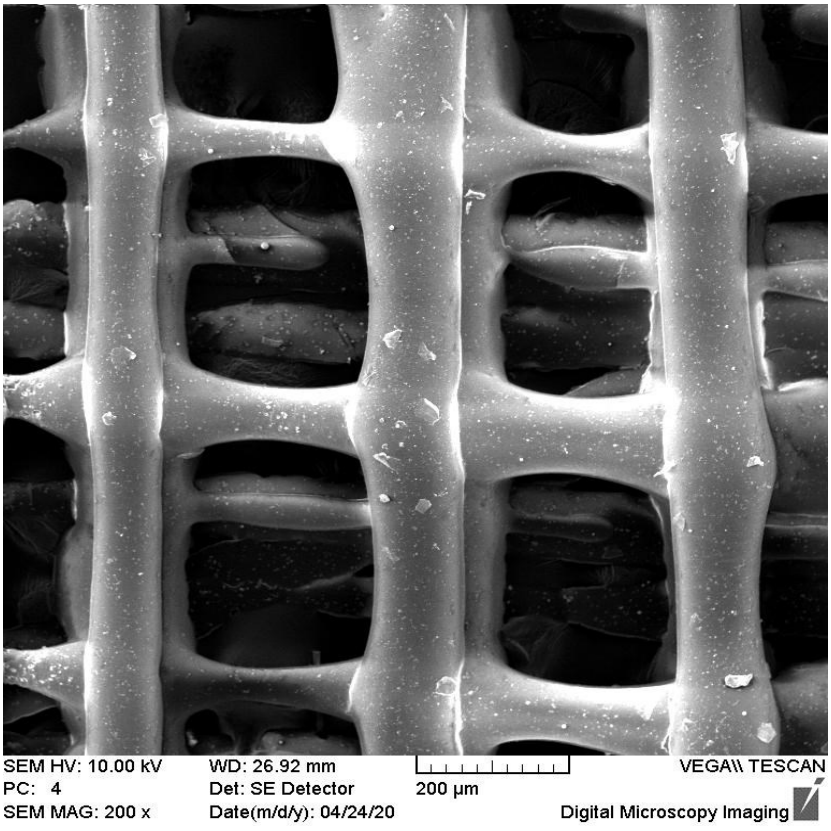

Figure 49 SEM SE image of 3D printed scaffold 50%.

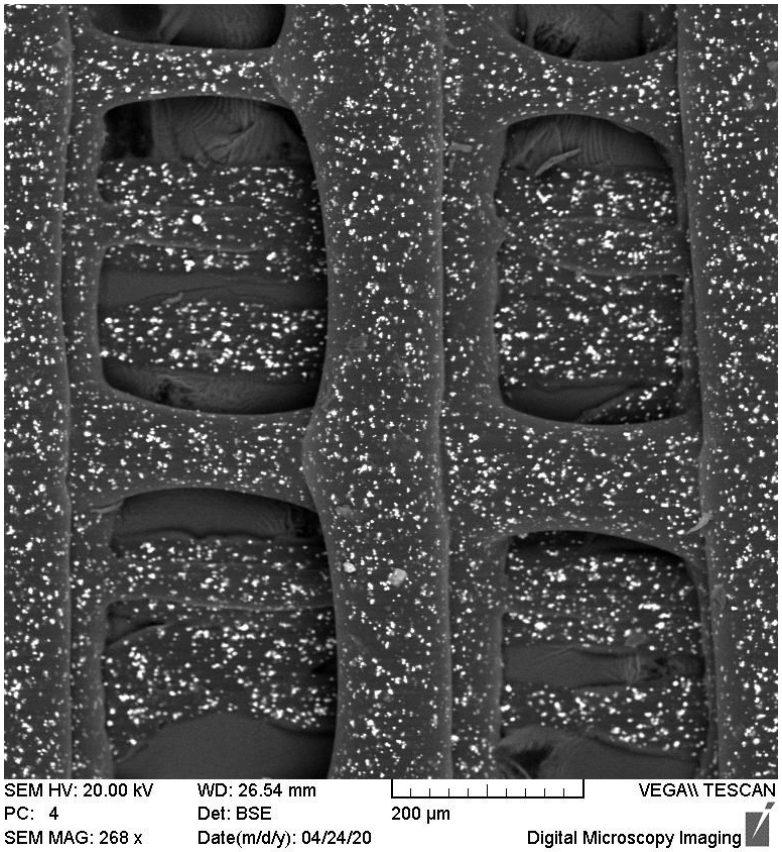

Figure 50 SEM BSE image of 3D printed scaffold 50%.

According to Figs. 46-52, all printed scaffolds have the corresponding structure. Images acquired in BSE mode (Figs. 48, 50 and 52) show polymer matrix with white points indicating the presence of CIP as a part of scaffold structure. Fig. 46 presents the scaffold 0% with the organized structure consisting of relatively thin fibers with no CIP inside and quite big gaps between. The scaffold 5% (Fig. 48) has CIP already and his fibers a little bit wider than in case of the scaffold 0%. In case of the scaffold 30% (Fig. 50) higher diamter is clearly seen and the amount of CIP is much more noticeable, gaps are smaller than in the previous scaffolds. The scaffold 50% (Fig. 52) has absolutely the biggest fiber width, the most abundant CIP particles and the smallest gaps. Here can be concluded, that the distribution of the CIPs is homogenous for all investigated samples.

The element analysis was done for monitoring of CIP dispersity in the scaffold. Every color point means certain chemical element. In this case it was green (Carbon), blue (Oxygen) and red (Iron).

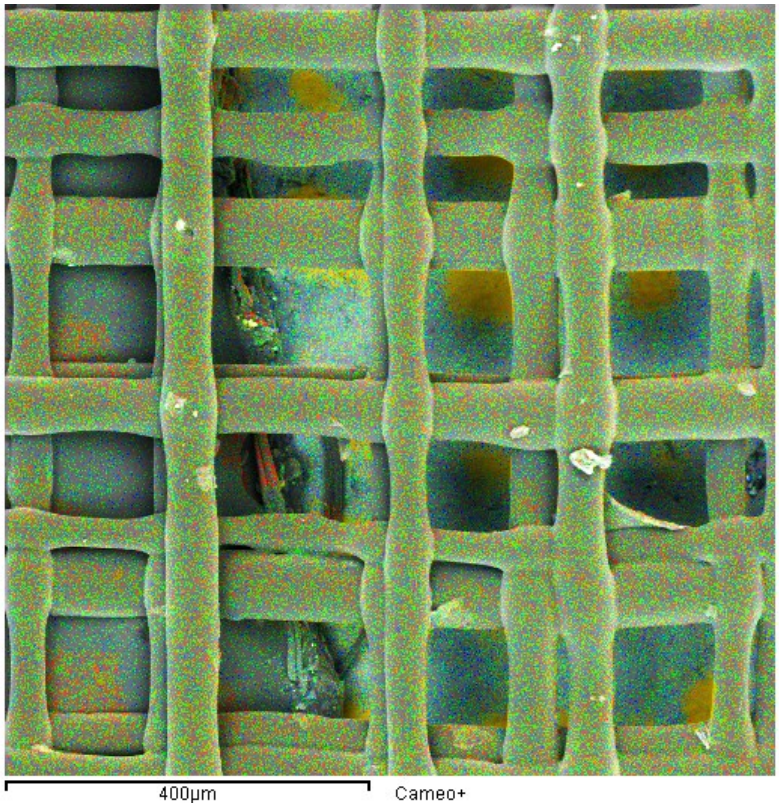

Figure 51 Element analysis for scaffold 0% including Fe, C and O.

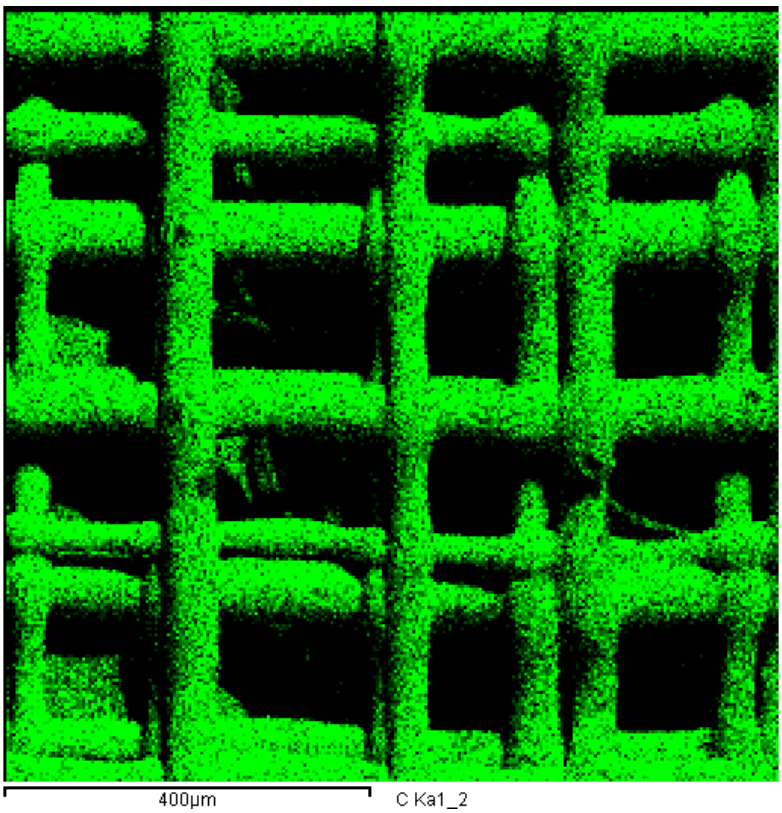

Figure 52 Carbon in the structure of the scaffold 0%.

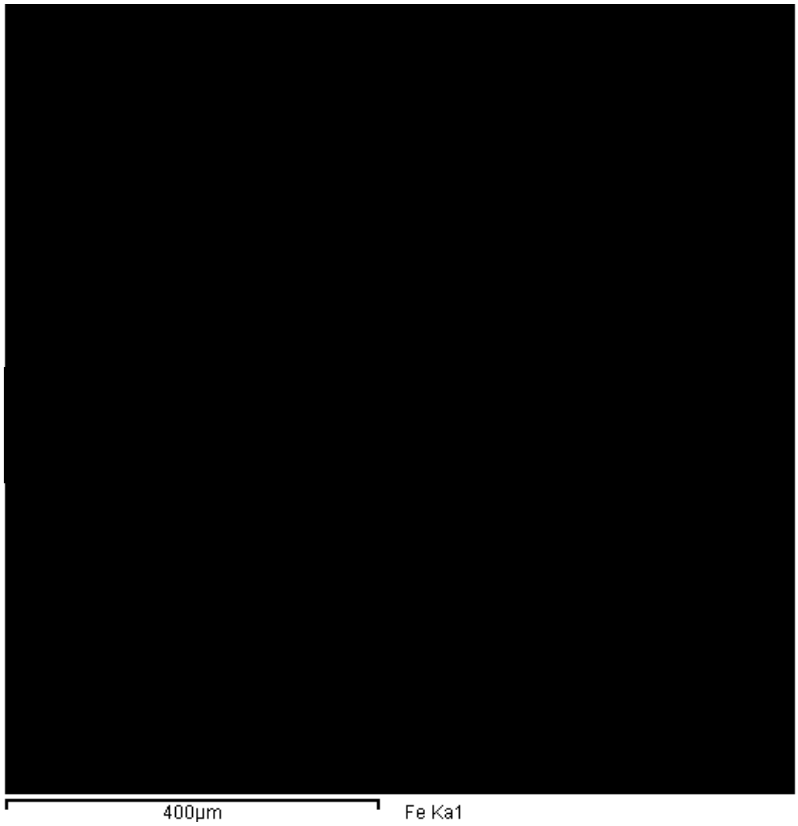

Figure 53 Iron in the structure of the scaffold 0%.

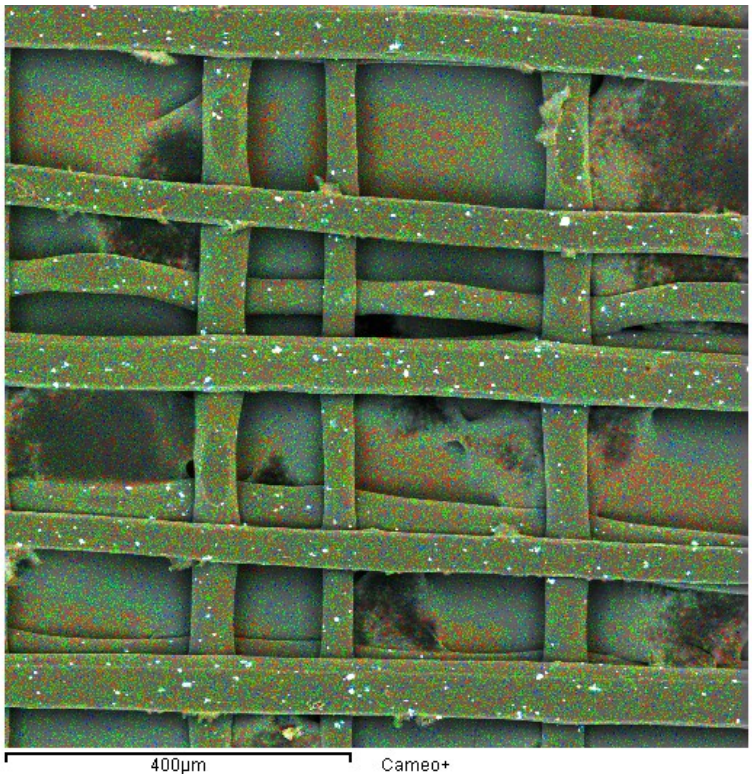

Figure 54 Element analysis for scaffold 5% including Fe, C and O.

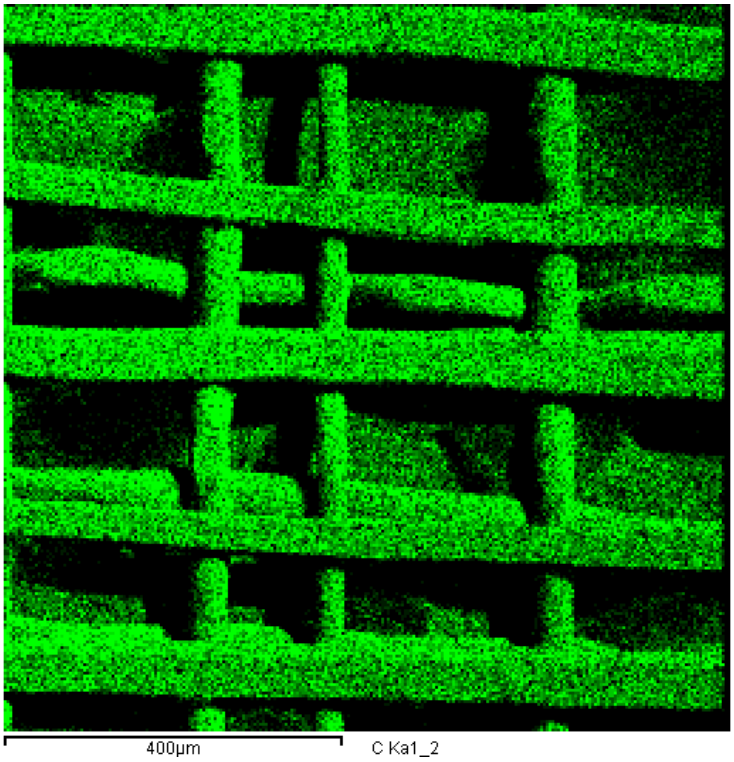

Figure 55 Carbon in the structure of the scaffold 5%.

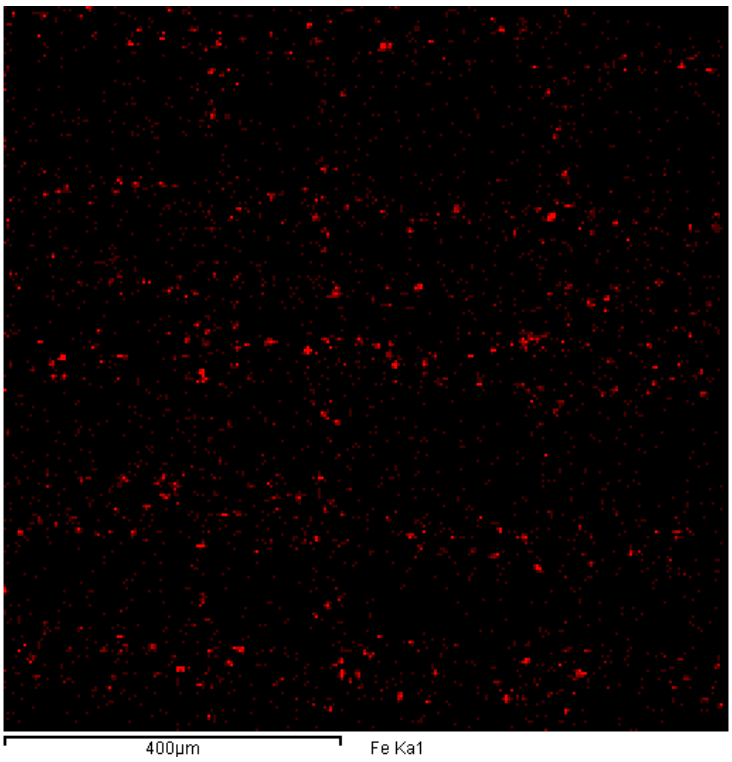

Figure 56 Iron in the structure of the scaffold 5%.

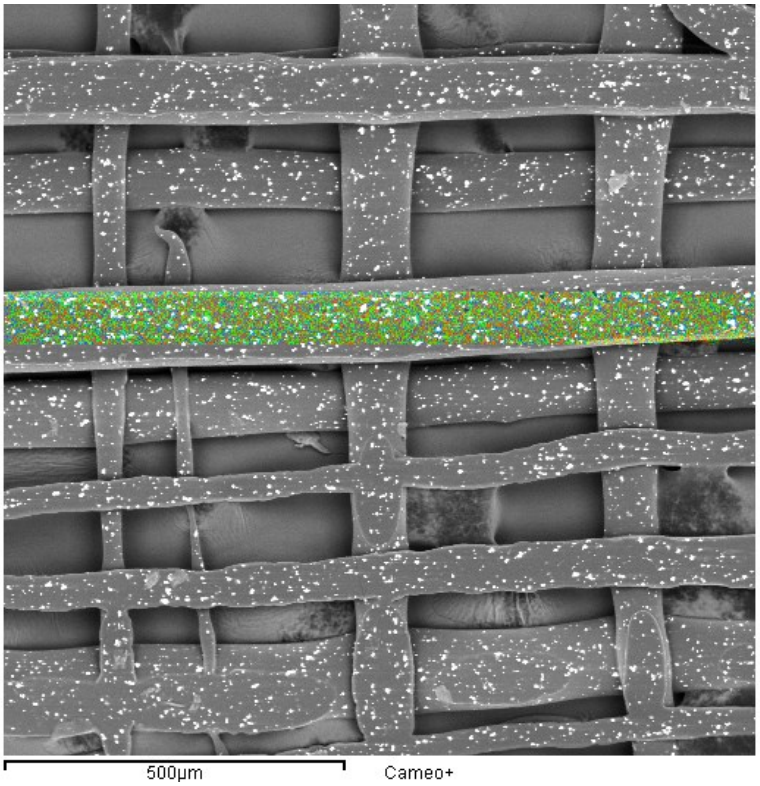

Figure Element analysis for scaffold 30% including Fe, C and O.

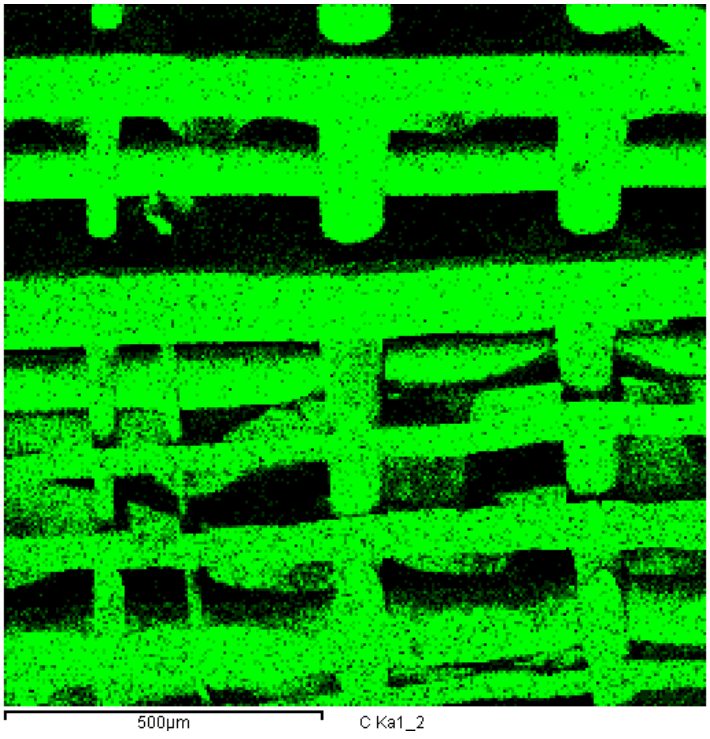

Figure 57 Carbon in the structure of the scaffold 30%.

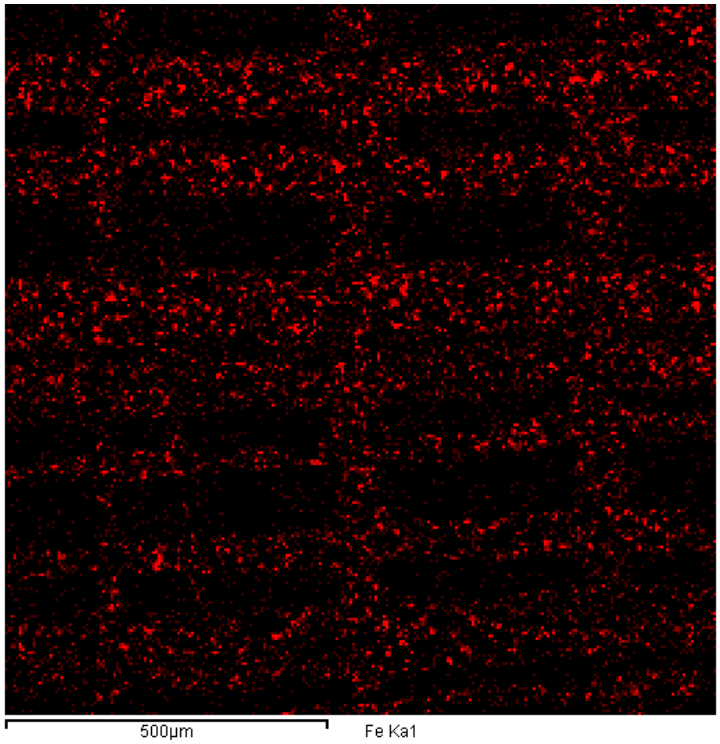

Figure 58 Iron in the structure of the scaffold 30%.

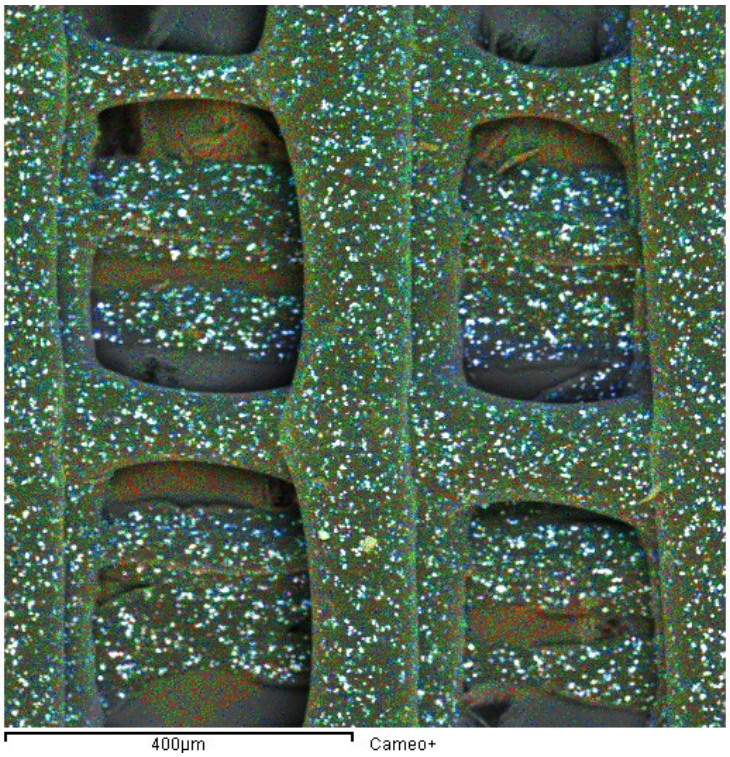

Figure 59 Element analysis for scaffold 50% including Fe, C and O.

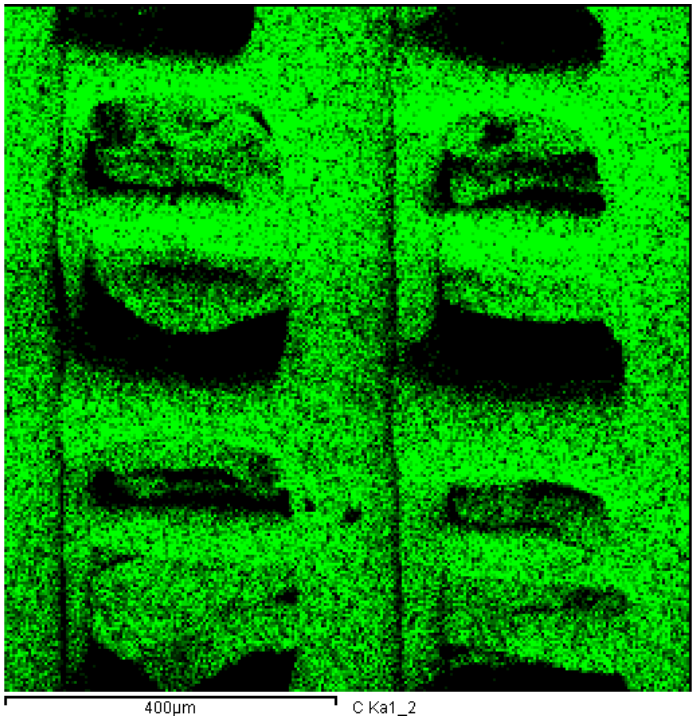

Figure 60 Carbon in the structure of the scaffold 50%.

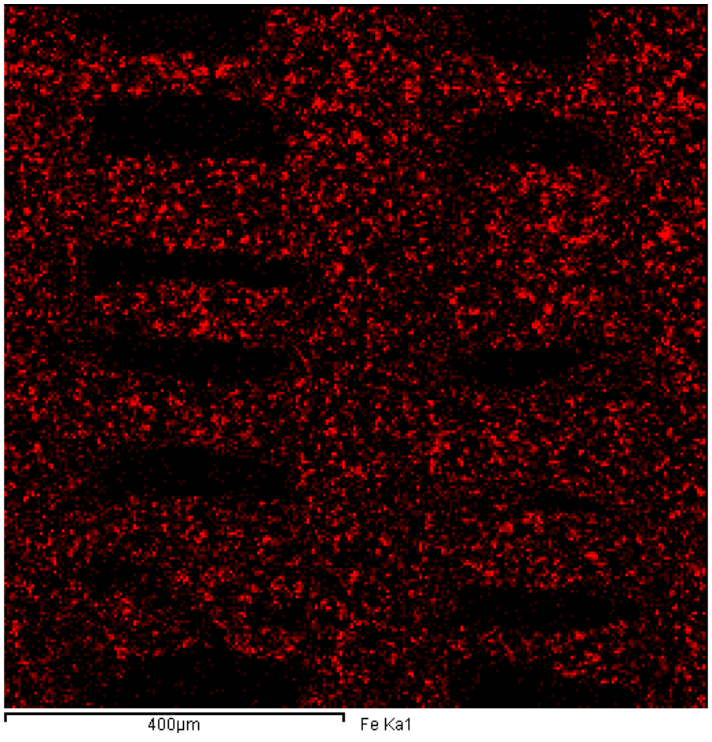

Figure 61 Iron in the structure of the scaffold 50%.

Figs. 58, 60, 63 prove the fact, that scaffolds 5%, 30% and 50% contain CIP in the individual fibers and those are homogenously dispersed in the matrix. The scaffold 5% (Fig. 58) has the lowest CIP concentration, the scaffold structure determination only according to iron particles is not possible. Fig. 60 shows more visible scaffold structure due to higher iron representation in fibers. In case of the scaffold 50% (Fig. 63) iron concentration is the highest among all scaffolds, every single fiber is clearly visible.

8.6 Magnetic field

The scaffold with sufficient amount of magnetic particles should be significantly influenced by magnetic field. In this experiment three samples were tested – 5%, 30% and 50%.

A sample was held and inserted to inactive magnetic field. After activation of the magnetic field strength, scaffold motion according to intensity of magnetic field was observed. The minimal intensity needed to lift scaffold towards the pole was taken as an optimal value (Figs. 69, 71).

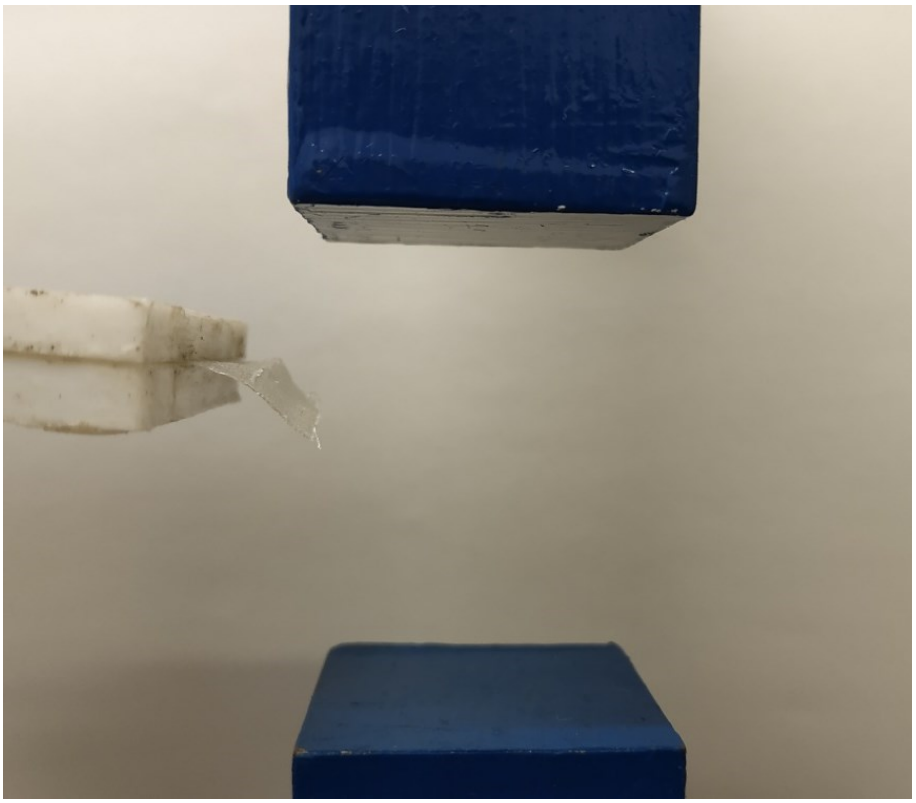

Figure 62 Image of the scaffold 0% in the absence of magnetic field strength.

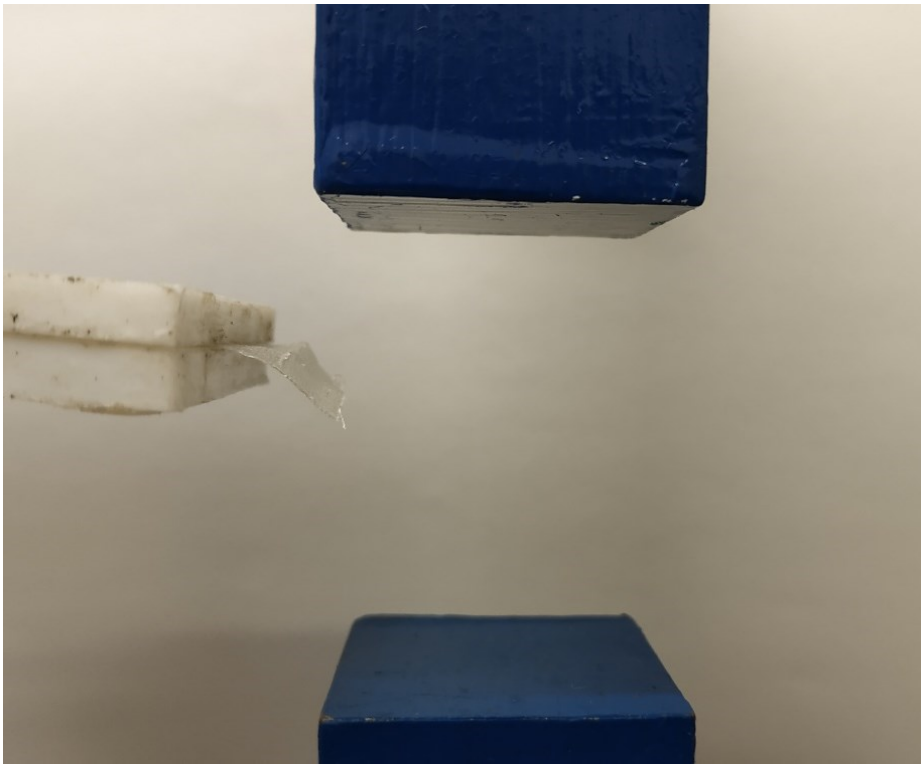

Figure 63 Image of the scaffold 0% in the presence of magnetic field strength, 150 kA/m (no effect).

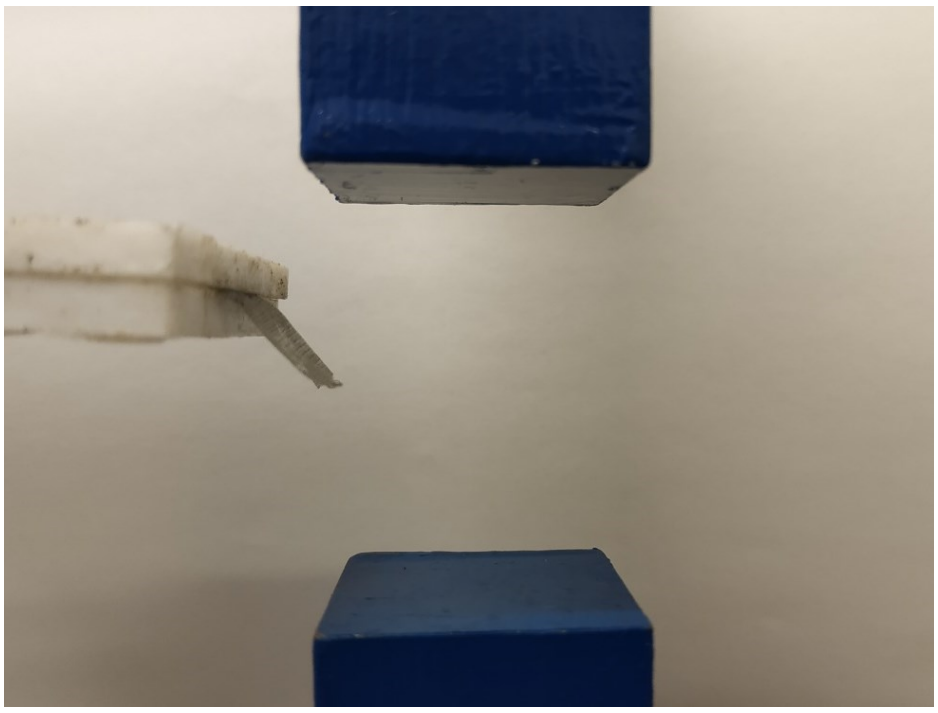

Figure 64 Image of the scaffold 5% in the absence of magnetic field strength.

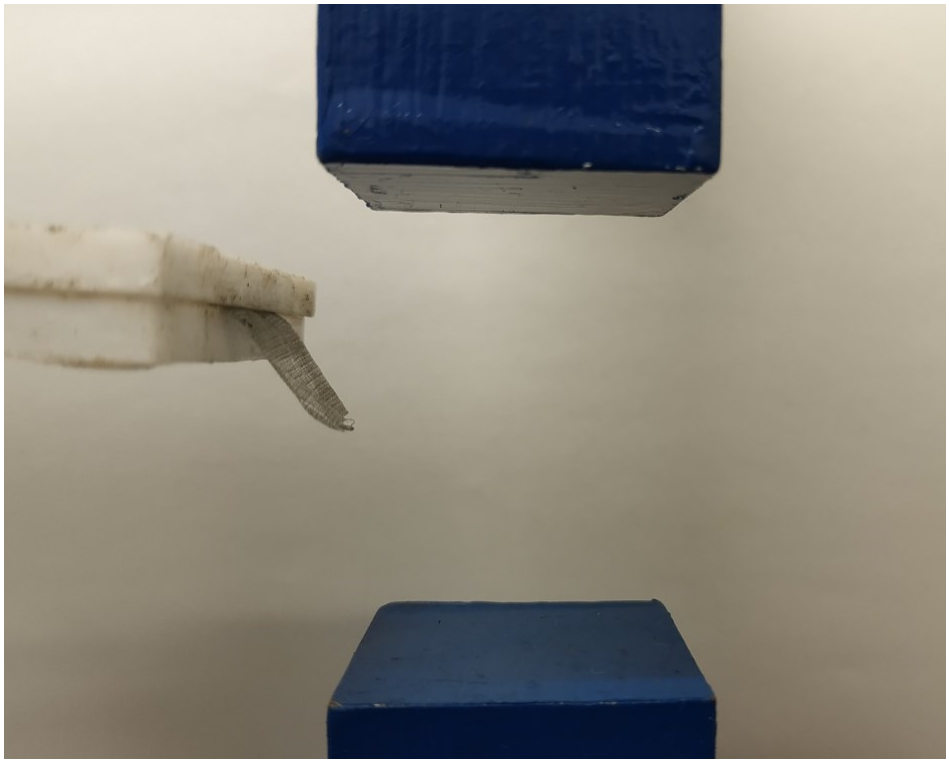

Figure 65 Image of the scaffold 5% in the presence of magnetic field strength, 150 kA/m (no effect).

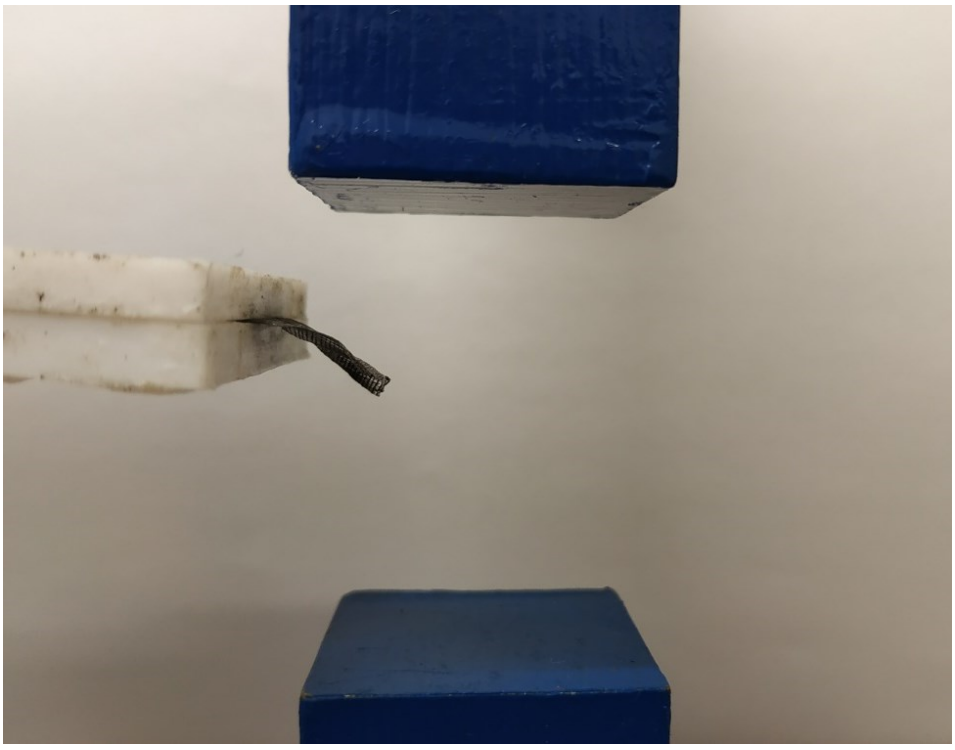

Figure 66 Image of the scaffold 30% in the absence of magnetic field strength.

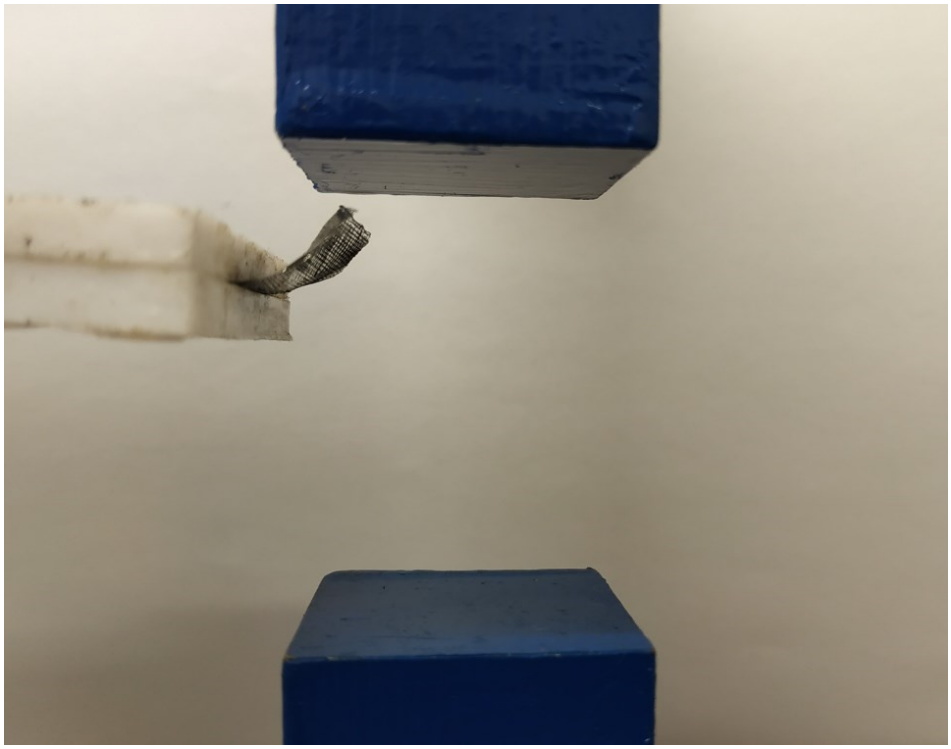

Figure 67 Image of the scaffold 30% in the presence of magnetic field strength, 110 kA/m.

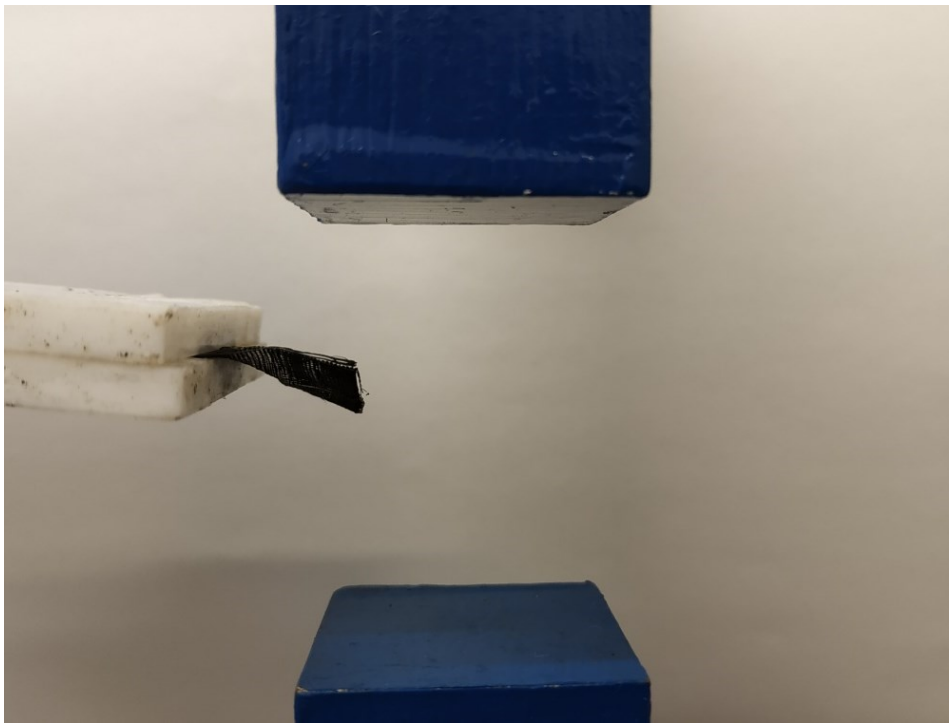

Figure 68 Image of the scaffold 50% in the absence of magnetic field strength.

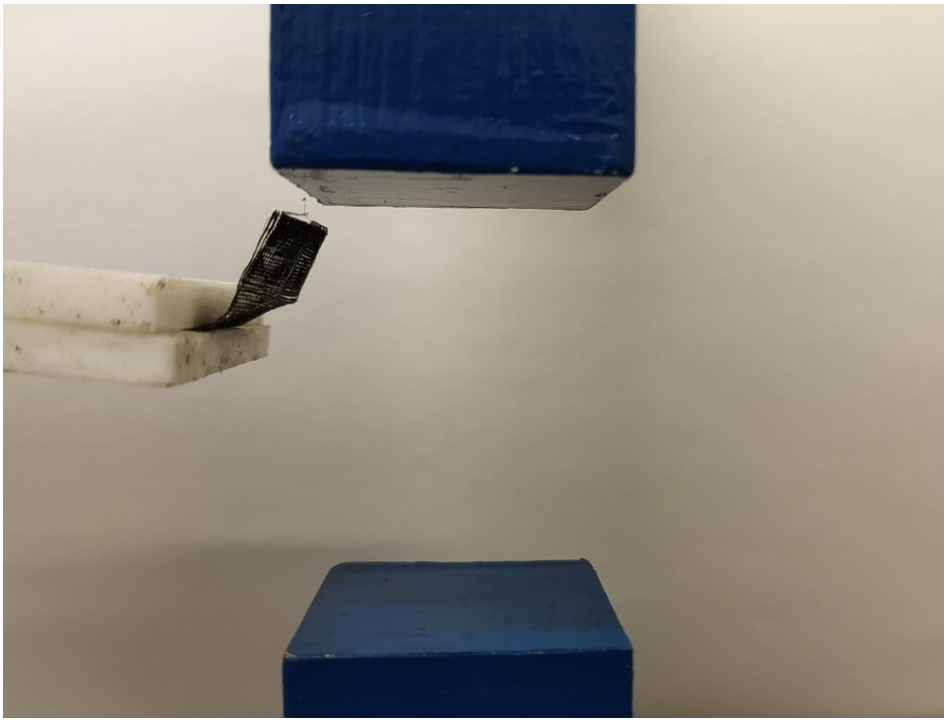

Figure 69 Image of the scaffold 50% in the presence of magnetic field strength, 80 kA/m.

According to Figs. 65 and 67, and as was expected the magnetic field does not influence the scaffolds 0% and 5% as well this concentration seems to be not enough for activation in magnetic field. Fig. 69 shows that the scaffold 30% is significantly influenced by magnetic field and that the motion is reversible when the field is switched on and off. For scaffold function, the minimal value of magnetic field is 110 kA/m which is relatively small value. Such sample could be suitable for functional magnetic scaffold.

As can be seen in Fig. 71, magnetic field has the biggest impact on the scaffold 50%. However, there is a negligible difference in comparison to the scaffold 30%. Moreover, here only magnetic field of 80 kA/m is enough for reversible motion. This sample is very promising and can be used as a functional magnetic scaffold.

8.7 Cytotoxicity

Table 5 Relative cell viability and concentration of all samples.

Extract conc./ Sample	100%		50%	
	Average	Error	Average	Error
V0	65.57	3.71	81.68	3.21
V5	81.81	2.74	89.29	2.63
V30	85.45	3.54	84.03	4.71
V50	90.37	2.87	96.62	3.68

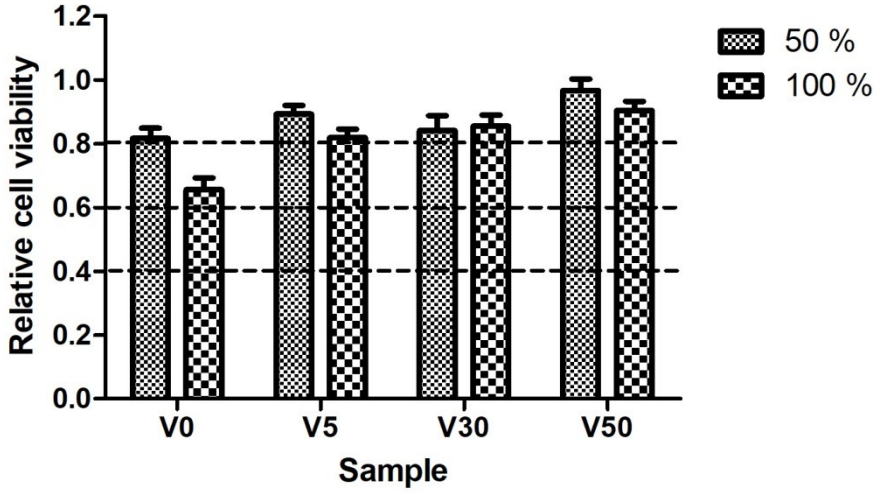

Figure 70 The dependence of relative cell viability on concentration for all samples.

According to the results of test CIP has tendency to positively influence biocompatibility of samples. Also, the few amounts of Vistamaxx in samples with higher CIP amount could have less negative impact to biocompatibility. For example according to the Fig. 72, the Sample 0% in concentration 100% reduces viability approximately about 30%. On the other hand, the sample 50% in concentration 100% reduces viability just about 3%. In case of concentration 50% it could even support cell proliferation. The reason of this tendency could be a negative influence of Vistamaxx to cells or iron presence that is beneficial for cell culture. However, these results mean that magnetic scaffold is completely biocompatible and could be used with cells.

CONCLUSION

In this work the masterbatches containing thermoplastic elastomer Vistamaxx with CIP concentration 0%, 5%, 10%, 30% and 50% was successfully prepared. DSC investigations of the neat Vistamaxx and various masterbatches showed the presence of two glass transition temperatures one melting temperature and exotermic peak at relatively high temperature 192 °C - 213 °C. Presence of the CIPs does not significantly influence the characteristic temperatures, however contribute to suppression of the exotermic peak in second heating, while pronounce the cold crystallization. Viscoelastic and rheological tests revealed that, the small CIP concentration (5%) can significantly decreased values of complex viscosity and improve masterbatch flow properties. Expectantly, addition of 30% and 50% of particles lead to the significant increase of the complex viscosity. On the other hand, with increasing temperature complex viscosity significantly decreases and in case of sample 50% the difference is about 2000 Pa.s between 150 °C and 190 °C. The results clearly indicated that even sample 50% can be suitable for additive manufacturing techniques especially for processing by melt-electrowriting technique (MEW).

The scaffold structure elucidation showed, that scaffolds printed by MEW technique, have decently organized fibers with fibre diameter in the range from 45 μm to 135 μm based on the amount of CIPs. In the magnetic properties test scaffolds 30% and 50% showed the best results among other samples, both are able to provide reversible motion upon magnetic field stimulation. Minimal required magnetic field intensity for sample 30% is 110 kA/m and in case of 50% value is 80 kA/m. Cytotoxicity tests showed that the CIP presence has a positive impact on scaffold biocompatibility. The sample with no CIP in gained only around 0.7 relative cell variability for undiluted solutions, on the other hand sample 50% in the same undiluted solution has approximately 1.0 relative cell.

All this information proves that this type of masterbatch can be easily processed using MEW and have optimal properties for successful scaffold fabrication. Moreover, the non-cytotoxic character is very promising for application of these scaffolds in process of stem cell differentiation upon magnetic field stimulation.

BIBLIOGRAPHY

Aldebs, A., Zohora, F., Nosoudi, N., Singh, S., & Ramirez-Vick, J. (2020). Effect of Pulsed Electromagnetic Fields on Human Mesenchymal Stem Cells Using 3D Magnetic Scaffolds. *Bioelectromagnetics*, *41*(3), 175-187. doi: 10.1002/bem.22248

Andonegi, M., Heras, K., Santos-Vizcaíno, E., Igartua, M., Hernandez, R., de la Caba, K., & Guerrero, P. (2020). Structure-properties relationship of chitosan/collagen films with potential for biomedical applications. *Carbohydrate Polymers*, *237*, 116159. doi: 10.1016/j.carbpol.2020.116159

Bakshi, P., Selvakumar, D., Kadirvelu, K., & Kumar, N. (2020). Chitosan as an environment friendly biomaterial – a review on recent modifications and applications. *International Journal Of Biological Macromolecules*, *150*, 1072-1083. doi: 10.1016/j.ijbiomac.2019.10.113

Bavaresco, B., Comín, R., Salvatierra, N., & Cid, M. (2020). Three-dimensional printing of collagen and hyaluronic acid scaffolds with dehydrothermal treatment crosslinking. *Composites Communications*, *19*, 1-5. doi: 10.1016/j.coco.2020.02.001

Bazrafshan, Z., & Stylios, G. (2019). Spinnability of collagen as a biomimetic material: A review. *International Journal Of Biological Macromolecules*, *129*, 693-705. doi: 10.1016/j.ijbiomac.2019.02.024

Brown, T., Dalton, P., & Hutmacher, D. (2011). Direct Writing By Way of Melt Electrospinning. *Advanced Materials*, *23*(47), 5651-5657. doi: 10.1002/adma.201103482

Brown, T., Dalton, P., & Hutmacher, D. (2016). Melt electrospinning today: An opportune time for an emerging polymer process. *Progress In Polymer Science*, *56*, 116-166. doi: 10.1016/j.progpolymsci.2016.01.001

Bu, H., Yang, H., Shen, L., Liu, W., & Li, G. (2020). Glutamic acid concentration dependent collagen mineralization in aqueous solution. *Colloids And Surfaces B: Biointerfaces*, *190*, 110892. doi: 10.1016/j.colsurfb.2020.110892

Blum, C., Schlegelmilch, K., Schilling, T., Shridhar, A., Rudert, M., & Jakob, F. et al. (2019). Extracellular Matrix-Modified Fiber Scaffolds as a Proadipogenic Mesenchymal Stromal Cell Delivery Platform. ACS Biomaterials Science & Engineering, 5(12), 6655-6666. doi: 10.1021/acsbiomaterials.9b00894

Burgaz, E., & Goksuzoglu, M. (2020). Effects of magnetic particles and carbon black on structure and properties of magnetorheological elastomers. *Polymer Testing*, *81*, 106233. doi: 10.1016/j.polymertesting.2019.106233

Carter, S., Costa, P., Vaquette, C., Ivanovski, S., Hutmacher, D., & Malda, J. (2016). Additive Biomanufacturing: An Advanced Approach for Periodontal Tissue Regeneration. *Annals Of Biomedical Engineering*, *45*(1), 12-22. doi: 10.1007/s10439-016-1687-2

Catt, S. (2020). Melt Electrowriting: Where Are We Now? - Advanced Science News. Retrieved 25 April 2020, from https://www.advancedsciencenews.com/melt-electrowriting-where-are-we-now/

Conrad, T., & Roeder, R. (2020). Effects of porogen morphology on the architecture, permeability, and mechanical properties of hydroxyapatite whisker reinforced polyetheretherketone scaffolds. *Journal Of The Mechanical Behavior Of Biomedical Materials*, *106*, 103730. doi: 10.1016/j.jmbbm.2020.103730

Chen, C., Bai, Z., Cao, Y., Dong, M., Jiang, K., & Zhou, Y. et al. (2020). Enhanced piezoelectric performance of BiCl3/PVDF nanofibers-based nanogenerators. Composites Science And Technology, 192, 108100. doi: 10.1016/j.compscitech.2020.108100

Cyphert, E., Bil, M., Recum, H., & Święszkowski, W. (2020). Repurposing biodegradable tissue engineering scaffolds for localized chemotherapeutic delivery. *Journal Of Biomedical Materials Research Part A*, *108*(5), 1144-1158. doi: 10.1002/jbm.a.36889

Dalton, P. (2017). Melt electrowriting with additive manufacturing principles. *Current Opinion In Biomedical Engineering*, *2*, 49-57. doi: 10.1016/j.cobme.2017.05.007

Dong, J., Zhou, W., Wang, C., Lu, L., Luo, F., & Zhu, D. (2019). Anisotropic particle geometry effect on magnetism and microwave absorption of carbonyl iron/polyimide composites. *Journal Of Magnetism And Magnetic Materials*, *491*, 165643. doi: 10.1016/j.jmmm.2019.165643

Dong, R., Ma, P., & Guo, B. (2020). Conductive biomaterials for muscle tissue engineering. *Biomaterials*, *229*, 119584. doi: 10.1016/j.biomaterials.2019.119584

Drained of blood, the heart is white : woahdude. (2020). Retrieved 27 April 2020, from https://www.reddit.com/r/woahdude/comments/5zj452/drained_of_blood_the_heart_is_white/

Electrospinning Technique. (2020). Retrieved 30 April 2020, from https://www.weistron.com/electrospinning-tech/

Farzin, A., Fathi, M., & Emadi, R. (2017). Multifunctional magnetic nanostructured hardystonite scaffold for hyperthermia, drug delivery and tissue engineering applications. *Materials Science And Engineering: C*, *70*, 21-31. doi: 10.1016/j.msec.2016.08.060

Frontiers. (2020). Retrieved 30 April 2020, from https://www.frontiersin.org/Community/AbstractDetails.aspx?ABS_DOI=10.3389/conf.FBIOE.2016.01.02089&eid=2893&sname=10th_World_Biomaterials_Congress

Haider, A., Haider, S., Rao Kummara, M., Kamal, T., Alghyamah, A., & Jan Iftikhar, F. et al. (2020). Advances in the scaffolds fabrication techniques using biocompatible polymers and their biomedical application: A technical and statistical review. *Journal Of Saudi Chemical Society*, *24*(2), 186-215. doi: 10.1016/j.jscs.2020.01.002

Hedayati, S., Behravesh, A., Hasannia, S., Bagheri Saed, A., & Akhoundi, B. (2020). 3D printed PCL scaffold reinforced with continuous biodegradable fiber yarn: A study on mechanical and cell viability properties. *Polymer Testing*, *83*, 106347. doi: 10.1016/j.polymertesting.2020.106347

Hrynevich, A., Elçi, B., Haigh, J., McMaster, R., Youssef, A., & Blum, C. et al. (2018). Dimension-Based Design of Melt Electrowritten Scaffolds. Small, 14(22), 1800232. doi: 10.1002/smll.201800232

http://www.kapelan-media.com, K. (2020). Magnetic Particles : Particles and Kits for Magnetic separation. Retrieved 25 April 2020, from http://www.chemicell.com/products/magnetic_particles/magnetic_particle_separation.html

Chemistry Society, SS, HKUSU. (2020). Retrieved 29 April 2020, from https://www.chemsoc.hkusu.hku.hk/academic_article/academic_article_16_05_24.html

Chen, C., Bai, Z., Cao, Y., Dong, M., Jiang, K., & Zhou, Y. et al. (2020). Enhanced piezoelectric performance of BiCl3/PVDF nanofibers-based nanogenerators. *Composites Science And Technology*, *192*, 108100. doi: 10.1016/j.compscitech.2020.108100

Cheng, Y., Xu, Y., Qian, Y., Chen, X., Ouyang, Y., & Yuan, W. (2020). 3D structured self-powered PVDF/PCL scaffolds for peripheral nerve regeneration. *Nano Energy*, *69*, 104411. doi: 10.1016/j.nanoen.2019.104411

Chung, L., Maestas, D., Housseau, F., & Elisseeff, J. (2017). Key players in the immune response to biomaterial scaffolds for regenerative medicine. *Advanced Drug Delivery Reviews*, *114*, 184-192. doi: 10.1016/j.addr.2017.07.006

Jang, D., Yoon, H., Nam, I., & Lee, H. (2020). Effect of carbonyl iron powder incorporation on the piezoresistive sensing characteristics of CNT-based polymeric sensor. *Composite Structures*, *244*, 112260. doi: 10.1016/j.compstruct.2020.112260

Jazayeri, H., Lee, S., Kuhn, L., Fahimipour, F., Tahriri, M., & Tayebi, L. (2020). Polymeric scaffolds for dental pulp tissue engineering: A review. *Dental Materials*, *36*(2), e47-e58. doi: 10.1016/j.dental.2019.11.005

Jin, G., & Li, K. (2014). The electrically conductive scaffold as the skeleton of stem cell niche in regenerative medicine. *Materials Science And Engineering: C*, *45*, 671-681. doi: 10.1016/j.msec.2014.06.004

Jodati, H., Yılmaz, B., & Evis, Z. (2020). A review of bioceramic porous scaffolds for hard tissue applications: Effects of structural features. *Ceramics International*. doi: 10.1016/j.ceramint.2020.03.192

Kajbafzadeh, A., Tourchi, A., Mousavian, A., Rouhi, L., Tavangar, S., & Sabetkish, N. (2014). Bladder muscular wall regeneration with autologous adipose mesenchymal stem cells on three-dimensional collagen-based tissue-engineered prepuce and biocompatible nanofibrillar scaffold. *Journal Of Pediatric Urology*, *10*(6), 1051-1058. doi: 10.1016/j.jpurol.2014.03.010

Kim, J., Kim, W., & Kim, G. (2020). Scaffold with micro/nanoscale topographical cues fabricated using E-field-assisted 3D printing combined with plasma-etching for enhancing myoblast alignment and differentiation. *Applied Surface Science*, *509*, 145404. doi: 10.1016/j.apsusc.2020.145404

Kim, W., Kim, M., & Kim, G. (2018). 3D-Printed Biomimetic Scaffold Simulating Microfibril Muscle Structure. *Advanced Functional Materials*, *28*(26), 1800405. doi: 10.1002/adfm.201800405

Koo, J., Kang, J., Shin, S., Jegal, J., Cha, H., & Choy, S. et al. (2020). Biobased thermoplastic elastomer with seamless 3D-Printability and superior mechanical properties empowered by in-situ polymerization in the presence of nanocellulose. *Composites Science And Technology*, *185*, 107885. doi: 10.1016/j.compscitech.2019.107885

Lanfer, B., Seib, F., Freudenberg, U., Stamov, D., Bley, T., Bornhäuser, M., & Werner, C. (2009). The growth and differentiation of mesenchymal stem and progenitor cells cultured on aligned collagen matrices. *Biomaterials*, *30*(30), 5950-5958. doi: 10.1016/j.biomaterials.2009.07.039

Lee, J., & Kim, G. (2020). A cryopreservable cell-laden GelMa-based scaffold fabricated using a 3D printing process supplemented with an in situ photo-crosslinking. *Journal Of Industrial And Engineering Chemistry*, *85*, 249-257. doi: 10.1016/j.jiec.2020.02.007

Liu, C., Wu, S., Yan, Y., Dong, Y., Shen, X., & Huang, C. (2019). Application of magnetic particles in forensic science. *Trac Trends In Analytical Chemistry*, *121*, 115674. doi: 10.1016/j.trac.2019.115674

Lovejoy, D. (1993). Magnetic particles, their characteristics and application. *Magnetic Particle Inspection*, 117-147. doi: 10.1007/978-94-011-1536-0_6

Mahato, R. (2017). Microneedles in Drug Delivery. Emerging Nanotechnologies For Diagnostics, Drug Delivery And Medical Devices, 331-353. doi: 10.1016/b978-0-323-42978-8.00013-9

Meng, Z., He, J., Cai, Z., Wang, F., Zhang, J., & Wang, L. et al. (2020). Design and additive manufacturing of flexible polycaprolactone scaffolds with highly-tunable mechanical properties for soft tissue engineering. *Materials & Design*, *189*, 108508. doi: 10.1016/j.matdes.2020.108508

Naderi, P., Zarei, M., Karbasi, S., & Salehi, H. (2020). Evaluation of the effects of keratin on physical, mechanical and biological properties of poly (3-hydroxybutyrate) electrospun scaffold: Potential application in bone tissue engineering. *European Polymer Journal*, *124*, 109502. doi: 10.1016/j.eurpolymj.2020.109502

O'Brien, F. (2011). Biomaterials & scaffolds for tissue engineering. *Materials Today*, *14*(3), 88-95. doi: 10.1016/s1369-7021(11)70058-x

Owens, G., Singh, R., Foroutan, F., Alqaysi, M., Han, C., & Mahapatra, C. et al. (2016). Sol–gel based materials for biomedical applications. *Progress In Materials Science*, *77*, 1-79. doi: 10.1016/j.pmatsci.2015.12.001

Parenteau, T., Bertevas, E., Ausias, G., Stocek, R., Grohens, Y., & Pilvin, P. (2014). Characterisation and micromechanical modelling of the elasto-viscoplastic behavior of

thermoplastic elastomers. *Mechanics Of Materials*, *71*, 114-125. doi: 10.1016/j.mechmat.2013.06.010

Paris, J., Román, J., Manzano, M., Cabañas, M., & Vallet-Regí, M. (2015). Tuning dual-drug release from composite scaffolds for bone regeneration. *International Journal Of Pharmaceutics*, *486*(1-2), 30-37. doi: 10.1016/j.ijpharm.2015.03.048

Pillai, M., Kumar, G., Houshyar, S., Padhye, R., & Bhattacharyya, A. (2020). Effect of nanocomposite coating and biomolecule functionalization on silk fibroin based conducting 3D braided scaffolds for peripheral nerve tissue engineering. *Nanomedicine: Nanotechnology, Biology And Medicine*, *24*, 102131. doi: 10.1016/j.nano.2019.102131

Pina, S., Ribeiro, V., Marques, C., Maia, F., Silva, T., Reis, R., & Oliveira, J. (2019). Scaffolding Strategies for Tissue Engineering and Regenerative Medicine Applications. *Materials*, *12*(11), 1824. doi: 10.3390/ma12111824

Pomeroy, J., Helfer, A., & Bursac, N. (2019). Biomaterializing the promise of cardiac tissue engineering. *Biotechnology Advances*. doi: 10.1016/j.biotechadv.2019.02.009

Rahmati Nejad, M., Yousefzadeh, M., & Solouk, A. (2020). Electrospun PET/PCL small diameter nanofibrous conduit for biomedical application. *Materials Science And Engineering: C*, *110*, 110692. doi: 10.1016/j.msec.2020.110692

Ranjbari, E., Bazgir, S., & Shirazi, M. (2020). Needleless electrospinning of poly(acrylic acid) superabsorbent: Fabrication, characterization and swelling behavior. *Polymer Testing*, *84*, 106403. doi: 10.1016/j.polymertesting.2020.106403

Ronca, A., Maiullari, F., Milan, M., Pace, V., Gloria, A., & Rizzi, R. et al. (2017). Surface functionalization of acrylic based photocrosslinkable resin for 3D printing applications. *Bioactive Materials*, *2*(3), 131-137. doi: 10.1016/j.bioactmat.2017.04.002

Saadatmand, M., Yazdanshenas, M., Khajavi, R., Mighani, F., Toliyat, T. (2019). Patterning the surface roughness of a nano fibrous scaffold for transdermal drug release, *International Journal of Nano Dimension*, 10(1), 78-88.

Sadtler, K., Wolf, M., Ganguly, S., Moad, C., Chung, L., & Majumdar, S. et al. (2019). Divergent immune responses to synthetic and biological scaffolds. *Biomaterials*, *192*, 405-415. doi: 10.1016/j.biomaterials.2018.11.002

Sarwar, Z., Krugly, E., Danilovas, P., Ciuzas, D., Kauneliene, V., & Martuzevicius, D. (2019). Fabrication and characterization of PEBA fibers by melt and solution

electrospinning. *Journal Of Materials Research And Technology*, *8*(6), 6074-6085. doi: 10.1016/j.jmrt.2019.10.001

Seyedi, F., Farsinejad, A., & Nematollahi-Mahani, S. (2017). Fibrin scaffold enhances function of insulin producing cells differentiated from human umbilical cord matrix-derived stem cells. *Tissue And Cell*, *49*(2), 227-232. doi: 10.1016/j.tice.2017.03.001

Seymour, R., & Kauffman, G. (1992). Elastomers: III. Thermoplastic elastomers. *Journal Of Chemical Education*, *69*(12), 967. doi: 10.1021/ed069p967

Shi, Q., Shui, H., Chen, Q., & Li, Z. (2020). How does mechanical stimulus affect the coupling process of the scaffold degradation and bone formation: An in silico approach. *Computers In Biology And Medicine*, *117*, 103588. doi: 10.1016/j.compbiomed.2019.103588

Shuai, C., Yang, W., He, C., Peng, S., Gao, C., & Yang, Y. et al. (2020). A magnetic micro-environment in scaffolds for stimulating bone regeneration. *Materials & Design*, *185*, 108275. doi: 10.1016/j.matdes.2019.108275

Sivashankari, P., & Prabaharan, M. (2020). Three-dimensional porous scaffolds based on agarose/chitosan/graphene oxide composite for tissue engineering. *International Journal Of Biological Macromolecules*, *146*, 222-231. doi: 10.1016/j.ijbiomac.2019.12.219

Tanasa, E., Zaharia, C., Hudita, A., Radu, I., Costache, M., & Galateanu, B. (2020). Impact of the magnetic field on 3T3-E1 preosteoblasts inside SMART silk fibroin-based scaffolds decorated with magnetic nanoparticles. *Materials Science And Engineering: C*, *110*, 110714. doi: 10.1016/j.msec.2020.110714

Thangavel, K., Roshini, T., Balaprakash, V., Gowrisankar, P., Sudha, S., & Mohan, M. (2020). Structural, morphological and antibacterial properties of ZnO nanofibers fabricated by electrospinning technique. *Materials Today: Proceedings*. doi: 10.1016/j.matpr.2020.03.241

Tian, M., Xue, C., Chang, Y., Shen, J., Zhang, Y., Li, Z., & Wang, Y. (2020). Collagen fibrils of sea cucumber (Apostichopus japonicus) are heterotypic. *Food Chemistry*, *316*, 126272. doi: 10.1016/j.foodchem.2020.126272

Wang, C., Huang, W., Zhou, Y., He, L., He, Z., & Chen, Z. et al. (2020). 3D printing of bone tissue engineering scaffolds. *Bioactive Materials*, *5*(1), 82-91. doi: 10.1016/j.bioactmat.2020.01.004

Wang, W., Lu, W., Goodwin, A., Wang, H., Yin, P., & Kang, N. et al. (2019). Recent advances in thermoplastic elastomers from living polymerizations: Macromolecular architectures and supramolecular chemistry. *Progress In Polymer Science*, *95*, 1-31. doi: 10.1016/j.progpolymsci.2019.04.002

Waterman, P. (2020). Rapid Tech Firms Aid Medical and Dental Fields - Digital Engineering. Retrieved 29 April 2020, from https://www.digitalengineering247.com/article/rapid-tech-firms-aid-medical-and-dental-fields/

Xia, Y., Sun, J., Zhao, L., Zhang, F., Liang, X., & Guo, Y. et al. (2018). Magnetic field and nano-scaffolds with stem cells to enhance bone regeneration. *Biomaterials*, *183*, 151-170. doi: 10.1016/j.biomaterials.2018.08.040

Yang, T., Liu, Q., Chan, L., & Liu, Z. (2007). Magnetic signature of heavy metals pollution of sediments: case study from the East Lake in Wuhan, China. *Environmental Geology*, *52*(8), 1639-1650. doi: 10.1007/s00254-006-0609-2

Yang, Y., Wang, G., Liang, H., Gao, C., Peng, S., Shen, L., & Shuai, C. (2018). Additive manufacturing of bone scaffolds. *International Journal Of Bioprinting*, *5*(1). doi: 10.18063/ijb.v5i1.148

Yeo, M., & Kim, G. (2019). Nano/microscale topographically designed alginate/PCL scaffolds for inducing myoblast alignment and myogenic differentiation. *Carbohydrate Polymers*, *223*, 115041. doi: 10.1016/j.carbpol.2019.115041

Yousefi, A., James, P., Akbarzadeh, R., Subramanian, A., Flavin, C., & Oudadesse, H. (2016). Prospect of Stem Cells in Bone Tissue Engineering: A Review. *Stem Cells International*, *2016*, 1-13. doi: 10.1155/2016/6180487

Zhao, P., Gu, H., Mi, H., Rao, C., Fu, J., & Turng, L. (2017). Fabrication of scaffolds in tissue engineering: A review. *Frontiers Of Mechanical Engineering*, *13*(1), 107-119. doi: 10.1007/s11465-018-0496-8

LIST OF ABBREVIATIONS

3D Three-dimensional

BSE Backscattered Electrons

CIP Carbonyl Iron Powder

DMA Dynamic Mechanical Analysis

DPSC Dental Pulp Stem Cells

DSC Differential Scanning Calorimetry

ECM Extracellular Matrix

EMF Electromagnetic Field

G″ Loss modulus

G′ Storage modulus

GO Graphene Oxide

MEW Melt-electrowriting technique

MSC Mesenchymal Stem Cells

NP Nanoparticles

PANi Polyaniline

PCL Polycaprolactone

PGA Polyglycolic acid

PLA Polylactic acid

PLGA Poly(lactic-co-glycolic acid)

PVDF Polyvinylidene Fluoride

SE Secondary Electron

SEM Scanning Electron Microscope

SFM Solid Free Mold technique

TE Tissue Engineering

TPE Thermoplastic Elastomer

LIST OF FIGURES

LIST OF TABLES